ULTRAFAST TRANSIENT ABSORPTION AND FLUORESCENCE STUDIES ON THE STABILITY AND CHARGE SEPARATION/RECOMBINATION DYNAMICS OF SEMICONDUCTOR NANOCRYSTALS IN PRESENCE OF SOME MOLECULAR SYSTEMS

A Thesis Submitted for the Degree of DOCTOR OF PHILOSOPHY

by

Chandra Sekhar Mutyala



School of Chemistry
University of Hyderabad
Hyderabad-500 046
India
May 2016

Dedicated

 $\mathcal{T}o$

My Family

"There comes a point in your life when you need to stop reading other people's books and write your own."

Albert Einstein

CONTENTS

Statement	i
Declaration	iii
Certificate	V
Acknowledgement	vii
List of Publications	ix
Presentations	xi
Thesis Layout	xii
Chapter 1 Introduction	1
1.1. Quantum Dots (QDs)	2
1.1.1. Passivation of surface trap state and solu	ability 5
1.1.2. Core/Shell QDs	7
1.1.2.1. Type-I Core/Shell QDs	7
1.1.2.2. Type-II Core/Shell QDs	8
1.1.2.3. Reverse Type-I Core/Shell QDs	8
1.1.2.4. Synthesis of Core/Shell QDs	8
1.1.3. Alloy QDs	9
1.1.4. Doped QDs	11
1.1.5. Multiple exciton generation	12
1.1.6. Applications	14
1.2. Ionic Liquids	15
1.2.1. Properties	17
1.2.1.1. Viscosity and density	17
1.2.1.2. Melting point	19
1.2.1.3. Thermal stability and volatility	19
1.2.1.4. Conductivity and ionic diffusion	20
1.2.1.5. Polarity	21
1.2.1.6. Structural characterization and heter	rogeneity 21
1.2.1.7. Other properties	23
1.2.2. Applications	24
1.3. Fluorescence quenching	24

	1.3.1. Energy transfer	24
	1.3.1.1. Radiative energy transfer	25
	1.3.1.2. Non-radiative energy transfer	25
	1.3.1.2.1. Förster resonance energy transfer	26
	1.3.1.2.2. Dexter energy transfer	28
	1.3.2. Photo-induced electron transfer	29
	1.4. Motivation behind the thesis	30
	References	35
Chapter 2	Material, Methods and Instrumentation	43
	2.1. Materials	44
	2.2. Synthesis of ligands and quantum dots	45
	2.2.1. 1-methyl-(11-undecanethiol) imidazolium bromide	45
	2.2.2. 3-mercaptoutyric acid	45
	2.2.3. Quantum dots in non-polar media	46
	2.2.3.1. CdTe/HDA/TOPO/TOP	46
	2.2.3.2. CdTe/TOP/OA	46
	2.2.3.3. CdSe/HDA/TOPO/TOP	47
	2.2.4. Quantum dots in polar media	48
	2.2.5. Quantum dots in ionic liquid	48
	2.3. Methods for purification of conventional solvents	48
	2.4. Purification of ionic liquid	49
	2.5. Sample preparation	49
	2.5.1. Steady state and time-resolved absorption and	
	emission measurements	49
	2.5.2. TEM measurements	49
	2.5.3. ICP-OES measurements	50
	2.6. Instrumentation and data analysis	50
	2.6.1. Time-correlated single photon counting fluorimeter	50
	2.6.1.1. Data analysis	52
	2.6.2. Femtosecond pump-probe setup	53
	2.6.2.1. Data analysis	55

	2.7. Measurement of emission quantum yield	55
	2.8. Determination of the size and concentration of QDs in	
	Solution	55
	2.9. Error limits	56
	References	57
Chapter 3	CdTe Quantum Dots in Ionic Liquid: Stability and Hole	
	Scavenging in the Presence of a Sulfide Salt	59
	3.1. Introduction	60
	3.2. Results and Discussion	63
	3.2.1. Steady state and time-resolved experiments	63
	3.2.2. Ultrafast transient absorption measurements	67
	3.3. Conclusion	71
	References	72
Chapter 4	Nature of Interactions between Oppositely Charged	
	Photo-excited CdTe Quantum Dots and Cresyl Violet	75
	4.1. Introduction	76
	4.2. Results	78
	4.2.1. Steady state measurements	78
	4.2.2. Time-resolved measurements	79
	4.2.3. Ultrafast transient absorption measurements	81
	4.3. Discussion	83
	4.4. Conclusion	90
	References	91
Chapter 5	Influence of Capping Agents on the Carrier Trapping	
	Dynamics of the Photo-excited CdTe Quantum Dots	93
	5.1. Introduction	94
	5.2. Results	95
	5.2.1. Steady state measurements	95
	5.2.2. Time-resolved photoluminescence measurements	99
	5.2.3. Ultrafast transient absorption measurements	100
	5.3. Discussion	104

	5.4. Conclusion	107
	References	108
Chapter 6	Charge Separation and Recombination Dynamics	
	between CdSe QDs and Methyl Viologen:	
	Dependence on the Stoichiometry of the Nanocrystals	111
	6.1. Introduction	112
	6.2. Results	114
	6.2.1. Steady state and time-resolved measurements	114
	6.2.2. Ultrafast transient absorption measurements	119
	6.3. Discussion	123
	6.4. Conclusion	127
	References	128
Chapter 7	Concluding Remarks	131
	7.1. Overview	132
	7.2. Future Scope	134

STATEMENT

I hereby declare that the matter embodied in the thesis entitled "Ultrafast Transient Absorption and Fluorescence Studies on the Stability and Charge Separation/Recombination Dynamics of Semiconductor Nanocrystals in Presence of Some Molecular Systems" is the result of investigations carried out by me in School of Chemistry, University of Hyderabad, India under the supervision of Prof.Anunay Samanta.

In keeping with the general practice of reporting scientific investigations, the acknowledgements have been made wherever the work described is based on the findings of other investigators. Any omission or error that might have crept in is regretted.

May 2016

Chandra Sekhar Mutyala

DECLARATION

I, Chandra Sekhar Mutyala hereby declare that this thesis entitled "Ultrafast Transient

Absorption and Fluorescence Studies on the Stability and Charge

Separation/Recombination Dynamics of Semiconductor Nanocrystals in Presence of

Some Molecular Systems" submitted by me under the supervision of Prof. Anunay

Samanta is a bonafide research work which is free from plagiarism. I also declare that it

has not been submitted previously in part or full to this University or any other University

or Institution for the award of any degree or diploma. I hereby agree that my thesis can

deposited in Shodganga/INFLIBNET.

A report on plagiarism from the University Library is enclosed.

Date:

Signature of the Supervisor

Signature of the Student

Name: Chandra Sekhar Mutyala

Regd. No: 10CHPH16

iii

SCHOOL OF CHEMISTRY UNIVERSITY OF HYDERABAD HYDERABAD-500 046, INDIA



Phone: +91-40-2313 4813 (O)

+91-40-2313 0715 (R)

Fax: +91-40-2301 1594

E-mail: anunay@uohyd.ac.in anunay.samanta@gmail.com

Prof. Anunay Samanta

CERTIFICATE

Certified that the work embodied in the thesis entitled "Ultrafast Transient Absorption and Fluorescence Studies on the Stability and Charge Separation/Recombination Dynamics of Semiconductor Nanocrystals in Presence of Some Molecular Systems" has been carried out by Mr. Chandra Sekhar Mutyala under my supervision and the same has not been submitted elsewhere for any degree.

Anunay Samanta

(Thesis Supervisor) School of Chemistry

University of Hyderabad

Dean

Acknowledgement

Though only my name appears on the cover page of this thesis, many people are the reason for its production. My sincere gratitude to my supervisor, Prof. Anunay Samanta, for his constant guidance, cooperation and encouragement. He has been quite helpful to me in both academic and personal fronts.

I would like to thank my doctoral committee members, Prof. Samudranil Pal and Prof. Tushar Jana for their suggestions and cooperation. I also thank the present and former Dean(s) and the faculty, School of Chemistry, for allowing me to avail the facilities in the department.

I thank Mr. M. Durga Prasad for Transmission Electron Microscope measurements at Centre for Nanotechnology, University of Hyderabad.

I am indebted to my teachers, R. Ravi Kumar, S. Sreedhar (DSP, Warangal), R. Sai Sakuntala and P. Kesava Rao from whom I was inspired at various stages of my life and to my friend /advisor, Anil Kumar, who introduced me to the world of chemistry. I am really fortunate to have Priyanka (Potti) and Sunil Kumar in my life with whom I share my victories and failures. I would like to thank all my school friends, Radha, Swathi, Gowri, Uday, Suresh, Sandeep, Vamsi, Chanti, Sailesh, Santhosh, Vinod, Shankar, Venkat ramana, Abhishek, Anil, Srikanth, Kranthi, Yesu, Pradeep, Ranjith, Manil for the beautiful moments I enjoyed.

I thank my bachelor mates, Midhun, Santhosh, Naveen (confy), Naidu, Santhosh (Roll. No-13), Vasu, Praveen, chinna and pedda Koti, Ramesh, Pavan, Praveen, Seshu, Saliu, Suvvi, Sandhya, Srividya for making my college days wonderful. I thank my friends Vasu and Ravana from my grandmother's village, who taught me how to steal coconuts and sugarcanes from the nearby fields.

I thank my master class mates, Dr. Ashok, Dr. Sudheer, Dr. Rajesh, Appi, Srinu, Rama rao, sudhakar, Dr. nagarjuna, Satti, Bejju, Praveen, Chaitanya, Vijay, Aleem, Dr. Pitta, Ojha, Babu, Gaurango, Naidu, Sneha for the beautiful memories.

I value my association with my lab seniors, Dr. Ravi kumar, Dr. Santhosh, Dr. Dinesh, Dr. Sanghamitra, Dr. Satyajit, Dr. Soumya, Dr. Tanmay, Dr. Shalini, and Dr. Ashok for their suggestion and discussions, which helped me a lot in

research and juniors Navendu, Sneha, Sudipta, Apurba, Saddam and Tasnim for maintaining a friendly and cooperative ambience in the lab. My special thanks to Dr. Shalini, Dr. Ashok and Sneha for enjoying with me in my success and helping me to overcome my weakness.

I am lucky to have other seniors in chemistry which include Dr. Sivaranjana Reddy, Dr. Sekhar Reddy, Dr. Trirupati Reddy, Dr. Pavan Kumar Reddy, Dr. Sivaramakrishna, Dr. Ramesh, Venkat Reddy, Dr. Bharani Shashank, Dr. Guru Brahmam and Dr. Ramu Yadav, Dr. Kishore, Dr. Karunakar, Vikranth, Sateesh, Obayya, Seshi and friends which include Dr. Naidu (bunny), Suresh, Murali, Ramakrishna (banda), Ramakrishna (Tammudu), Anil, Srujana, Srinu, Narendra, Kesav, Divya, Lasya, Suryanarayana. My special thanks to Naidu, Sudheer, Suresh, Ashok and Murali for being part of my life.

I acknowledge my university gang for all the awesome parties, especially, the cooks, Ashok, Shalini, Naidu, Narendra, Srinu, Manil, Sudheer (Head Cook) for the delicious food.

I would like to thank my cricket friends, Rakesh, Dheemudu, Prasanna, Ramji, Praveen, Ravi, Triupati, Lakshman, Sagar, Rithwik, Mahender, Sai, Khaja, Ravinder and others, Susheel, Gurajada, Uday, Kiran, Joshi, Sandeep, Sampath Reddy, Sai, Durga Rao and sreetam for the lovely memories in the university.

I am fortunate to have family friends, Amurutha, Saritha vadina, Srinivasa Rao garu and Vinodini garu, who stood my side during hard times.

I express my deep gratitude to my mother (Umadevi) and sister (Bharathi). Amma and Akka, without your support, I could not have reached to this stage. I also express my gratitude to by brother-in-law (Bhaskar) for his cooperation. I am fortunate to have a nephew (Lohitaksha), who is similar to me in personality.

Forgive me if I fail to mention your name, but I want to thank all the people who played a role in my life.



List of Publications

- 1. "Dual Fluorescence of Ellipticine: Exited State Proton Transfer from Solvent versus Solvent Mediated Intramolecular Proton Transfer" S. Banerjee, A. Pabbathi, M. Chandra Sekhar and A. Samanta, *J. Phys. Chem. A*, 115 (**2011**), 9217-9225.
- 2. "Intramolecular Cycloadditions of Photogenerated Azaxylylenes: An Experimental and Theoretical Study" A. Olga, W. Mukhina, C. Cronk, N. N. Bhuvan Kumar, M. Chandra Sekhar, and A. Samanta, *J. Phys. Chem. A*, 118 (2014), 10487-10496.
- 3. "CdTe Quantum Dots in Ionic Liquid: Stability and Hole Scavenging in the Presence of a Sulfide Salt" M. Chandra Sekhar, K. Santhosh, J. Praveen, N. Mondal, S. Soumya, and A. Samanta, *J. Phys. Chem. C*, 118(**2014**), 18481-18487. (Chapter 3)
- 4. "Ultrafast Transient Absorption Study of the Nature of Interaction between Oppositely Charged Photoexcited CdTe Quantum Dots and Cresyl Violet" M. Chandra Sekhar and A. Samanta, *J. Phys. Chem. C*, 119(2015), 15661-15668. (Chapter 4)
- 5. "Influence of Capping Agents on the Carrier Trapping Dynamics of Photo-excited CdTe QDs" M. Chandra Sekhar and A. Samanta (to be communicated). (Chapter 5)

6. "Charge Separation and Recombination Dynamics between CdSe QDs of Different Stoichiometry and Methyl Viologen: An Ultrafast Transient Absorption Study" M. Chandra Sekhar and A. Samanta (to be communicated). (Chapter 6)

Presentations

Oral Presentation

1. "CdTe Quantum Dots in Ionic Liquid: Stability and Hole Scavenging in the Presence of a Sulfide Salt" **ChemFest-2015**, **12**th **Annual In-House Symposium**, School of Chemistry, University of Hyderabad, 20th-21st February, 2015.

Poster Presentations

- 1. "Can Ionic Liquids Overcome the Limitations of CdTe Quantum Dots in Quantum Dot Sensitized Solar Cells? An Ultrafast Transient Absorption Study" **Trombay Symposium on Radiation and Photochemistry (TSRP-2014)**, Bhabha Atomic Research Centre, Mumbai, 6th-9th January, 2014.
- 2. "Photoinduced Electron Transfer between CdTe Quantum Dots and Cresyl Violet: An Ultrafast Transient Absorption Study" **8**th **Asian Photochemistry Conference (APC-2014)**, Indian Institute of Science and Education Research Thiruvananthapuram jointly with CSIR-National Institute for Interdisciplinary Science and Technology, Thiruvananthapuram, Kerala, 10th-13th November, 2014.

Thesis Layout

The thesis is divided into seven chapters. *Chapter 1* starts with a brief introduction on different types of semiconductor nanocrystals (quantum dots, QDs) and discusses some of their properties and applications. This chapter also introduces another class of materials, ionic liquids (ILs), along with their significant properties and applications in various fields. Further, excitation energy transfer and photoinduced electron transfer processes, which are responsible for the fluorescence quenching of the excited fluorophores, are also discussed. Chapter 2 provides detailed information on materials, procedures for synthesis of various QDs and ligands, methods for purification of solvents and sample preparation for various experiments. It also provides detailed information on the instrumentation and their data analysis. *Chapter 3* discusses about the stability of CdTe QDs including hole transfer process between CdTe QDs and sulfide ion in ILs. Chapter 4 deals with the mechanism responsible for the quenching of CdTe QDs fluorescence by an organic fluorophore. Chapter 5 demonstrates the influence of capping agents on the carrier trapping dynamics of photo-excited CdTe QDs. Chapter 6 discusses the effect of QDs surface stoichiometry on the charge separation and recombination dynamics between CdSe QDs and methyl viologen. Chapter 7 summarizes the results of the present studies and highlights their future scope.

Introduction

This chapter introduces different types of three-dimensionally confined metal chalcogenide semiconductor nanoparticles like core, core-shell and alloy quantum dots. Quantum confinement, which arises due to three-dimensional confinement of these nanoparticles leading to their size-dependent optical tunability, is discussed in detail. Other properties such as solubility, surface passivation, and multiple exciton generation are also discussed along with some of their applications. This chapter also provides an overview of another class of materials, ionic liquids, including their significant properties and applications in various fields. Further, the excitation energy transfer and photoinduced electron transfer processes, which are responsible for the fluorescence quenching of the excited fluorophores, are also discussed. Finally, the motivation behind this thesis is presented.

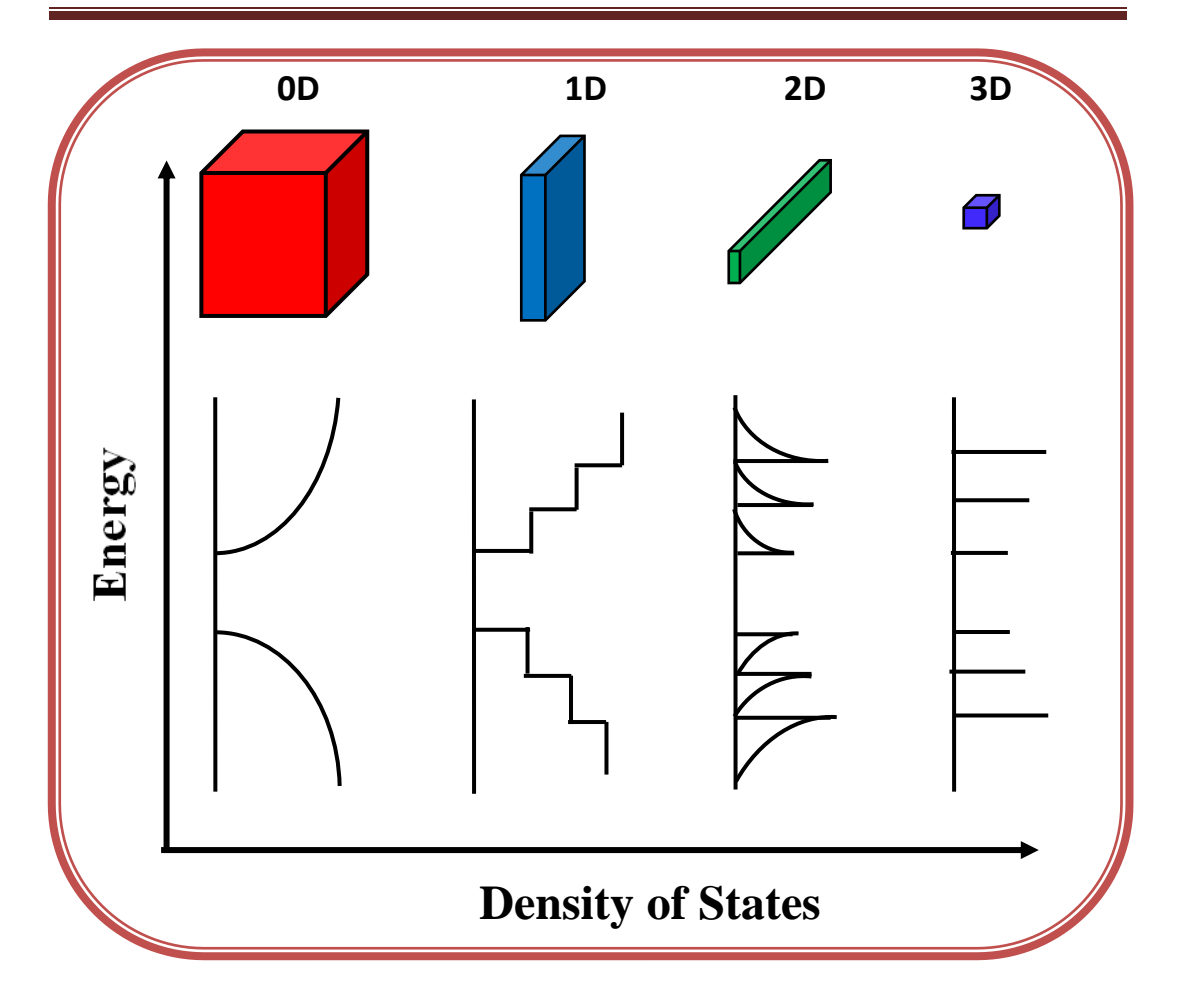
1.1. Quantum Dots

Quantum dots (QDs) are the semiconductor nanoparticles, which consist of hundreds to thousands of atoms. They were first discovered in the glass matrix by Alexei Ekimov¹ and in colloidal solution by Louis E. Brus², but the term "quantum dot" was given by Mark Reed.³ Unlike their bulk counterparts QDs exhibit size-dependent optical and electronic properties due to three dimensional quantum confinement of the exciton (electrostatically bound electron-hole pair) that are produced during photo-excitation of the QDs.³⁻⁷ As the size of the nanoparticles is comparable or smaller than the exciton Bohr radius (a_b, distance between electron-hole pair) of the bulk material and is given by

$$a_b = \frac{\varepsilon \hbar^2}{e^2} \left(\frac{1}{m_e^*} + \frac{1}{m_h^*} \right) \tag{1.1}$$

where, ε is the dielectric constant, h is the reduced Planck's constant, e is the electric charge, m_e* and m_h* are the effective masses of the electron and hole, respectively, the spatial motions of the excitons are confined leading to their quantum confinement. B-10 Due to the quantum confinement, the electronic energy states in the valence and conduction bands become quantized in case of QDs compared to the bulk semiconductor where they are quasi-continuous. B shows the effect of dimensionality confinement on the density of states of the semiconductors. The discreteness in the electronic energy levels of the QDs resembles that of an isolated atom or molecule, thus bridging the gap between the small molecules and bulk nanocrystals (Scheme 1.2). Hence the QDs show properties such as broad absorption (due to large density of states) and intense fluorescence (due to radiative recombination of photo-generated electrons and holes) similar to that of bulk semiconductors and molecular dyes. A show the electron is the electronic energy levels of the QDs show properties such as broad absorption (due to large density of states) and intense fluorescence (due to radiative recombination of photo-generated electrons and holes) similar to that of bulk semiconductors and molecular dyes.

The shift in the band gap (minimum energy required to excite the electron

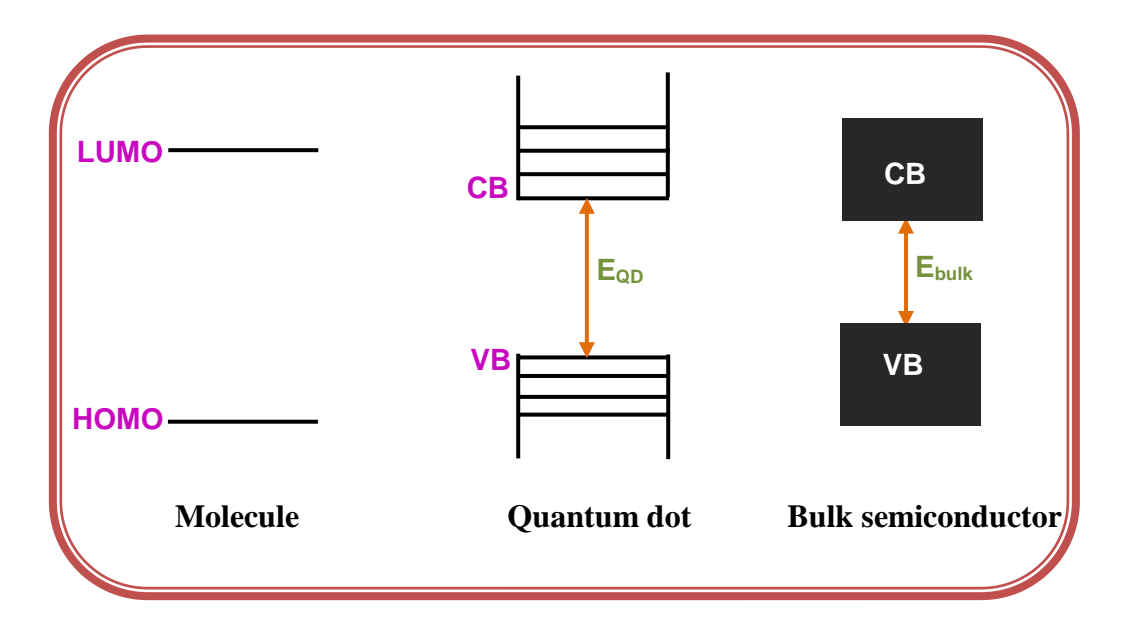


Scheme 1.1. The effect of dimensional confinement on the density of states in semiconductor nanocrystals.

from the valence band to the conduction band) of the QDs with respect to the bulk semiconductors can be calculated using 6,7

$$E_{QD} = E_{bulk} + \frac{\hbar^2 \pi^2}{2R^2 m_e^*} + \frac{\hbar^2 \pi^2}{2R^2 m_h^*} - \frac{1.8e^2}{4\pi \varepsilon_0 \varepsilon R} - 0.248 E_{Ry}^* \quad (1.2)$$

where, E_{bulk} represents the band gap of the bulk semiconductor and R is the radius of the QDs. The second and the third terms are the energies due to the confinement of electron and hole with m_e^* and m_h^* as effective mass of electron and hole, respectively. The Coulomb interaction energy between the electron and the hole is



Scheme 1.2. Comparison of electronic energy levels of the molecule, quantum dot and bulk semiconductor. E_{QD} and E_{bulk} are the band gap of the quantum dot and bulk semiconductor, respectively. CB and VB denote conduction band and valence band, respectively.

represented by the fourth term with ϵ as the dielectric constant, whereas, the spatial correlation between the electron and the hole is given by the final term, where E_{Ry}^* represents the exciton Rydberg energy. This Rydberg energy term is independent of QDs size and is usually negligible but can become effective in case of semiconductors with small dielectric constant. The equation 1.2 shows that the band gap of the QDs varies with their size (band gap increases as the size of the QDs decreases). In general, most of the cations of the QDs belong to IIIA, IVA and IIB groups, whereas, the anions to VA and VIA groups. These inorganic compositions increase the stability of the QDs against photobleaching. Due their broad absorption, intense and narrow fluorescence, size-dependent bandgap tunability and superior photostability, these materials are considered as promising alternatives to molecular fluorophores. These QDs can be synthesized by

Introduction

different techniques such as successive ionic layer adsorption and reaction (SILAR), chemical bath deposition (CBD), and colloidal synthesis.^{13, 23-25} Among these techniques, the colloidal method of synthesis results in QDs with a lesser heterogeneity in size.^{4, 26} In this colloidal method of synthesis, the QDs of different sizes can be prepared by varying either the reaction temperature or the time. For example, QDs of larger size can be synthesized by maintaining the reaction at high temperatures for a shorter time or at low temperatures for a longer time.

1.1.1. Passivation of surface states and solubility

As we are dealing with the nanoparticles of few nanometers in size, the surface area to volume ratio will be high. Hence the optical properties of the QDs are mainly governed by the surface atoms. Unlike the atoms inside the crystal, the atoms at the surface are not completely bonded leaving the non-bonding orbitals, also known as dangling orbitals, on the surface of QDs.^{4, 27} If these non-bonding/dangling orbitals lie within the bandgap of the semiconductors, they act as traps for the photo-generated carriers thus reducing the degree of overlap between the electron and hole and enhancing the non-radiative carrier recombination.⁴ In order to passivate these dangling orbitals, the QDs are coated with organic ligands such as trioctylphosphine (TOP), hexadecylamine (HDA), oleic acid (OA), trioctylphosphine oxide (TOPO), 3-mercaptopropanoic acid (3-MPA) (Chart 1.1).^{9, 28, 29} These ligands contain electron rich atoms such as N, S, O, P which can donate their lone pair of electrons to the dangling orbitals of the QDs to form metal-ligand coordinate covalent bond.⁴

In addition to the passivation of the dangling orbitals, these ligands also play a role in determining the solubility of the QDs. The capping agents such as TOP, HDA, OA and TOPO (Chart 1.1), which contain long alkyl chains, are used for dissolving the QDs in non-polar solvents such as chloroform and hexane, whereas the hydrophilic polymers like phosphine oxide and surfactants like HDA are used

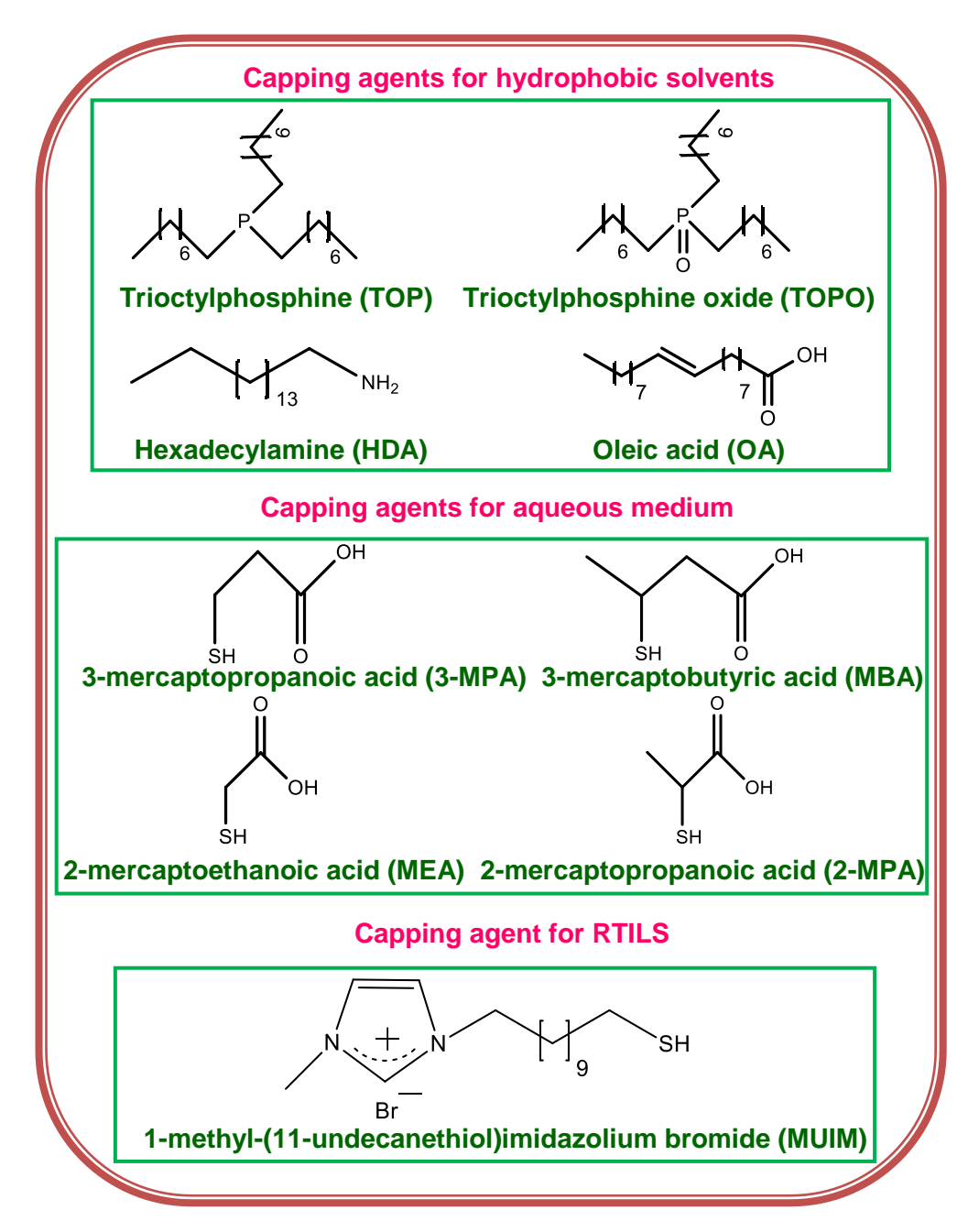


Chart 1.1. Structures of the capping agents used for the passivation of QDs surface and determining their solubility in different media.

for dissolving them in polar solvents.^{9, 29-33} The capping agents containing thiol and acid groups (mercapto acids, Chart 1.1) are commonly used for making the QDs

Introduction

soluble in aqueous medium.^{29, 33} Other than the conventional solvents, the QDs can also be dissolved in room temperature ionic liquids (RTILs). The first successful attempt to dissolve the QDs in RTILs was made by Nakashima and Kawai, where the 2-(dimethylamino)ethanethiol-capped CdTe QDs soluble in aqueous medium was extracted into the water immiscible RTILs (1-butyl-3-methylimidazolium bis(trifluoromethanesulfonyl)imide). However, this method of extraction was limited only to the hydrophobic RTILs.^{34, 35} Recently, Samanta and coworkers synthesized a task specific capping agent (1-methyl-(11-undecanethiol) imidazolium bromide (MUIM, Chart 1.1) and which can be used for dissolving the CdTe QDs in both hydrophobic and hydrophilic RTILs.³⁶

1.1.2 Core/Shell quantum dots

The surface atoms of the QDs cannot always be efficiently passivated by the organic ligands due to their site specific (cationic/anionic) binding.³⁷⁻⁴⁰ In addition, these QDs are susceptible to photo-oxidation, thus increasing the surface defects and decreasing their emission quantum yield (QY).⁴ The other possibility to passivate the surface atoms of the QDs is by growing an inorganic semiconductor shell around the core, resulting in core-shell QDs.^{4,41-45} This shell growth results in efficient passivation of the QDs surface atoms irrespective of the nature of the defects and enhancement of radiative carrier recombination and improved stability towards photo-oxidation.⁴²⁻⁴⁴ Based on the band gap of the shell these core/shell QDs are classified into three different types.

1.1.2.1 Type-I Core/Shell QDs

QDs of larger band gap compared to the core QDs are used as shell materials, where the conduction and valence bands of the shell are higher and lower in energy than that of the core, respectively (Scheme 1.3).^{48,49} This type of shell coating enables the confinement of photo-generated electrons and holes to the core only. The emission QY and stability of the core/shell QDs is much improved compared

Chapter 1

to the core QDs, but a red shift in their absorption and emission spectra is observed.^{41, 42, 45} This bathochromic shift observed in case of Type-I core/shell QDs is due to partial leakage of the exciton into the shell material. ^{41, 42, 45} CdSe/ZnS QDs is a typical example of Type-I core/shell QDs. ⁴⁵

1.1.2.2 Type-II Core/Shell QDs

QDs with either their valence or conduction band lying within the band gap of the core QDs are used as a shell material (Scheme 1.3). ^{4, 46} This structured band gap alignment of the core/shell QDs results in spatial separation of the photogenerated carriers that confines either the electron or hole to the core and the other one to the shell. Because of the spatial separation of the photo-generated carriers, these core/shell QDs exhibit novel properties that are different from the Type-I core/shell QDs. For example the excited state lifetimes of these materials are increased due to the decrease in spatial overlap between the electron and hole.^{4, 46} These systems not only enhance the quantum yield of the core but also allow to access wavelengths that are not possible with only core QDs.^{4, 46} CdTe/CdSe and CdSe/ZnTe are typical examples of Type-II systems.⁴⁶

1.1.2.3 Reverse Type-I Core/Shell QDs

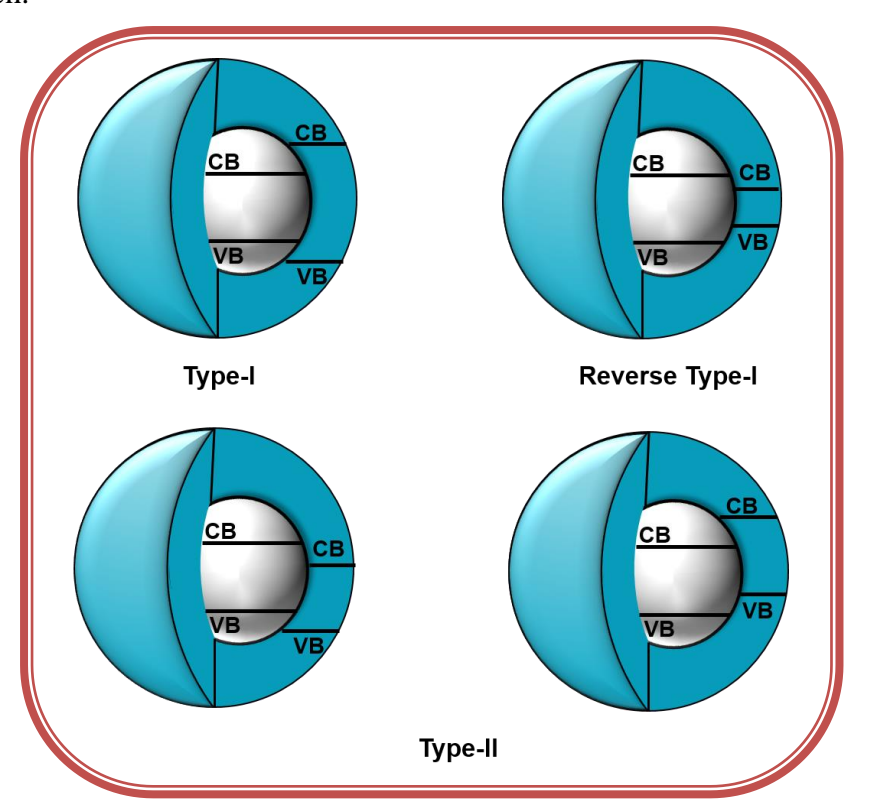
The band gap of the shell material for this type of Core/Shell QDs is smaller than the band gap of the core QDs (Scheme 1.3). A significant red shift in the emission maximum of the core/shell QDs of this type can be seen compared to core QDs.⁴¹ CdS/HgS, CdS/CdSe and ZnSe/CdSe are the well-studied reverse type-I systems.⁴⁷⁻⁴⁹

1.1.2.4 Synthesis of Core/Shell QDs

These core/shell QDs are synthesized by two-step procedure. ⁴¹Initially, core QDs are grown at higher temperatures and later the shell is grown on to the core at lower temperatures to prevent the self-nucleation of the shell materials and further

Introduction

growth of the core QDs. This shell is grown through SILAR (successive ion layer adsorption and reaction) method, where the cationic and anionic precursors required to form the shell are alternatively injected into the reaction mixture containing core QDs.⁴¹ The choice of these core and shell QDs depends on their lattice mismatch. For example, the core/shell QDs with less lattice mismatch exhibit higher emission QY compared to the core/shell QDs with more lattice mismatch.⁴

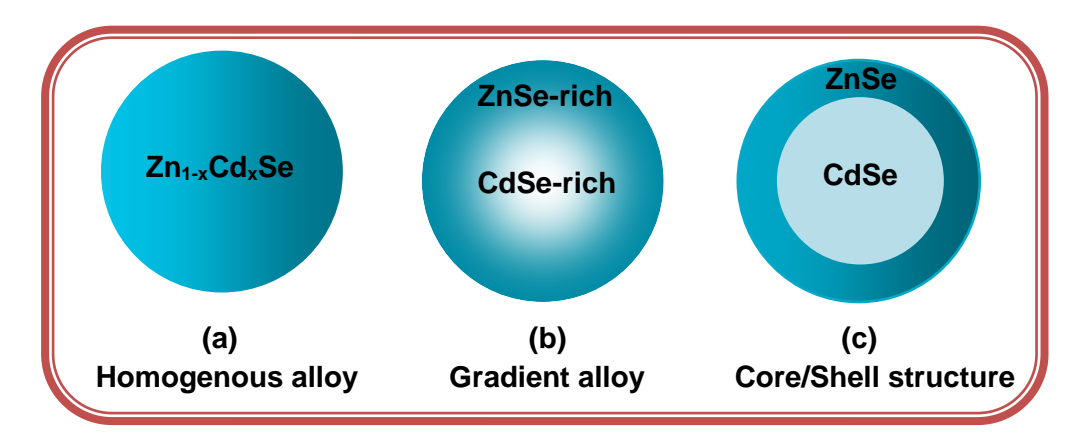


Scheme 1.3. The band gap alignment in different types of core/shell QDs. CB and VB represents the conduction and valence bands, respectively.

1.1.3 Alloy QDs

As the quantum efficiency of the core/shell QDs depends on their lattice mismatch, finding out the core and shell QD materials with less lattice mismatch is difficult.⁵⁰ Hence alloy semiconductor QDs that do not rely on their lattice

mismatch has become an alternative to obtain highly luminescent nanocrystals.⁵⁰ Based on the nanocrystal composition, these alloy QDs are classified into two types; 1) homogeneous alloy QDs with uniform nanocrystal composition, and 2) gradient alloy QDs, where the nanocrystal composition gradually varies from the center to the surface (e.g., Cd-rich at the center and Zn-rich at the surface).⁵⁰⁻⁵³ Scheme 1.4 shows the homogeneous alloy, gradient alloy and core/shell structure nanocrystals. Further, on the basis of their number of component elements, they are classified as ternary and quaternary alloy QDs.⁵¹ Ternary alloys are formed with the combination of two binary systems containing either a common cation or an anion. For example, alloying two binary systems C'A and C"A results in (C'A)_x(C"A)_{1-x} or simply C'_xC"_{1-x}A, where C' and C" represent two different cations and A is the common anion.⁵¹ An example of this type of alloy is Zn_{1-x}Cd_xSe.⁵² On the other hand, alloying of the two binary systems with common cation and two different anions results in CA'_xA"_{1-x} (e.g. CdTe_xSe_{1-x}).⁵³



Scheme 1.4. Schematic representations of the ZnCdSe QDs with (a) homogenous alloy (b) gradient alloy and (c) core/shell structure.

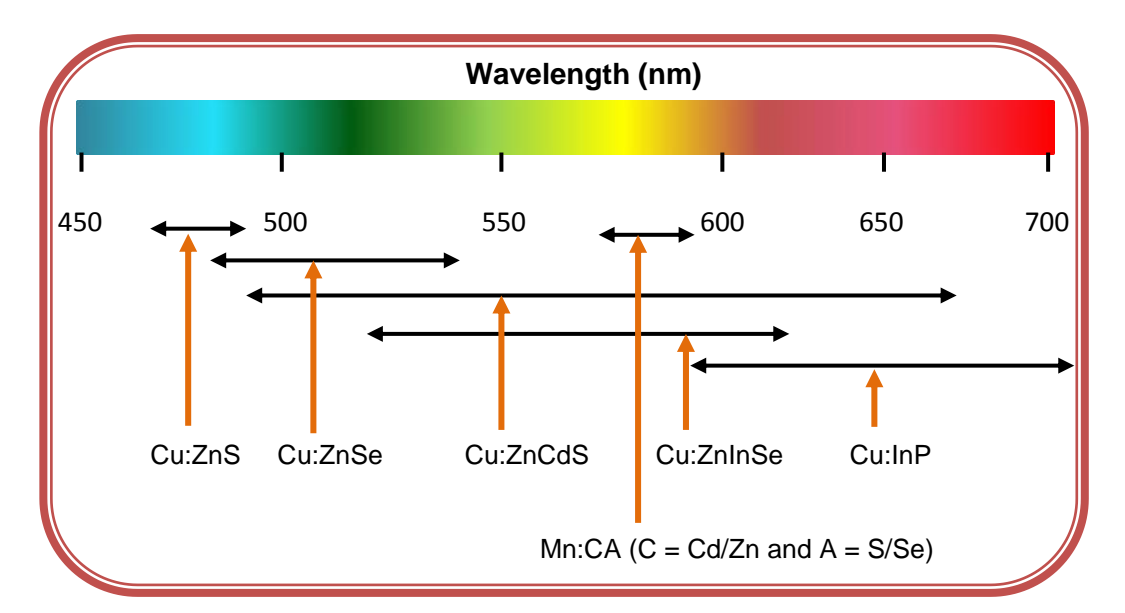
Quaternary alloys of the composition $C'_xC''_{1-x}A'_xA''_{1-x}$ are produced by the alloying of two binary systems with no element in common. $Zn_xCd_{1-x}S_ySe_{1-y}$ is an example of this type of alloy.⁵⁰ Quaternary alloys are also produced by the

Introduction

combination of two ternary systems (such as $CuInSe_2$ and $CuGaSe_2$) or from a ternary ($CuInS_2$) and a binary system (ZnS), where $CuIn_{1-x}Ga_xSe_2$ is an example of the former and ($CuInS_2$)_x(ZnS)_{1-x} is an example of the latter.^{54, 55} In addition to the size-dependent band gap tunability, these QDs also exhibit band gap tunability when their elemental composition is varied.⁵¹

1.1.4. Doped QDs

The other approach to modify the electronic and optical properties of the semiconductor QDs is by introducing impurity atoms (or dopants) into the lattice of the host semiconductors, typically, the optically active transition metal ions (e.g., Mn⁺²).⁵⁶⁻⁶⁰ These dopants introduce electronic states within the band gap of



Scheme 1.5. Schematic representation of the range of tunability in the emission of the QDs by incorporating different dopants. Figure is adopted from ref 60.

the semiconductor nanocrystals, which influence their photo-generated carrier separation and recombination dynamics resulting in red-shifted emission.^{56, 57} The

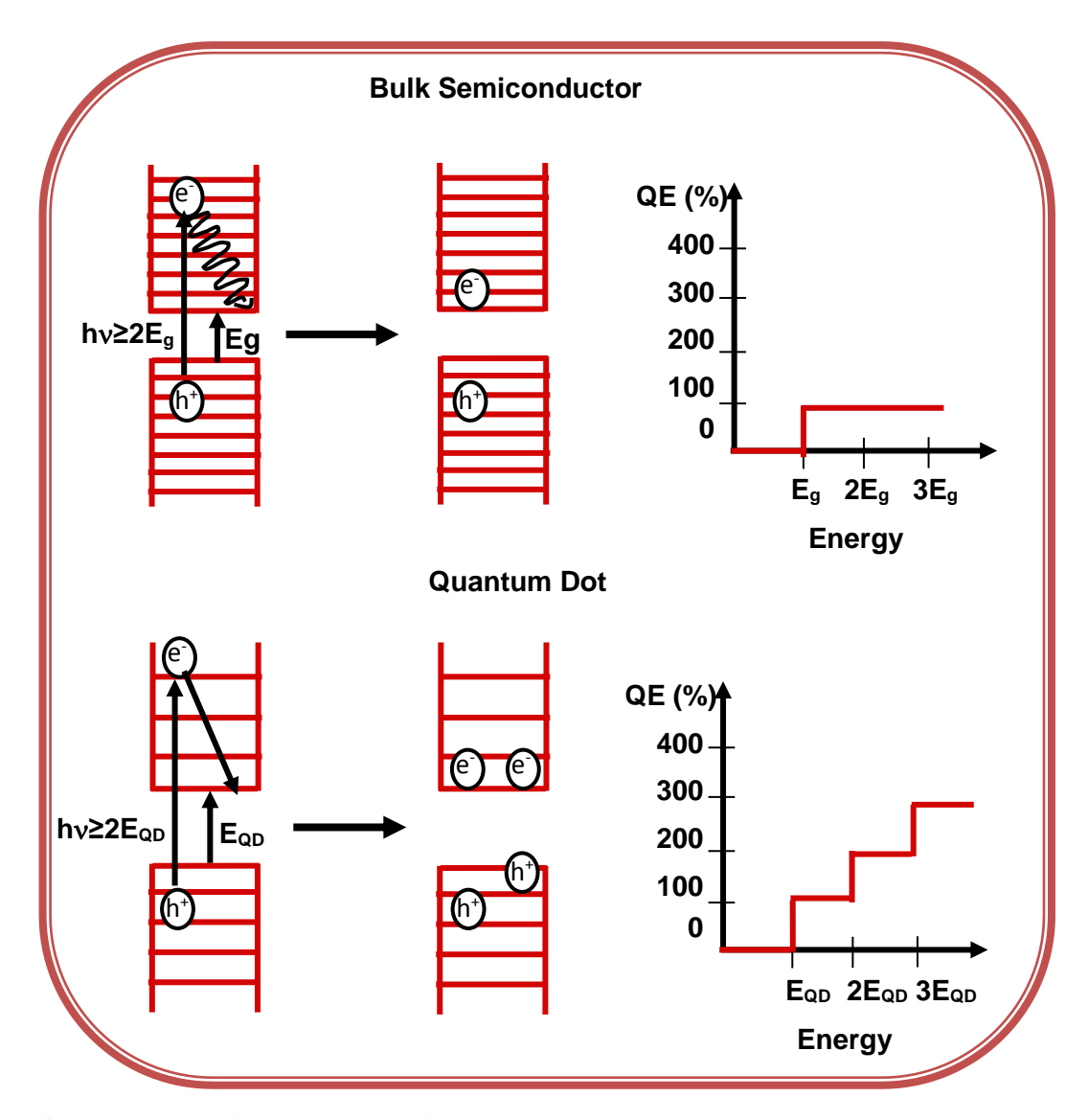
Chapter 1

emission tunability range of the QDs using transition metal ions like Mn^{+2} and Cu^{+2} as dopants are shown in Scheme 1.5.⁵⁶

1.1.5. Multiple exciton generation

In case of bulk semiconductors, when a photon of at least double the energy compare to their band gap is absorbed, the excess energy is dissipated as heat through electron-phonon interactions as the excited carriers relax to their lowest state. 61-65 However, in case of QDs, due to discrete nature of their energy levels, this phonon-assisted carrier thermalization is suppressed, leading the excess energy to generate another exciton. 61-65 Hence multiple exciton generation (MEG) or carrier multiplication is a phenomenon where a photon of higher energy (hv ≥ 2E_{QD}, E_{QD} is the band gap of QD) generates two or more excitons (Scheme 1.6). Due to these multiple excitons, the internal quantum efficiency (QE, conversion of photons to excitons) of the QDs exceeds 100 % for photon energies greater than their band gap, whereas in case of bulk semiconductor this QE is 100 %.63-65 Further, in case of QDs, a plot of QE vs energy exhibits a staircase like signature indicating that the photon with energy hv >2 E_{QD} potentially generates two excitons and for every E_{OD} increase in the photon energy the number of photogenerated excitons increases by one (Scheme 1.6). 63, 64 A QE of 700 % is reported by Klimov and coworkers for PbS and PbSe QDs by producing seven excitons from a photon with an energy of 7.8 E_{OD}.63 MEG is one of the important characteristics of the QDs through which the conversion efficiency of the solar energy into electrical energy can be enhanced beyond the Schokley and Queisser limit. 65-67 However, this MEG is limited by the Auger process in the QDs.

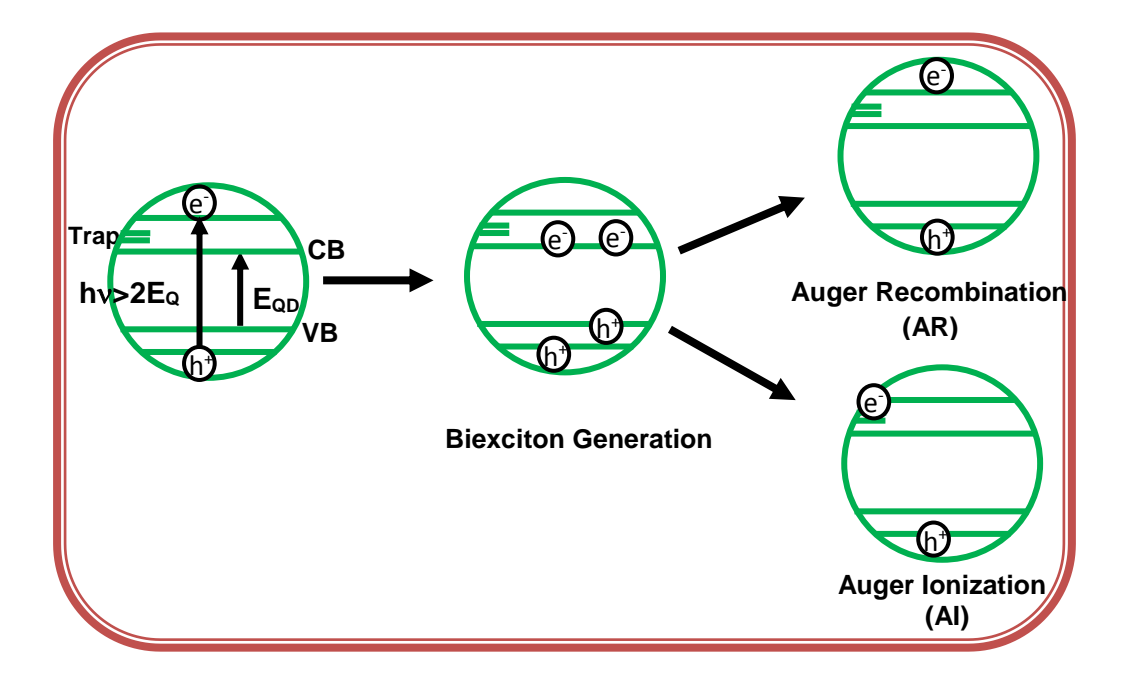
Auger process is a phenomenon where one of the excitons recombine by transferring the energy to other photo-generated electron (or hole) that is excited to the higher energy state within the QDs (Auger recombination, AR) or ejected from the core of the QDs to the higher energy surface states (Auger ionization, AI)



Scheme 1.6. Comparison of the photon to exciton conversion in bulk semiconductors and QDs. E_g and E_{QD} resemble the band gap of bulk semiconductor and QDs, respectively.

(Scheme 1.7).^{68, 69} Because of the relaxation in momentum conservation and enhanced Coulombic interactions in QDs, this AR/AI becomes efficient and occurs usually on tens-to-hundreds of picosecond timescales.^{68, 70} Hence, the extra electrons (or holes) generated through MEG must be separated by fast electron

(hole) injection from QDs to electron (hole) acceptors before they recombine through $AR/AI.^{70}$



Scheme 1.7. Schematic representation of the biexciton generation and Auger recombination (AR) and Auger ionization (AI) in QDs. VB and CB represents the valence and conduction bands, respectively.

1.1.6. Applications

Due to the high molar extinction coefficient, broad absorption spectra, tunable emission, photostability and long luminescence lifetime these materials are considered as alternatives to organic dye molecules in a wide range of applications such as biological reporters, light emitting diodes, fuel cells and photo-detector devices. These materials are also considered as alternatives to the silicon-based solar cells due to their cost effective synthesis and ability to generate multiple excitons. 68, 69, 76-80

Introduction

1.2. Ionic Liquids

Ionic liquids (ILs) are low-melting salts that constitute entirely of cations and anions. Unlike, the high melting salts like NaCl where the electrostatic interactions between the ions are strong, these materials possess weak Coulombic interactions between the ions due to which they exist as liquid at or below 100 °C.⁸¹ Room temperature ionic liquids (RTILs) are the sub class of ILs that exist as liquids at ambient temperature (20-30 °C) and pressure (1 bar).⁸² Because of high thermal stability, negligible vapor pressure and the ability to dissolve most of the organic and inorganic compounds, ILs are considered as potential replacements to volatile organic solvents used in chemical reaction, manufacturing and separation processes, and transition metal catalysis.⁸¹⁻⁸⁵

The first RTIL, ethyl ammonium nitrate, was discovered in 1914 by Walden. 86 Though the ILs discovered in the early 20th century, these materials were significantly explored in 1980s by Wilkes and coworkers using salts based on chloroaluminate anions (AlCl₄ or Al₂Cl₇).^{87, 88} Usually, ammonium, phosphonium, non-symmetrical imidazolium, pyridinium, pyrrolidinium, and piperidinium cations are used in RTILs, whereasAlCl₄, AlCl₇, BF₄, PF₆, SbF₆ (CF₃SO₂)₂N⁻ and CF₃SO₃ are used as anions (Chart 1.2). In majority of the cases, the reactivity, hydrophobicity and hydrophilicity of the ILs are decided by their anions and hence, based on the anions, these ILs are divided into four categories.⁸⁹ The ILs with AlCl₄ or Al₂Cl₇ as anions are considered as first category of ILs. However, highly hygroscopic nature limits their storage and handling to inert atmosphere. The hygroscopic nature of these ILs is reduced by replacing the anions with nearly air stable anions such as BF₄, PF₆ and SbF₆, which are classified as second category of ILs.90 But, the limitations of the second category of ILs are the production of detectable amounts of HF acid on hydrolysis and their highly viscous nature.⁹¹ The third of ILs containing anions category such as

(CF₃SO₂)₂N⁻(Tf₂N⁻) and CF₃SO₃ are more stable towards the production of HF and are characterized by low melting points, low viscosities and high conductivities. However, these ILs are expensive and have a stronger binding ability towards Lewis acidic metal ions and also their disposal is difficult due to the presence of fluorine atoms. ⁹¹⁻⁹³ This led to the synthesis of fourth category of ILs that are low coordinating and less expensive containing non-fluorinated counter anions such as carboranes ([CB₁₁H₁₂]⁻, [CB₁₁H₆Cl₆]⁻ and orthoborates (Chart 1.2). ^{94, 95} Recently, RTILs based on natural amino acids are synthesized and used extensively for biological applications. ^{96, 97} In addition, task specific RTILs with specific functional groups such as ester, ether and chiral side chain being incorporated into the alkyl group of the cation and anion have been developed for their use in specific applications. ^{36, 98, 99}

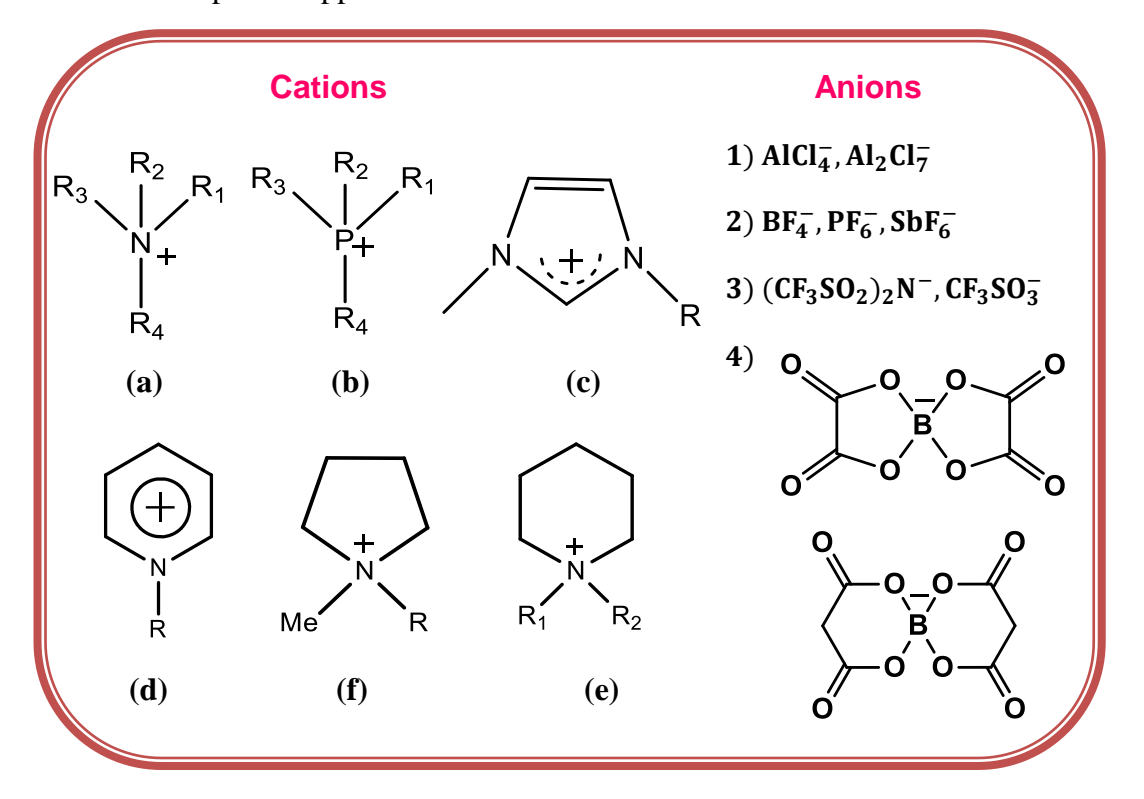


Chart 1.2 Structures of different cations and anions which are the constituents of ILs

1.2.1. Properties

ILs exhibit novel properties such as negligible vapor pressure, high thermal and chemical stability, wide liquidous range and electrochemical window, medium to high polarity, potential to dissolve most of the organic and inorganic substances, non-flammability and reusability. 81-85, 100-102 As the properties of ILs depend on the constituent ions, ILs with desired properties can be synthesized by varying their cations and anions and hence, these materials are also called as "designer solvents". 103

1.2.1.1. Viscosity and density

Compared to the conventional solvents, ILs are highly viscous. The lowest viscous IL is about 30 times higher in viscosity than conventional solvents like acetonitrile, water and alcohols (Table 1.1.) In general, the viscosity of the IL decreases with increase in temperature and follows a non-Arrhenius behavior. In most of the cases the variation in the viscosity against temperature can be represented by Vogel-Tammann-Fulcher (VFT) equation (1.3). ¹⁰⁴

$$\ln(\eta) = \ln(\eta_0) + \frac{DT_C}{T - T_C} \tag{1.3}$$

where, η and η_0 are the shear and reference viscosities, respectively, T_c represents the critical temperature at which η is infinite and D is the fragility parameter. The variation in the viscosity of the ILs on changing their cation-anion combination is primarily attributed to the variation in their van der Waals forces. This statement was supported by ILs with 1-alkyl-3-methylimidazolium as a cation and Tf_2N^- or BF_4^- as anions, where the viscosity increases with increase in the number of carbon atoms in the linear alkyl group of the cation. However, branching of the alkyl chain of 1-alkyl-3-methylimdiazolium cation decreases the viscosity of the IL. The other factors that affect the viscosity of ILs are the symmetry and hydrogen bonding between the counter anions. The higher viscosity observed in case of alcohol

Chapter 1

functionalized ILs compared to their alkyl counterparts is due to their hydrogen bonding ability. $^{105,\ 106}$ ILs with PF $_6^-$ as the counter anion exhibit higher viscosity compared to the Tf $_2$ N $^-$ due to the high symmetry and increase in hydrogen bonding. $^{107,\ 108}$ Hence, the viscosity increases in the order Tf $_2$ N $^-$ < BF_4^- < PF_6^- < CI $^-$. $^{107,\ 108}$ The viscosities are also affected by the presence of impurities such as halides and water. $^{109,\ 110}$ Interestingly, the studies on the microviscosities of the ILs by employing a fluorescent probe suggest that they are different from their bulk viscosity. 111

ILs are denser than most of the conventional solvents. The density of the ILs depends on the molar mass and volume of the counter anions. For example, ILs with 1-butyl-3-methylimdazolium ([bmim]) as cation and orthoborates as anion, the density decreases with increase in the volume of the anion. ^{95, 107, 108, 112, 113}

Table 1.1. Properties of some imidazolium ILs

IL	Tmp/oC	T _d / °C	η / cP	ρ / (g/cc)	σ/ (mS/cm)	E _T (30)
[emim][Cl]	86 ¹¹⁴		S	S		
[bmim][Cl]	65 ¹¹⁴		S	S		
[emim][BF ₄]	6114	447 ¹¹⁵	66.5 ⁸³	1.25^{83}	13 ¹¹⁶	49.1117
[prmim][BF ₄]	-17 ¹¹⁵	435 ¹¹⁵	103 ¹¹⁵	1.24 ¹¹⁵	5.9 ¹¹⁵	
[bmim][BF ₄]	-81 ¹¹⁸	435 ¹¹⁵	154 ⁸³	1.2^{83}	3.5^{115}	48.9 ¹¹⁷
[emim][PF ₆]	60^{119}		S	S	5.2116	S
[bmim][PF ₆]	-61 ¹¹⁸		371 ⁸³	1.37^{83}	1.5^{116}	52.3 ¹²⁰
[emim][Tf ₂ N]	-3 ¹²¹		34 ¹²¹	1.52^{121}	8.8 ¹²¹	47.7 ¹²²
[bmim][Tf ₂ N]	-4 ¹²¹	> 400 ¹¹⁵	52123	1.43^{123}	3.9^{123}	47.2^{122}

 T_{mp} -melting point; T_d -decomposition temperature; S-solid; η -viscosity; ρ -density; σ -specific conductivity and $E_T(30)$ -microscopic solvent polarity parameter.

1.2.1.2. Melting point

The melting points of many ILs are uncertain because they undergo supercooling and the value of the temperature corresponding to their phase transition varies depending on whether the IL is heated or cooled.⁸⁹ It was found that the melting point of the ILs decreases with increase in asymmetry and size of the cation and further increases with increase in the branching of the alkyl chain. 107, 108 The melting points of some common ILs are shown in Table 1.1. Though the relation between the melting points and the cations of ILs (especially imidazolium cations) were found, the influence of the anions remained uncertain.⁸⁹ Experiments such as NMR, IR and crystallography showed the influence of the anions on the melting point of the ILs based on the hydrogen bonding interactions between their cations and anions, 89, 124-129 but the results on such type of interactions are ambiguous. For example, higher melting point was observed in case of 1-butyl-2,3- dimethylimidazolium chloride ([bm2im][Cl]) compared to 1butyl-3- methylimidazolium chloride ([bmim][Cl]), though the latter has more number of C-H---Cl interactions per unit. 129 However, the low-melting point exhibited by the ILs with Tf₂N⁻ as the counter anion is attributed to the low charge density and lack of hydrogen bonding interaction.⁸⁹ Further, in case of ILs with spherical counter anions like BF₄ and PF₆, the increase in the melting point is also attributed to the strong hydrogen bonding interactions.⁸⁹ Hence, to some extent the effect of anions on the melting points of ILs can be explained by the delocalization of charge and hydrogen bonding interactions between the ions.

1.2.1.3. Thermal stability and volatility

Most of the ILs exhibit higher thermal stability with decomposition temperature greater than 400 °C (Table 1.1). The onset of the ILs thermal decomposition decreases with increase in the hydrophilicty of the anion.^{89, 101} The thermal stability of the ILs with different counter anions decreases in the

Chapter 1

order $PF_6^- > Tf_2N^- \sim BF_4^- > Cl^{-.89, 101}$ However, the thermal stability of the ILs for different cations is similar.⁸⁹

As mentioned earlier, one of the properties of ILs is their negligible vapor pressure and hence they cannot be distilled. However, ILs with significant vapor pressure that can be distilled at low pressure without any thermal decomposition was reported. ¹³⁰⁻¹³² Earle and coworkers were the first to distill aprotic ILs at 200-300 °C and low pressure but they could not provide the direct evidence of the ions vaporization in their distillation process. ¹³¹ Recently, Leone and coworkers detected the intact ion pair of the vaporized IL, 1-butyl-3-methylimidazolium tricyanomethanide, by tunable vacuum ultraviolet photoionization time-of-flight mass spectrometry technique. ¹³³

1.2.1.4. Conductivity and ionic diffusion

Conductivity of ILs is important for their use as electrolyte in electrochemical cells such as double layer capacitors, lithium ion batteries and fuel cells. As ILs are entirely composed of ions, larger values of conductivity are expected, but ILs with inorganic electrolytes exhibited values similar to those of organic solvents. 115, 116, 121, 123 The conductivities of some of the ILs are shown in Table 1.1. The dependence of the IL conductivity on the planarity of their cation is observed in few ILs, where the conductivity value decreases with decrease in the planarity of the cation (1-alkyl-3-methylimidazolium > N,N-dialkylpyrrolidinium > tetraalkylammonium. 116

As the conductivity of the ILs is determined by the diffusion of the constituent ions, understanding the diffusion of ions in ionic liquids is crucial for their use as electrolytes in electrochemical devices. In general, the diffusion of ions in solvents is related to their viscosity by Stokes-Einstein equation given below

$$D = \frac{\kappa T}{6\pi\eta r} \tag{1.4}$$

where, κ is the Boltzmann constant, T is the absolute temperature, η is the viscosity and r is the Stokes or hydrodynamic radius.

Similar to conventional solvents, ionic diffusion of most of the ILs obeys Stokes-Einstein relation. For instance, the ionic diffusion of [emim][Tf₂N] ($\eta = 37$ cP) is faster than in [emim][BF₄] ($\eta = 66$ cp).^{89, 111}

1.2.1.5 Polarity

The bulk polarity of any liquid can be assessed from their static dielectric constant (ϵ). The measured ϵ values of some of the ILs (= 9-13 at 25 °C) suggest that their polarity is similar to that of pyridine (ϵ = 12.3 at 25 °C), but is much less than that of acetonitrile (ϵ = 35.9 at 25 °C). ^{134, 135} However, the low ϵ values of ILs cannot explain most of their experimental observations, indicating that the ϵ is not the best parameter to define the polarity of ILs. ¹¹¹ It is generally considered that the microscopic solvent polarity parameter like E_T (30) to be more appropriate as it is a measure of all microscopic interactions (hydrogen bonding, Coulombic, electron pair donor and acceptor forces etc.) between the solute and solvent molecules. ⁸⁹ Hence, the polarity of the ILs is commonly expressed in terms of E_T (30) values, which are determined using the solvatochromic probes like coumarin 153, nile red (chart 1.3). ^{117, 120, 136, 137} The polarity of the ILs estimated from these E_T (30) values states that they are in between acetonitrile and methanol. ^{120, 138}

1.2.1.6 Structural characterization and heterogeneity

In order to understand the effect of ILs on the chemical reactions and other processes, knowledge on their structural organization is essential. Various theoretical and experimental studies were carried out to understand the structure of the ILs in both the solid and liquid phases. Most of the ILs crystallize as polymorphs but ILs which are glass formers are difficult to crystallize. However, efforts have been made to identify the crystal structures of ILs by in situ

Chart 1.3. Structures of some solvatochromic probes used for estimation of the polarity of ILs.

crystallization at low temperatures. ¹⁴⁶ ILs containing counter anions such as BF_4^- and PF_6^- which are symmetric, rigid and small in size could be easily crystallized compared to ones containing flexible anions like Tf_2N^- and $CF_3SO_3^-$. ^{127, 144, 147-149} The hydrogen bonding interactions between the cations and anions are detected from the crystal structures of imidazolium based ILs, but for the ILs existing as liquid salts the presence of such type of interactions is ambiguous. ¹²⁷⁻¹²⁹ For example, the presence and absence of hydrogen bonding interactions are detected in BF_4^- and Tf_2N^- salts in their liquid state, respectively, but in case of PF_6^- salts they are uncertain. ^{121, 125, 150, 151} Further, molecular dynamics simulations have also been performed to understand the liquid structure of ILs. These studies have shown that the liquid structures of ILs are similar to those of membranes and worm-like micelles. ¹⁵²⁻¹⁵⁵

The heterogeneity in ILs containing local structure is characterized by various studies such as small- and wide-angle X-ray scattering (SWAXS), neutron scattering, fluorescent spectroscopic studies and molecular simulation studies. 104, 117, 152, 156-158 However, the heterogeneity of ILs is not well understood. For instance, the molecular dynamic simulation and SWAXS studies support the nanoscale organization of the local structure of ILs, 152, 156 but the neutron scattering and computational studies do not support it. 157, 158

1.2.1.7 Other properties

The other important properties of ILs are their refractive index and miscibility with aqueous and organic media. The refractive indices of ILs, especially [bmim][X] salts, are comparable to organic solvents. Based on the miscibility of the ILs with aqueous media, they are categorized as hydrophobic and hydrophilic. This hydrophilic and hydrophobic nature of ILs is majorly determined by their anions. For example, salts containing X^- , BF_4^- and RSO_4^- as anions are hydrophobic in nature whereas PF_6^- and Tf_2N^- as anions are hydrophobic. The solubility of PF_6^- and Tf_2N^- in water can be increased by incorporating the -OH functional group in the alkyl chain of the cation. On the other hand, an increase in the number of carbon atoms in the alkyl chain length increases the hydrophobicity of the ILs and decreases their miscibility in aqueous medium. $^{107, 108, 112}$

As most of the physical properties like viscosity, ^{109, 110, 159} polarity, ^{138,160, 161} solvation ^{138,161, 162} and electrochemical behavior ^{163, 164} of ILs vary with addition of conventional solvents, the applications of these materials can be widened by adding the conventional solvents. For instance, the mixture of ILs with the conventional solvents results in less viscous solvent mixture that influences the ionic association or dissociation phenomenon. ^{163, 164}

1.2.2 Applications

ILs have become promising alternatives to volatile organic solvents in catalysis, chemical reactions, mass spectrometry and separation processes due to the high thermal stability, low volatility and ability to dissolve large number of organic and inorganic compounds. S3-85 ILs serve as good electrolytes in lithium-ion batteries, fuel cells, double-layer capacitors and actuators due to the high proton conductivity, low reactivity and wide electrochemical window. Only, 101, 165, 166 Biocompatible ILs are used as solvents for bio-catalysis, enzyme-based reactions and protein folding and unfolding studies. A6, 96, 167 ILs are also used as solvents for the synthesis of inorganic semiconductor nanoparticles, metal oxide nanowires and nanorods. Transition metal nanoparticles synthesized in ILs exhibit high stability and good catalytic activity. Recently, the hole transfer between the CdTe QDs and sulfide redox couple (where the former acts as a light harvester and latter as electrolyte in solar cells, respectively) is observed when the aqueous medium is replaced with ILs. 171

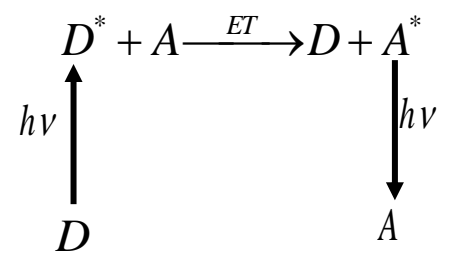
1.3. Fluorescence quenching

Fluorescence is a process by which the electronically excited molecules relax to their ground state by emitting a photon. A decrease in the fluorescence intensity of the molecules by any process is termed as fluorescence quenching.¹⁷² Two such common processes, which result in the reduction of fluorescence intensity of the molecules are energy transfer and electron transfer.

1.3.1 Energy transfer

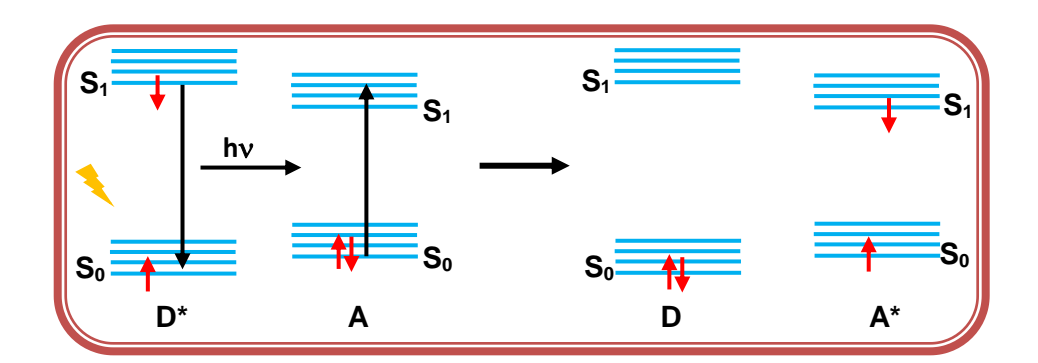
Energy transfer (ET) is a phenomenon where the excited donor (D) molecule transfers its energy in a radiative or non-radiative fashion to the acceptor molecule (A) which is in its ground state, resulting in the emission of the latter.¹⁷³ The efficiency of this process depends on the extent of overlap between the emission

spectrum of the donor and absorption spectrum of the acceptor.¹⁷³ Based on the mode of the energy transfer, they are classified as radiative and non-radiative energy transfer.



1.3.1.1 Radiative energy transfer

The donor molecule (D) transfers its excitation energy to the acceptor molecule (A) in the form of photon (Scheme 1). This type of energy transfer does not require any interaction between the quenching partners but requires the spectral overlap between them.¹⁷³



Scheme 1.8. Radiative energy transfer between the donor and acceptor. S_0 and S_1 represent the ground and first excited singlet states of the molecules, respectively.

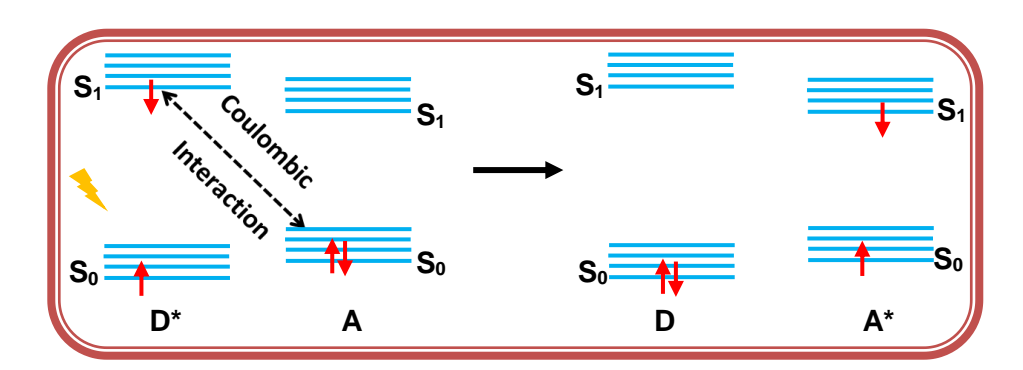
1.3.1.2 Non-radiative energy transfer

The excitation energy of the donor molecule is transferred to the acceptor molecule non-radiatively (without emission of photon). The interaction between

the quenching partners along with their spectral overlap is required for the energy transfer. Based on the type of interactions (long- or short-range) between the quenching partners, this energy transfer is classified as Förster Resonance Energy Transfer (FRET) and Dexter Energy Transfer (DET). 172-174

1.3.1.2.1 Förster resonance energy transfer (FRET)

FRET is a non-radiative energy transfer that results due to the long range dipole-dipole (Coulombic) interactions between the donor and acceptor molecule. ¹⁷³ In addition to the spectral overlap between the donor emission and acceptor absorption, FRET depends on the donor-acceptor distance and the relative orientation of their transition dipoles. Typically, FRET can be observed between the donor and acceptor which are separated by 10-100 Å. ^{172, 174}



Scheme 1.9. Schematic representation of the excitation energy transfer from donor to acceptor through FRET mechanism.

According to the Förster theory, the rate constant of FRET (k_{FRET}) from donor to acceptor is given by

$$k_{FRET}(r) = \frac{1}{\tau_D} \left[\frac{R_0}{r} \right]^6 \tag{1.5}$$

where, r is the distance between the donor and acceptor, τ_D represents the lifetime of the donor molecule and R_0 is the Förster distance, which is defined as the

distance at which the efficiency of energy transfer is 50 % and is given by

$$E = \frac{R_0^6}{R_0^6 + r^6} \tag{1.6}$$

Förster distance, R₀ (Angstroms) can be calculated by

$$R_0 = 0.211 \left[\kappa^2 n^{-4} Q_D J(\lambda) \right]^{\frac{1}{6}}$$
 (1.7)

where κ^2 represents the relative orientation of the transition dipoles of donor and acceptor in space, Q_D is the fluorescence QY of the donor, n is the refractive index of the medium and J (λ) is the overlap integral that represents the spectral overlap between the donor emission and acceptor absorption (Figure 1.1) and is given by

$$J(\lambda) = \int_{0}^{\infty} F_{D}(\lambda) \varepsilon_{A}(\lambda) \lambda^{4} d\lambda$$
 (1.8)

 F_D (λ) is corrected fluorescence intensity of the donor that is normalized to unity and $\epsilon_A(\lambda)$ represents the extinction coefficient of the acceptor at λ .

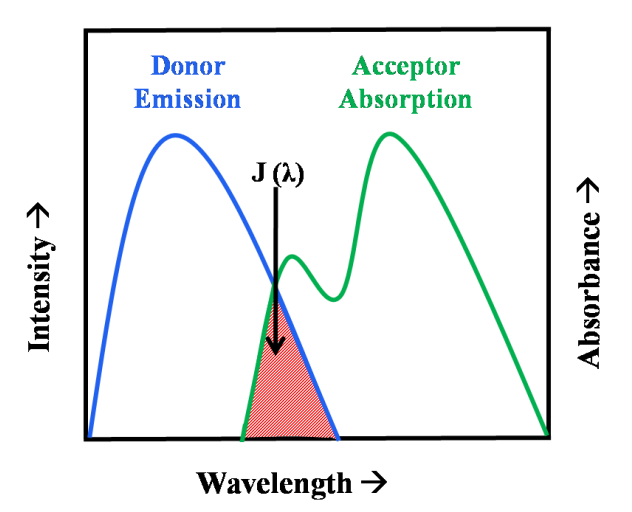


Figure 1.1. The spectral overlap between the donor emission and acceptor absorption

1.3.1.2.2. Dexter energy transfer (DET)

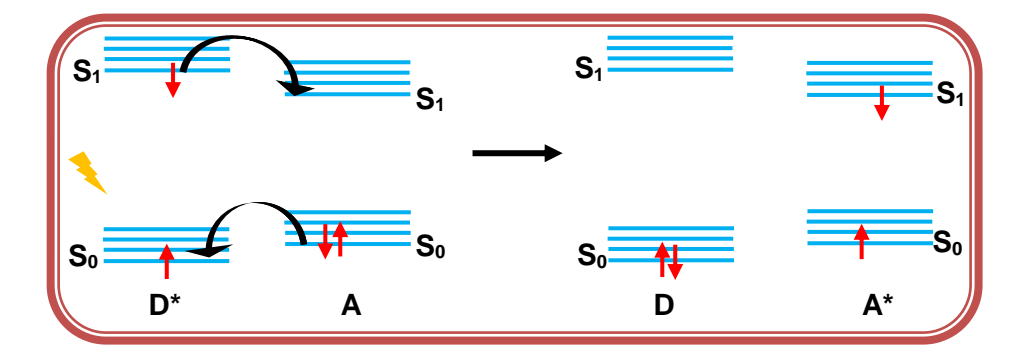
DET results due to the short range interactions (electron exchange) between the donor and acceptor molecules (Scheme 1.10). 173, 174 For the electron exchange to occur, the molecular orbital overlap between the donor and acceptor is required along with the spectral overlap between the donor emission and acceptor absorption. Since this exchange mechanism requires overlap of the molecular orbitals, it is effective only at short donor-acceptor distances (< 10 Å). 173, 174 The rate of DET (k_{DET}) from donor to acceptor is given by

$$k_{DET} = KJ(\lambda) \exp\left(\frac{-2r}{L}\right)$$
(1.9)

where K represents the orbital interaction, r is the distance between the donor and acceptor, L is the sum of the donor and acceptor radii and $J(\lambda)$ represents the spectral overlap integral which is given by

$$J(\lambda) = \int_{0}^{\infty} F_{D}(\lambda)\varepsilon_{A}(\lambda)d\lambda \tag{1.10}$$

 F_D (λ) and ϵ_A (λ) represent the corrected fluorescence intensity of the donor and extinction coefficient of the acceptor, respectively.



Scheme 1.10. Schematic representation of the excitation energy transfer between the donor and acceptor through DET mechanism.

Excitation energy transfer is widely used as a tool to determine the distance

between two sites in macromolecules.¹⁷⁵ It is also used to improve the efficiency of solar cells,¹⁷⁶⁻¹⁷⁸ light-emitting diodes¹⁷⁹ and to find the probes that can act as sensors.¹⁸⁰⁻¹⁸² Experimentally, energy transfer between the quenching partners can be identified using the steady state and time-resolved emission techniques.¹⁸³⁻¹⁸⁶

1.3.2. Photo-induced electron transfer (PET)

PET plays a key role in photosynthesis,¹⁸⁷ logic gates,¹⁸⁸ sensing,¹⁸⁹ molecular electronic devices¹⁹⁰ and solar cells.¹⁹¹ PET can be intermolecular or intramolecular. Generally, the photoexcited species can act either as a donor or as an acceptor. On the basis of the electron donating or accepting ability of the photoexcited species, the electron transfer can be termed as oxidative or reductive electron transfer (Scheme 1.11).¹⁷³ The rate of electron transfer between the donor and acceptor is given by

$$k_{PFT} = Z \exp(-\Delta G */RT)$$
 (1.11)

Z is the collisional frequency and ΔG^* is the activation free energy, which is related to the standard free energy (ΔG^0) by

$$\Delta G^* = \frac{(\Delta G^0 + \lambda)^2}{4\lambda} \tag{1.12}$$

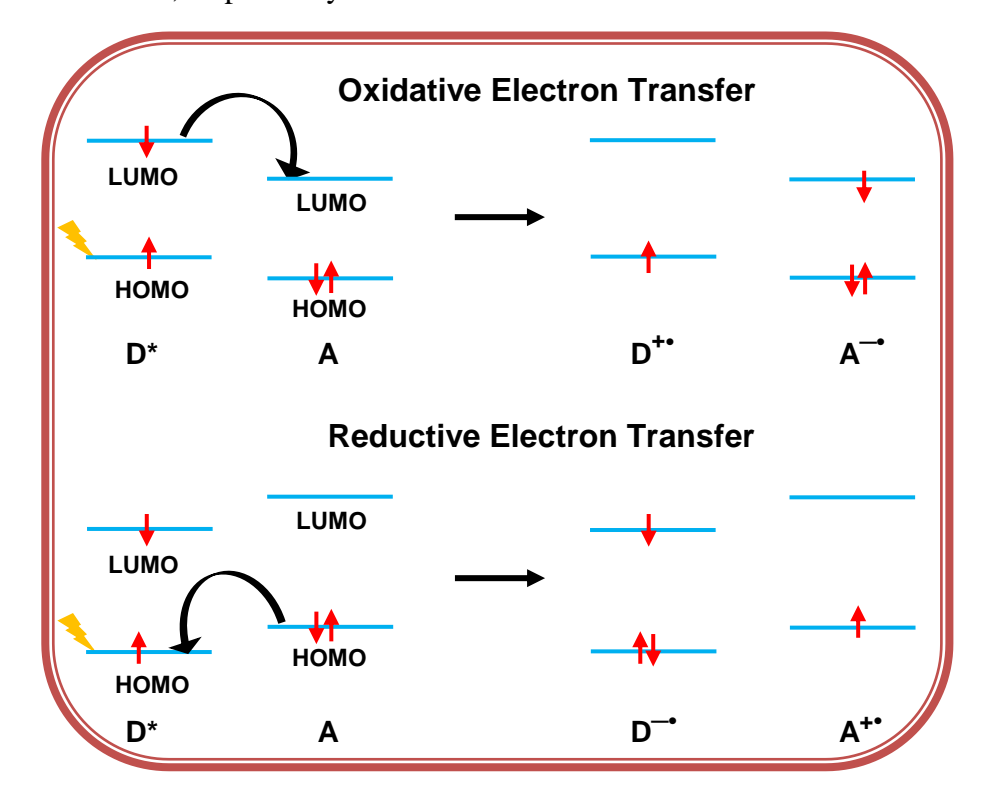
with λ as the reorganization energy.

 ΔG^0 is expressed in terms of oxidation (E_D^{ox}) and reduction (E_A^{red}) potentials of the donor and acceptor molecules, respectively, by

$$\Delta G = E_D^{ox} - E_A^{red} - E_{0,0} - e^2 / \varepsilon r \tag{1.13}$$

where, $E_{0,0}$ is the energy difference between the lowest vibrational level of the first excited state and ground state of either the excited donor or acceptor. The fourth term is the Coulombic interaction energy of the ion pair formed with e representing the electron charge, ε and r as the dielectric constant of the solvent and distance

between the ions, respectively.¹⁷³



Scheme 1.11. Illustration of the oxidative and reductive electron transfer.

PET between the donor and acceptor can be characterized using various techniques such as femtosecond pump-probe,^{63, 186}nanosecond laser flash photolysis,^{192, 193} ESR or spin trapping,¹⁹⁴ scavenging or trapping intermediates¹⁹⁵ and transient photocurrent measurements.¹⁹⁶

1.4. Motivation behind the thesis

As stated earlier, QDs have become a promising alternative to molecular fluorophores in a variety of applications ranging from photovoltaics to biological imaging due to their significant properties such as broad absorption spectra, narrow emission spectra, size-dependent optical tunability, long photoluminescence lifetime and superior photostability. ^{20-22, 197, 198} As majority of the applications of the QDs are related to their luminescence, which depends on the trapping of the

photogenerated carriers and also on the dynamics of their charge separation and recombination, a clear understanding of these processes is essential. 198-201

The main objective of our work presented in this thesis is to synthesize the QDs with appropriate ligands that effectively passivate the surface atoms of the QDs enhancing their radiative carrier recombination and investigate their exciton quenching dynamics in the presence of molecular systems.

As a major part of the solar energy contains visible and infrared light, small band gap semiconductor QDs such as CdSe, CdTe, PbS and PbSe which absorb in the visible and infrared region are considered as ideal solar energy harvesters. 201-203 Recently, Kamat and coworkers reported that CdSe QDs are better systems for harvesting the solar energy compared to CdTe QDs in quantum dot sensitized solar cells (ODSSCs), though the electron transfer efficiency is higher for the later system.²⁰⁴ The poor performance of CdTe QD as light harvesters is attributed to rapid corrosion of the surface compared to its hole transfer in the presence of commonly used hole scavenger, sulfide redox couple in aqueous medium.²⁰⁴ This limitation can be overcome either by replacing the redox couple or the solvent medium in which the corrosion of the QDs reduces. However, the former attempt was found to be ineffective. 204 Recent synthesis of highly luminescent CdTe QDs capped with task specific ionic liquids (MUIM, Chart 1.4) exhibiting good stability in IL³⁶ gave the idea that it might be possible to prevent/reduce the corrosion of the QDs in presence of sulfide redox couple in IL and enhance their hole transfer ability.

Understanding the exciton quenching dynamics of the QDs is crucial for their applications ranging from solar cells to biological applications.^{71-75, 197-199, 201} Two such processes which are responsible for emission quenching of the QDs are energy and charge transfer (electron and hole).¹⁸⁶ The factors that govern energy transfer between a donor and an acceptor is the spectral overlap of the donor

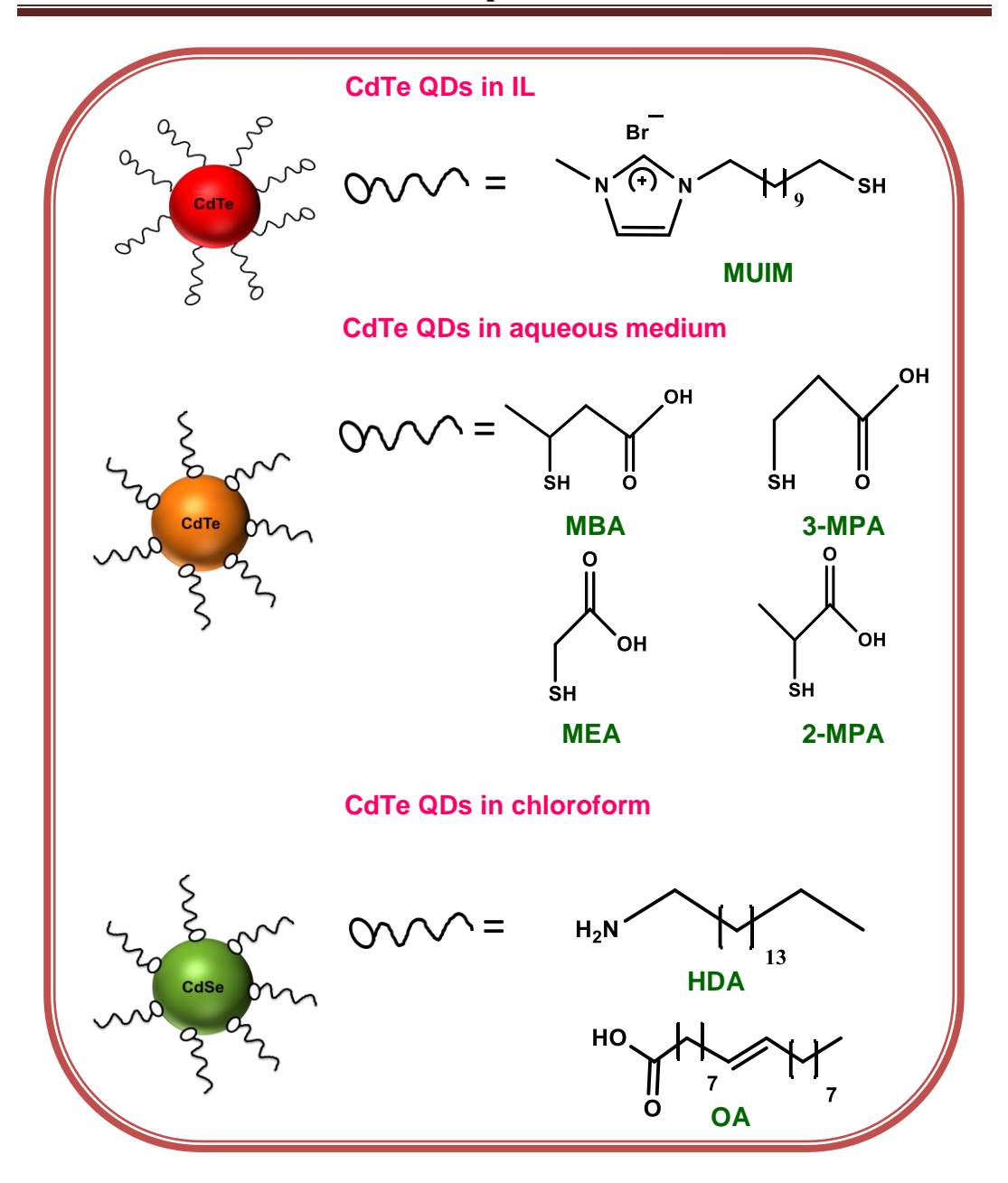


Chart 1.4. Structures of the capping agents and the QDs employed in the present study.

emission and acceptor absorption and the donor-acceptor distance. In the case of charge transfer, the potential difference between the donor and acceptor is one of

the most crucial factors. Most of the energy transfer studies between QDs and organic molecules are confirmed based on their spectral overlap criterion and the decrease of the lifetime of the donor in the presence of acceptor. ²⁰⁵⁻²⁰⁹ In order to unambiguously establish that the above parameters are insufficient to confirm the energy transfer process and that one should consider other possibilities carefully before attributing the quenching of QDs fluorescence to the energy transfer process, we have studied the quenching of MPA capped CdTe QDs fluorescence by cresyl violet (CV, chart 1.5).

In case of nanoparticles with few nanometers in size (QDs), passivation of the surface atoms plays a significant role in enhancing their luminescence.²⁸ Hence, finding out appropriate ligands that effectively passivate the surface atoms of the QDs is essential. In addition to the passivation of surface atoms, the luminescence of QDs also depends on the method of their synthesis. The two procedures used for synthesis of water soluble CdTe QDs are i) direct synthesis of QDs in the aqueous medium and ii) initial synthesis of organic ligand capped QDs in high boiling solvents and later replacing the organic ligand with water soluble ligands (ligand replacement method).^{29, 33} Fang et. al., synthesized CdTe ODs capped with a series of mercapto acids (Chart 1.4) directly in the aqueous medium and found maximum QY for the 3-mercaptobutyric acid (MBA, Chart1.4) capped CdTe QDs.³³ The reported QY of CdTe QDs capped with other agents was however found low.³³ As the ligand replacement method is known to produce highly luminescent QDs, we have synthesized a series of mercapto acid capped CdTe QDs (chart 1.4) by this ligand replacement procedure and studied their exciton dynamics.

The stoichiometry of the QDs is another factor that needs to be considered while synthesizing highly luminescent QDs, as most of the ligands used for passivating the surface atoms of the QDs are specific in their binding. ^{37-39, 210} For

example, ligands containing groups like amine, oxide and acid are shown to bind strongly with the cationic sites of the QDs, while ligands like trialkylphosphine are preferred to passivate the anionic sites of the QDs.^{37-39, 210} Hence, effective passivation of the QDs surface atoms by the ligands depends on the stoichiometry of the former. The photoluminescence properties of the QDs with different stoichiometry are well studied,^{37, 40} but the influence of the latter on the charge separation and recombination dynamics of the QDs is an unexplored area. To understand the effect of QDs stoichiometry on the charge separation and recombination process, we have chosen CdSe QDs (Chart 1.4) with different stoichiometry as donor and methyl viologen (MV⁺²) (chart 1.5) as acceptor and investigated the dynamics.

Chart 1.5. Structures of the molecular acceptors used in the present study.

References

- 1. Ekimov, A. I.; Efros, A. L.; Onushchenko, A. A., Solid State Commun. 1985, 56, 921.
- 2. Rosetti, R.; Nakahara, S.; Brus, L. E., J. Chem. Phys. 1983, 79, 1086.
- 3. Reed, M. A.; Randall, J. N.; Aggarwal, R. J.; Matyi, R. J.; Moore, T. M.; Wetsel, A. E., *Phys. Rev. Lett.* **1988**, 535.
- 4. Smith, A. M.; Nie, S., Acc. Chem. Res. **2010**, 43, 190.
- 5. Kippeny, T.; Swafford, L. A.; Rosenthal, S. J., *J. Chem. Edu.* **2002,** 79, 1094.
- 6. Brus, L. E., J. Chem. Phys. **1984**, 80, 4403.
- 7. Brus, L. E., J. Chem. Phys. **1983**, 79, 5566.
- 8. Alivisatos, A. P., J. Phys. Chem. **1996**, 100, 13226.
- 9. Murray, C. B.; Norris, D. J.; Bawendi, M. G., J. Am. Chem. Soc. 1993, 115, 8706.
- 10. Nirmal, M.; Brus, L., Acc. Chem. Res. 1999, 32, 407.
- 11. Bawendi, M. G.; Steigerwarld, M. L.; Brus, L. E., *Annu. Rev. Phys. Chem.* **1990,** 41, 477.
- 12. Rasmussen, M. A.; Ramakrishna, S.; Weiss, E. A.; Seideman, T., *J. Chem. Phys.* **2014**, 140, 144102.
- 13. Yu, W. W.; Qu, L.; Guo, W.; Peng, X., Chem. Mater. 2003, 15, 2854.
- 14. Wang, Y.; Herron, N., J. Phys. Chem. **1991,** 95, 525.
- 15. Bera, D.; Qian, L.; Tseng, T. K.; Holloway, P. H., *Materials* **2010,** 3, 2260.
- 16. Chen, Z.; Brein, S. O., ACS Nano 2008, 2, 1219.
- 17. Machol, J. L.; Wise, F. W.; Patel, R.; Tanner, D. B., *Physica A* **1994,** 207, 427.
- 18. Wu, K.; Song, N.; Liu, Z.; Zhu, H.; Cordoba, R. W.; Lian, T., *J. Phys. Chem. A* **2013**, 117, 7561.
- 19. Gao, X.; Nie, S., *Trends Biotechnol.* **2003**, 21, 371.
- 20. Hodes, G., J. Phys. Chem. C 2008, 112, 17778.
- 21. Hod, I.; Gonzalez-Pedro, V.; Tachan, Z.; Fabregat-Santiago, F.; Mora-Sero, I.; Bisquert, J.; Zaban, A., *J. Phys. Chem. Lett.* **2011**, 2, 3032.
- 22. Genger, U. R.; Grabolle, M.; Jaricot, S. C.; Nitschke, R.; Nann, T., *Nature Methods* **2008,** 5, 763.
- 23. Blackburn, J. L.; Selmarten, D. C.; Nozik, A. J., *J. Phys. Chem. B* **2003**, 107, 14154.
- 24. Piris, J.; Ferguson, A. J.; Blackburn, J. L.; Norman, A. G.; Rumbles, G.; Selmarten, D. C.; Kopidakis, N., *J. Phys. Chem. C* **2008**, 112, 7742.
- 25. Guijarro, N.; Lana-Villarreal, T.; Shen, Q.; Toyoda, T.; Gomez, R., *J. Phys. Chem. C* **2010,** 114, 21928.
- 26. Wang, H.; Barcelo, I.; Villarreal, L. T.; Gomez, R.; Bonn, M.; Canovas, E., *Nano. Lett.* **2014**, 14, 5780.
- 27. Chen, X.; Lou, Y.; Samia, A. C.; Burda, C., *Nano Lett.* **2003,** 3, 799.
- 28. Pokrant, S.; B.Whaley, K., Eur. Phys. J. D. **1999**, 6, 255.
- 29. Wuister, S. F.; Swart, I.; Driel, F. V.; Hickey, S. G.; Donega, D. D. M., *Nano Lett.* **2003,** 3, 503.
- 30. Kloper, V.; Osovsky, R.; Olesiak, J. K.; Sashchiuk, A.; Lifshitz, E., *J. Phys. Chem. C* **2007**, 111, 10336.

Chapter 1

- 31. Kim, S. W.; Kim, S.; Tracy, J. B.; A. Jasanoff; Bawendi, M. G., *J. Am. Chem. Soc.* **2005,** 127, 4556.
- 32. Fan, H.; Leve, E. W.; Scullin, C.; Gabaldon, J.; Tallant, D.; Bunge, S.; Boyle, T.; Wilson, M. C.; Brinker, C. J., *Nano Lett.* **2005**, 5, 645.
- 33. Fang, T.; Ma, K.; Ma, L.; Bai, J.; Li, X.; Song, H.; Guo, H., *J. Phys. Chem. C* **2012,** 116, 12346.
- 34. Nakashima, T.; T. Kawai, *Chem. Commun.* **2005**, 1643.
- 35. Nakashima, T.; Nonoguchi, Y.; Kawai, T., *Polym. Adv. Technol.* **2008,** 19, 1401.
- 36. Santhosh, K.; Samanta, A., J. Phys. Chem. C 2012, 116, 20643.
- 37. Jasieniak, J.; Mulvaney, P., J. Am. Chem. Soc. 2007, 138, 876.
- 38. Woo, Y. J.; Lee, S.; Lee, S.; Kim, D. W.; Lee, K.; K. Kim; An, J. H.; Lee, C. D.; Jeong, S., J. Am. Chem. Soc. **2016**, 138, 876.
- 39. Gao, Y.; Peng, X., J. Am. Chem. Soc. **2015**, 137, 4230.
- 40. Omogo, B.; Aldana, F. J.; Heyes, D. C., J. Phys. Chem. C 2013, 117, 2317.
- 41. Reiss, P.; Protiere, M.; Li, L., Small **2009**, 5, 154.
- 42. Dabbousi, B. O.; Rodriguez-Viejo, J.; Mikulec, F. V.; Heine, J. R.; Mattoussi, H.; Ober, R.; Jensen, K. F.; Bawendi, M. G., *J. Phys. Chem. B* **1997**, 101, 9463.
- 43. Peng, X.; Schlamp, M. C.; Kadavanich, A. V.; Alivisatos, A. P., *J. Am. Chem. Soc.* **1997,** 119, 7019.
- 44. Chaudhuri, R. G.; Paria, S., Chem. Rev. 2012, 112, 2373.
- 45. Hines, M. A.; Guyot-Sionnest, P., J. Phys. Chem. 1996, 100, 468.
- 46. Kim, S.; Fisher, B.; Eisler, J. H.; Bawendi, M., J. Am. Chem. Soc. **2003**, 125, 11466.
- 47. Mews, A.; Eychmuller, A.; Giersig, M.; Schooss, D.; Weller, H., *J. Phys. Chem* **1994,** 98, 934.
- 48. Battaglia, D.; Li, J. J.; Wang, Y. J.; Peng, X. G., *Angew. Chem. Int. Ed.* **2003,** 42, 5035.
- 49. Zhong, X. H.; Xie, R. G.; Zhang, Y.; Basche, T.; Knoll, W., *Chem. Mater.* **2005,** 17, 4038.
- 50. Bae, W. K.; Char, K.; Hur, H.; Lee, S., Chem. Mater. **2008**, 20, 531.
- 51. Regulacio, M. D.; Han, M. Y., Acc. Chem. Res. **2010**, 5, 621.
- 52. Groeneveld, E.; Witteman, L.; Lefferts, M.; Ke, X.; Bals, S.; Tendeloo, G. V.; Donega, C. M., ACS Nano **2013**, 7, 7913.
- 53. Bailey, R. E.; Nie, S., J. Am. Chem. Soc. **2003**, 125, 7100.
- 54. Tang, J.; Hinds, S.; Kelley, S. O.; Sargent, E. H., *Chem. Mater.* **2008**, 20, 6906.
- 55. Pan, D. C.; Weng, D.; Wang, X. L.; Xiao, Q. F.; Chen, W.; Xu, C. L.; Yang, Z. Z.; Lu, Y. F., *Chem. Commun.* **2009**, 4221.
- 56. Pradhan, N.; Sarma, D. D., J. Phys. Chem. Lett. **2011**, 2, 2818.
- 57. Santra, P. K.; Kamat, P. V., J. Am. Chem. Soc. **2012**, 134, 2508.
- 58. Bhargava, R. N.; Gallagher, D.; Hong, X.; Nurmikko, A., *Phys. Rev. Lett.* **1994,** 72, 416.
- 59. Jana, S.; Srivastava, B. B.; Pradhan, N., J. Phys. Chem. Lett. **2011**, 2, 1747.
- 60. Zeng, R.; Rutherford, M.; Xie, R.; Zou, B.; Peng, X., Chem. Mater. 2010, 22, 2107.

- 61. Nozik, A. J.; Beard, M. C.; Luther, J. M.; Law, M.; Ellingson, R. J.; Johnson, J. C., *Chem. Rev.* **2010**, 110, 6873.
- 62. Shabaev, A.; Hellberg, C. S.; Efros, A. L., Acc. Chem. Res. 2013, 46, 1242.
- 63. Schaller, R. D.; Sykora, M.; Pietryga, J. M.; Klimov, V. I., Nano. Lett. 2006, 6, 424.
- 64. Stewart, J. T.; Padilha, L. A.; Bae, W. K.; Koh, W. K.; Pietryga, J. M.; Klimov, V. I., *J. Phys. Chem. Lett.* **2013**, 4, 2061.
- 65. Semonin, O. E.; Luther, J. M.; Choi, S.; Chen, H. Y.; Gao, J.; Nozik, A. J.; Beard, M. C., *Science* **2011**, 334, 1530.
- 66. Tisdale, W. A.; Williams, K. J.; Timp, B. A.; Norris, D. J.; Aydil, E. S.; Zhu, X. Y., *Science* **2010**, 328, 1543.
- 67. Schokley, W.; Queisser, H. J., J. Appl. Phys. **1961**, 32, 510.
- 68. Klimov, V. I., Annu. Rev. Phys. Chem. 2007, 58, 635.
- 69. Schaller, R. D.; Klimov, V. I., *Phys. Rev. Lett.* **2004,** 92, 186601/1.
- 70. Zidek, K.; Zheng, K.; Abdellah, M.; Lenngren, N.; Chabera, P.; Pullerits, T., *Nano Lett.* **2012**, 12, 6393.
- 71. Bakalova, R.; Zhelev, Z.; Ohba, H.; Baba, Y., J. Am. Chem. Soc. **2005**, 127, 11328.
- 72. Hoshino, K.; Gopal, A.; Glaz, M. S.; Bout, D. A. V.; Zhang, X., *Appl. Phys. Lett.* **2012**, 101, 043118.
- 73. Vaillancourt, J.; Vasinajindakaw, P.; Lu, X., Optics and Photonics Lett. **2011,** 4, 57.
- 74. Huang, J.; Mulfort, L. K.; Du, P.; Chen, L. X., J. Am. Chem. Soc. **2012**, 134, 16472.
- 75. Suriñach, C. G.; Albero, J.; Stoll, T.; Fortage, J.; Collomb, M. N.; Deronzier, A.; Palomares, E. E.; Llobet, A., *J. Am. Chem. Soc.* **2014**, 136, 7655.
- 76. Nozik, A. J., J. Chem. Phys. Lett. 2008, 3, 457.
- 77. Kamat, P. V., Acc. Chem. Res. 2012, 45, 1906.
- 78. Robel, I.; Subramanian, V.; Kuno, M.; Kamat, P. V., *J. Am. Chem. Soc.* **2006,** 128, 2385.
- 79. Etgar, L.; Zhang, W.; Gabriel, S.; Hickey, S. G.; Nazeeruddin, M. K.; Eychmuller, A.; Liu, B.; Gratzel, M., *Adv. Mater.* **2012**, 24, 2202.
- 80. Yang, Z.; Chen, C. Y.; Roy, P.; Chang, H. T., Chem. Commun. 2011, 47, 9561.
- 81. Wassercheid, P.; Kein, W., Angew. Chem. Int. Ed. 2000, 39, 3772.
- 82. Samanta, A., J. Phys. Chem. Lett. **2010,** 1, 1557.
- 83. Seddon, K. R., Ionic Liquids, Industrial Applications for Green Chemistry, American Chemical Society, Washington DC,. **2002**.
- 84. Dubreuil, J. F.; Bourahla, K.; Rahmouni, M.; Bazureau, J. P.; Hamelin, J., *Catal. Commun.* **2002**, 3, 185.
- 85. Hallett, J. P.; Welton, T., Chem. Rev. 2011, 111, 3508.
- 86. Walden, P., Bull. Acad. Imper. Sci. (St. Petersberg) 1914, 1800.
- 87. Wilkes, J. S.; Levinsky, J. A.; Wilson, R. A.; Hussey, C. L., *Inorg. Chem.* **1982,** 21, 1263.
- 88. Boon, J. A.; Levinsky, J. A.; Pflug, J. L.; Wilkes, J. S., *J. Org. Chem.* **1986**, 51, 480.
- 89. Chiappe, C.; Pieraccini, D., J. Phys. Org. Chem. **2005**, 18, 275.
- 90. Sheldon, R., Chem. Commun. 2001, 2399.

Chapter 1

- 91. Wasserscheid, P.; Welton, T., *Ionic Liquids in Synthesis, Wiley-VCH, Weinheim* **2003**.
- 92. Golding, J. J.; MacFarlane, D. R.; Spiccia, L.; Forsyth, G. B.; Skelton, B. W.; White, A. H., *Chem. Commun.* **1998**, 18, 1593.
- 93. Polyakov, O. G.; Ivanova, S. M.; Gaudinski, C. M.; Miller, S. M.; Anderson, O. P.; Strauss, S. H., *Organometallics* **1999**, 18, 3769.
- 94. Larsen, A. S.; Holbery, J. D.; Tham, F. S.; Reed, C. A., *J. Am. Chem. Soc.* **2000,** 122, 7264.
- 95. Xu, W.; L. M. Wang; Nieman, R. A.; Angell, C. A., *J. Phys. Chem. B* **2003,** 107, 11749.
- 96. Sankaranarayanan, K.; Sathyaraj, G.; Nair, B. U.; Dhathathreyan, A., *J. Phys. Chem. B* **2012**, 116, 4175.
- 97. Ohno, H.; Fukumoto, K., Acc. Chem. Res. 2007, 40, 1122.
- 98. Davis, J. H., Chem. Lett. **2004**, 33, 1072.
- 99. Lee, S., Chem. Commun. 2006, 1049.
- 100. Enomoto, T.; Nakamori, Y.; Matsumoto, K.; Hagiwara, R., *J. Phys. Chem. C* **2011**, 115, 4324.
- 101. Ngo, H. L.; Compte, K. L.; Hargens, L.; McEwen, A., *Thermochim. Acta* **2000,** 357, 97.
- 102. Lewandowski, A.; Swiderska-Mocek, A., J. Power Sources 2009, 194, 601.
- 103. Freemantle, M., Chem. Eng. News 1998, 76, 32.
- 104. Santhosh, K.; Banerjee, S.; Rangaraj, N.; Samanta, A., *J. Phys. Chem. B* **2010,** 114, 1967.
- 105. Holbrey, J. D.; Turner, M. B.; Reichert, W. M.; Rogers, R. D., *Green Chem.* **2003,** 5, 731.
- 106. Branco, L. C.; Rosa, J. N.; Ramos, J. J. M.; Afonso, C. A. M., *Chem. Eur. J.* **2002,** 8, 3671.
- 107. Dzyuba, S.; Bartsch, R. A., ChemPhysChem 2002, 3, 161.
- 108. Carda-Borch, S.; Berthold, A.; Armstrong, D. W., *Anal. Bioanal. Chem.* **2003,** 375, 191.
- 109. Seddon, K. R.; Stark, A.; Torres, M. J., Pure Appl. Chem. **2000**, 72, 2275.
- 110. Widegren, J. A.; Laesecke, A.; Magee, J. W., Chem. Commun. 2005, 1610.
- 111. Paul, A.; Samanta, A., J. Phys. Chem. B 2008, 112, 16626.
- 112. Huddleston, J. G.; Visser, A. E.; Reichert, W. M.; Willauer, H. D.; Broker, G. A.; Rogers, R. D., *Green Chem.* **2001**, *3*, 156.
- 113. Pringle, J. M.; Golding, J.; Baranyai, K.; Forsyth, C. M.; Deacon, G. B.; Scott, J. L.; MacFarlane, D. R., *New J. Chem.* **2003,** 27, 1504.
- 114. Dupont, J.; Souza, R. F. D.; Suarez, P. A. Z., *Chem. Rev.* **2002,** 102, 3667.
- 115. Nishida, T.; Tashiro, Y.; Yamamoto, M. J., Fluorine Chem. 2003, 120, 135.
- 116. Buzzeo, M. C.; Evans, R. G.; Compton, R. G., ChemPhysChem **2004**, 5, 1106.
- 117. Aki, S. N. V. K.; Brennecke, J. F.; Samanta, A., Chem. Commun. 2001, 413.
- 118. Law, G.; Watson, P. R., Langmuir **2001**, 17, 6138.
- 119. Fuller, J.; Carlin, R. T.; Long, H. C. D.; Haworth, D., Chem. Commun. 1994, 299.

- 120. Reichardt, C., Green Chem. 2005, 7, 339.
- 121. Bonhote, P.; Dias, A.; Papageorgiou, N.; Kalyanasundaram, K.; Gratzel, M., *Inorg. Chem.* **1996**, 35, 1168.
- 122. Karmakar, R.; Samanta, A., J. Phys. Chem. A 2002, 106, 6670.
- 123. MacFarlane, D. R.; Meakin, P.; Sun, J.; Amini, N.; Forsyth, M., *J. Phys. Chem. B* **1999,** 103, 4164.
- 124. Jeon, Y.; Sung, J.; Seo, C.; Lim, H.; Cheong, H.; M. Kang; Moon, B.; Ouchi, Y.; Kim, D., *J. Phys. Chem. B* **2008**, 112, 4735.
- 125. Mele, A.; Tran, C. D.; Lacerda, S. H. D. P., Angew. Chem. Int. Ed. 2003, 42, 4364.
- 126. Mele, A.; Romano, G.; Giannone, M.; Ragg, E.; Fronza, G.; Raos, G.; Marcon, V., *Angew. Chem. Int. Ed.* **2006**, 45, 1123.
- 127. Gordon, C. M.; Holbrey, J. D.; Kennedy, A. R.; Seddon, K. R., *J. Mater. Chem.* **1998,** 8, 2627.
- 128. Wilkes, J. S.; Zaworotko, M. J., Chem. Commun. 1992, 965.
- 129. Kolle, P.; Dronskowski, R., *Inorg. Chem.* **2004**, 43, 2803.
- 130. Wasserscheid, P., Nature 2006, 439, 797.
- 131. Earle, M. J.; Esperanca, J. M. S. S.; Gilea, M. A.; Lopes, J. N. C.; Rebelo, L. P. N.; Magee, J. W.; Seddon, K. R.; Widegren, J. A., *Nature* **2006**, 439, 831.
- 132. Taylor, A. W.; Lovelock, K. R. J.; Deyko, A.; Licence, P.; Jones, R. G., *Phys. Chem. Phys.* **2010**, 12, 1772.
- 133. Chambreau, S. D.; Vaghjiani, G. L.; Koh, C. J.; Golan, A.; Leone, S. R., *J. Phys. Chem. Lett.* **2012**, 3, 2910.
- 134. Wakai, C.; Oleinikova, A.; Ott, M.; Weingartner, H., *J. Phys. Chem. B* **2005,** 109, 17028.
- 135. Daguenet, C.; Dyson, P. J.; Krossing, I.; Oleinikova, A.; Slattery, J.; Wakai, C.; Weingartner, H., *J. Phys. Chem. B* **2006**, 110, 12682.
- 136. Crowhurst, L.; Mawdsley, P. R.; Perez-Arlandis, J. M.; Salter, P. A.; Welton, T., *Phys. Chem. Chem. Phys.* **2003**, 5, 2790.
- 137. Anderson, J. L.; Ding, J.; Welton, T.; Armstorng, D. W., *J. Am. Chem. Soc.* **2002,** 124, 14247.
- 138. Mellein, B. R.; Aki, S. N. V. K.; Ladewski, R. L.; Brennecke, J. F., *J. Phys. Chem. B* **2007**, 111, 6452.
- 139. Russina, O.; Triolo, A.; Gontrani, L.; Caminiti, R., J. Phys. Chem. Lett. 2012, 3, 27.
- 140. Fruchey, K.; Lawler, C. M.; Fayer, M. D., J. Phys. Chem. B 2012, 116, 3054.
- 141. Canongia, L. J. N. A.; Costa, G. M. F.; Padua, A. A. H., *J. Phys. Chem. B* **2006,** 110, 16816.
- 142. Castner, J. E. W.; Margulis, C. J.; Maroncelli, M.; Wishart, J. F., *Annu. Rev. Phys. Chem.* **2011**, 62, 85.
- 143. Mudring, A. V., Aust. J. Chem. **2010**, 63, 544.
- 144. Hamaguchi, H.; Saha, S.; Ozawa, R.; Hayashi, S., Raman and X-ray studies on the structure of [bmim]X (X = Cl, Br, I, [BF4], [PF6]): rotational isomerism of the [bmim]+ cation. *In Ionic Liquids IIIA: Fundamentals, Progress, Challenges, and Opportunities,*

Chapter 1

- *Properties and Structure*, Rogers, R. D., Seddon, K. R., Eds.; Am. Chem. Soc.: Washington, 2005; pp 68.
- 145. Jayaraman, S.; Maginn, E. J., J. Chem. Phys. 2007, 127, 214504.
- 146. Choudhury, A. R.; Winterton, N.; Steiner, A.; Cooper, A. I.; Johnson, K. A., *J. Am. Chem. Soc.* **2005**, 127, 16792.
- 147. Hardacre, C.; Holbrey, J. D.; Nieuwenhuyzen, M.; Youngs, T. G. A., *Acc. Chem. Res.* **2007**, 40, 1146.
- 148. Triolo, A.; Mandanici, A.; Russina, O.; Rodriguez-Mora, V.; Cutroni, M., *J. Phys. Chem. B* **2006**, 110, 21357.
- 149. Holbrey, J. D.; Reichert, W. M.; Rogers, R. D., Dalton Trans. 2004, 2267.
- 150. Hardacre, C.; Holbrey, J. D.; Mullan, C. L.; Nieuwenhuyzen, M.; Youngs, T. G. A.; Bowron, D. T., *J. Phys. Chem. B* **2008**, 112, 8049.
- 151. Suarez, P. A. Z.; Dullius, J. E. L.; Souza, R. F.; Dupont, J., *J. Chim. Phys. Phys. Chim. Biol.* **1998**, 95, 1626.
- 152. Wang, Y.; Voth, G. A., J. Am. Chem. Soc. 2005, 127, 12192.
- 153. Lopes, J. N. C.; Padua, A. A. H., J. Phys. Chem. B 2006, 110, 3330.
- 154. Jiang, W.; Wang, Y.; Voth, G. A., J. Phys. Chem. B 2007, 111, 4812.
- 155. Wang, Y.; Jiang, W.; Yan, T.; Voth, G. A., Acc. Chem. Res. 2007, 40, 1193.
- 156. Triolo, A.; Russina, O.; Bleif, H. J.; Cola, E. D., J. Phys. Chem. B 2007, 111, 4641.
- 157. Hardacre, C.; Holbery, J. D.; Mullan, C. L.; Youngs, T. G. A.; Bowron, D. T., *J. Chem. Phys.* **2010**, 133, 074510.
- 158. Annapureddy, H. V. R.; Kashyap, H. K.; Biase, P. M. D.; Margulis, C. J., *J. Phys. Chem. B* **2010**, 114, 16838.
- 159. Rodriguez, H.; Brennecke, J. F., J. Chem. Engg. Data **2006**, 51, 2145.
- 160. Fletcher, K. A.; Baker, S. N.; Baker, G. A.; Pandey, S., New J. Chem. 2003, 27, 1706.
- 161. Seth, D.; Chakraborty, A.; Setua, P.; Sarkar, N., J. Phys. Chem. B 2007, 111, 4781.
- 162. Chakrabarty, D.; Seth, D.; Chakraborty, A.; Sarkar, N., *J. Phys. Chem. B* **2005**, 109, 5753.
- 163. Li, W.; Zhang, Z.; Han, B.; Hu, S.; Xie, Y.; Yang, G., J. Phys. Chem. B **2007**, 11, 6452.
- 164. Tokuda, H.; Baek, S. J.; Watanabe, M., *Electrochemistry* **2005,** 73, 620.
- 165. Armand, M.; Endres, F.; MacFarlane, D. R.; Ohno, H.; Scrosati, B., *Nat. Mater.* **2009**, 8, 621.
- 166. Ding, J.; Zhou, D.; Spinks, G.; Wallace, G.; Forsyth, S.; Forsyth, M.; MacFarlane, D., *Chem. Mater.* **2003**, 15, 2392.
- 167. Fujita, K.; Ohno, H., Biopolymers **2010**, 93, 1093.
- 168. Yang, L. X.; Zhu, Y. J.; Wang, W. W.; Tong, H.; Ruan, M. L., *J. Phys. Chem. B* **2006**, 110, 6609.
- 169. Okazaki, K. I.; Kiyama, T.; Hirahara, K.; Tanaka, N.; Kuwabata, S.; Torimoto, T., *Chem. Commun.* **2008**, 691.
- 170. Migowski, P.; J. Dupont, Chem. Eur. J. 2007, 13, 32.
- 171. Sekhar, M. C.; Santhosh, K.; Kumar, J. P.; Mondal, N.; Soumya, S.; Samanta, A., *J. Phys. Chem. C* **2014**, 118, 18481.

- 172. Lakowicz, J. R., Principles of Fluorescence Spectroscopy, Second ed.; Kluwer Academic/Plenum Publishers. **1999**.
- 173. Valeur, B., Molecular Fluorescence- Principles and Applications, WILEY-VCH Verlag GmbH. **2002**.
- 174. Peng, H. Q.; Niu, L. Y.; Chen, Y. Z.; Wu, L. Z.; Tung, C. H.; Yang, Q. Z., *Chem. Rev.* **2015,** 115, 7502.
- 175. Deniz, A. A.; Dahan, M.; Grunwell, J. R.; Ha, T.; Faulhaber, A. E.; Chemla, S. D.; Weiss, S.; Schultz, P. G., *Proc Natl Acad Sci U S A.* **1999**, 96, 3670.
- 176. Choi, H.; Santra, P. K.; Kamat, P. V., ACS Nano **2012**, 6, 5718.
- 177. Miyasaka, T., J. Phys. Chem. Lett. **2011**, 2, 262.
- 178. Panda, D. K.; Goodson, F. S.; Ray, S.; Saha, S., Chem. Commun. 2014, 50, 5358.
- 179. Reineke, S.; Lindner, F.; Schwartz, G.; Seidler, N.; Walzer, K.; Lussem, B.; Leo, K., *Nature* **2009**, 459, 234.
- 180. Fan, J.; Hu, M.; Zhan, P.; Peng, X., Chem. Soc. Rev. 2013, 42, 29.
- 181. Chen, G.; Song, F.; Xiong, X.; Peng, X., Ind. Eng. Chem. Res. 2013, 52, 11228.
- 182. Genovese, D.; Rampazzo, E.; Bonacchi, S.; Montalti, M.; Zaccheroni, N.; Prodi, L., *Nanoscale* **2014**, 6, 3022.
- 183. Funston, A. M.; Jasieniak, J. J.; Mulvaney, P., Adv. Mater. 2008, 20, 4274.
- 184. Medintz, I. L.; Pons, T.; Susumu, K.; Boeneman, K.; Dennis, A. M.; Farrell, D.; Deschamps, J. R.; Melinger, J. S.; Bao, G.; Mattoussi, H., *J. Phys. Chem. C* **2009**, 113, 18552.
- 185. Soujon, D.; Becker, K.; Rogach, A. L.; Feldmann, J.; Weller, H.; Talapin, D. V.; Lupton, J. M., *J. Phys. Chem. C* **2007**, 111, 11511.
- 186. Boulesbaa, A.; Huang, Z.; Wu, D.; Lian, T., J. Phys. Chem. C 2010, 114, 962.
- 187. Nocera, D. G., Acc. Chem. Res. 2012, 45, 767.
- 188. Anderson, M.; Sinks, L. E.; Hayes, R. T.; Y. Zhao; Wasielewski, M. R., *Angew. Chem. Int. Ed.* **2003**, 42, 3139.
- 189. Huang, J. H.; Wen, H.; Sun, Y. Y.; Chou, P. T.; Fang, J. M., *J. Org. Chem.* **2005,** 70, 5827.
- 190. Kondratenko, M.; Moiseev, A. G.; Perepichka, D. F., *J. Mater. Chem.* **2011,** 21, 1470.
- 191. Julliard, M.; Chanon, M., Chem. Rev. 1983, 83, 425.
- 192. In the Exciplex; Gordon, M.; Ware. R., EDs.; Academic Press: New York. 1974.
- 193. Mataga, N., Pure and Appl. Chem. **1984,** 56, 1255.
- 194. Schaap, A. P.; Zaklika, K. A.; Kaskar, B.; Fung, L. V. M., *J. Am. Chem. Soc.* **1980,** 102, 389.
- 195. Gassman, P. G.; Olson, K. D., J. Am. Chem. Soc. 1982, 104, 3740.
- 196. Jarnigan, R. C., Acc. Chem. Res. 1971, 4, 420.
- 197. Bruchez, M.; Moronne, M.; Gin, P.; Weiss, S.; Alivisatos, A. P., *Science* **1998**, 281, 2013.
- 198. Chan, W. C. W.; Nie, S., Science 1998, 281, 2016.
- 199. Yang, J.; Wang, J.; Zhao, K.; Izuishi, T.; Li, Y.; Shen, Q.; Zhong, X., *J. Phys. Chem. C* **2015,** 119, 28800.

Chapter 1

- 200. Abdellah, M.; Marschan, R.; Zidek, K.; Messing, E. M.; Abdelwahab, A.; Chabera, P.; Zheng, K.; Pullerits, T., *J. Phys. Chem. C* **2014**, 118, 25802.
- 201. Kamat, P. V., J. Phys. Chem. Lett. 2013, 4, 908.
- 202. Yang, Y.; Rodríguez-Córdoba, W.; Lian, T., J. Am. Chem. Soc. **2011**, 133, 9246.
- 203. Bae, W. K.; Joo, J.; Padilha, L. A.; Won, J.; Lee, D. C.; Lin, Q.; Koh, W.; Luo, H.; Klimov, V. I.; Pietryga, J. M., *J. Am. Chem. Soc.* **2012**, 134, 20160.
- 204. Bang, J. H.; Kamat, P. V., ACS Nano 2009, 3, 1467.
- 205. Goldman, E. R.; Medintz, I. L.; Whitley, J. L.; Hayhurst, A.; Clapp, A. R.; Uyeda, H. T.; Deschamps, J. R.; Lassman, M. E.; Mattoussi, H., *J. Am. Chem. Soc.* **2005**, 127, 6744.
- 206. Zhou, D.; Piper, J. D.; Abell, C.; Klenerman, D.; Kang, D. J.; Ying, L., *Chem. Commun.* **2005**, 4807.
- 207. Nikiforov, T. T.; Beechem, J. M., Analytical Biochemistry 2006, 357, 68.
- 208. Sadhu, S.; Patra, A., ChemPhysChem 2008, 9, 2052.
- 209. Sadhu, S.; Tachiya, M.; Patra, A., J. Phys. Chem. C 2009, 113, 19488.
- 210. Bullen, C.; Mulvaney, P., Langmuir 2006, 22, 3007.

Materials, Methods and Instrumentation

This chapter provides detailed information on the source of various chemicals/materials used in this study. It also provides methods of purification of the conventional solvents and procedures for the synthesis of various quantum dots and ligands. Methods of estimation of the size of the QDs and its concentration using empirical equation are discussed. Details on the method of sample preparation for spectral studies, transmission electron microscopy (TEM) and inductively coupled plasma-optical emission spectrometer (ICP-OES) studies are described. Details on UV-vis spectrophotometer and spectrofluorimeter, time-correlated single photon counting fluorimeter and femtosecond pump-probe setups are provided along with the procedures for data analysis.

2.1. Materials

Cresyl violet perchlorate (CV) and methyl viologen dichloride hydrate (MV⁺²) were purchased from Sigma-Aldrich and sodium sulfide from local suppliers. For the synthesis of CdTe and CdSe QDs, precursors like cadmium acetate was procured from local suppliers, cadmium oxide, tellurium and selenium powders were purchased from Sigma-Aldrich. Ligands like hexadecylamine (HDA), trioctylphosphine oxide (TOPO), trioctylphosphine (TOP), oleic acid (OA), 3-mercaptopropanoic acid (3-MPA), 2-mercaptopropanoic acid (2-MPA), 2mercaptoethanoic acid (MEA) used for capping the QDs were obtained from Sigma-Aldrich. Crotonoic acid and thioacetic acid, used for the synthesis of ligand (3-Mercaptobutyric acid (MBA)), were acquired from Sigma-Aldrich. The taskspecific capping agent, 1-methyl-(11-undecanethiol) imidazolium bromide (MUIM), used for dissolution of CdTe QDs in ionic liquid (ILs) was synthesized using 1-methylimidazole and 11-bromoundecanethiol procured from Sigma-Aldrich. IL, 1-butyl-3-methylimidazolium hexafluorophosphate, [bmim][PF₆], was obtained from Kanto Chemicals (Japan). The reference Rhodamine 6G, used for determination of the quantum yield of the QDs, was acquired from Sigma-Aldrich.

Solvents (GR grade) used for their spectral studies were procured from Merck. These solvents were purified using various drying agents such as calcium chloride, iodine and magnesium turnings which were procured from local suppliers. Hydrochloric acid required for cleaning the magnesium turnings and molecular sieves for the storage of dry solvents were also procured from local suppliers. The NMR spectra of the synthesized ligands were recorded by dissolving the compound in deuterated solvent, chloroform-d, acquired from Merck.

2.2. Synthesis of ligands and quantum dots

2.2.1. 1-methyl-(11-undecanethiol) imidazolium bromide (MUIM)

Scheme 2.1. Synthesis of 1-methyl-(11-undecanethiol) imidazolium bromide.

The task-specific capping agent, MUIM, was synthesized following a known procedure. Briefly, 11-bromoundecanethiol was first added dropwise to 1-methylimidazole under ice bath in the 1.5:1 mole ratio and then the reaction was carried out at room temperature under nitrogen atmosphere for 24 h. The light yellow colored solid MUIM was treated with ethyl acetate to remove the unreacted starting materials and dried under vacuum for several hours.

2.2.2. 3-mercaptobutyric acid (MBA)

MBA was synthesized by following reported procedures with some modifications.^{2, 3} Thioacetic acid (2.6 g) was added to crotonoic acid (3 g) in a round bottom flask and the reaction was allowed to stand at 30 °C for 24 h. The reaction was heated at 100 °C for 2 h and then cooled to room temperature where it was further allowed to stand for 30 h. The mixture was treated with 25 mL of concentrated ammonia and 25 mL of deionized water. The solution was acidified (pH = 3) by adding sulfuric acid and extracted with diethyl ether (100 mL). The aqueous phase was separated from the organic phase and further treated with diethyl ether to obtain the remaining MBA. The ether was removed on a rotary evaporator and the product was purified by column chromatography. ¹³C NMR (CDCl₃, ppm) 24.73, 30.80, 45.54, 177.56; ¹H NMR (CDCl₃, ppm) 1.41 (d, 3H), 1.88 (d, 1H), 2.66 (m, 2H), 3.38 (m, 1H), 10.80 (b, 1H).

Scheme 2.2. Synthesis of 3-mercaptobutyric acid.

2.2.3. Quantum dots in non-polar media

2.2.3.1. CdTe/HDA/TOPO/TOP

TOPO- and HDA-capped CdTe QDs were prepared following a reported procedure with minor modifications.⁴ Briefly, Cd(CH₃COO)₂ (0.41 g) and Te (0.16 g) were mixed in a reagent bottle to which TOP (5 mL) was added and sonicated till a clear solution was obtained. In a two-necked round-bottom flask (RB), a mixture of HDA (5 g) and TOP (3 mL) was heated to 80 °C in argon atmosphere and then the sonicated solution was injected into the RB and the temperature was slowly increased to 140 °C. When the QDs of desired size were obtained (monitored through emission) the RB was removed out of the heating mantle and allowed to cool to room temperature. To remove excess ligands, methanol was added to the reaction mixture and the precipitate was separated by centrifugation. This precipitate was dissolved in chloroform to obtain the CdTe QDs.

2.2.3.2. CdTe/TOP/OA

TOP- and OA-capped CdTe QDs were also synthesized based on a reported

procedure.⁵ Briefly, Te (0.0128 g) powder was added to a reagent bottle containing TOP (0.5 mL) and sonicated until a clear yellowish color solution was obtained. This clear solution was further diluted with ODE (1.5 mL). In a two-necked round bottom flask (RB), the Cd precursor solution was prepared by mixing CdO (0.0256 g) and OA (200 μL) to ODE (10 mL) and the reaction mixture was heated to 100 °C under vacuum until a red homogeneous mixture appeared. Further, in an Argon atmosphere, the temperature of the solution was raised to 310 °C and the reaction was heated until grey-to-black precipitate appeared. After the appearance of grey-to-black precipitate, the clear solution containing the Te and TOP was injected into the RB. Once the desired size of the QDs was obtained (monitored through emission), the RB was removed from the heating mantle and allowed to cool to room temperature to arrest the further growth of the nanocrystals. To isolate the CdTe QDs from the excess starting materials, ethanol/acetone mixture was added and the obtained precipitate was separated by centrifugation and dissolved in chloroform.

2.2.3.3. CdSe/HDA/TOPO/TOP

CdSe QDs were synthesized by following a standard procedure.¹ Briefly, CdO (0.067 g, 0.52 mmol), and OA (1.4 mmol) were added to a two-necked round bottom flask (RB) containing TOPO (2.7 g) and HDA (5 g) and the reaction mixture was heated to 100 °C under argon atmosphere. Further, the temperature of the reaction mixture was increased to 300 °C and maintained till the CdO dissolved completely. At this stage, the solution of Se (0.041 g, 0.52 mmol) powder dissolved in TOP (5.3 mL) was injected and the reaction was carried out until the QDs of desired sized (by monitoring the emission of the sample) was obtained. When the desired size of the QDs was reached, the RB was removed from the heating mantle and allowed to cool to room temperature. The excess starting materials were removed by adding methanol to the crude QDs solution and the

obtained precipitate was centrifuged. The precipitate separated by centrifugation was dissolved in chloroform to obtain fluorescent CdSe QDs. The CdSe QDs with different stoichiometry were synthesized by maintaining the same amount of CdO but varying the amount of Se.

2.2.4. Quantum dots in polar media

Water soluble mercapto acid-capped CdTe QDs were prepared by following reported procedure.⁴ For instance, 3-MPA-capped CdTe QDs were prepared by adding 0.5 M methanolic solution of 3-MPA-KOH (20 mol % excess KOH) slowly to the CdTe QDs dissolved in CHCl₃ until the particles flocculate. The precipitate was separated by centrifugation and dissolved in water to obtain the fluorescent CdTe QDs.

2.2.5. Quantum dots in ionic liquid

MUIM-capped CdTe QDs were also prepared by following a reported procedure.¹ A CHCl₃ solution of MUIM (0.05 M) was added slowly to a CHCl₃ solution of CdTe QDs until the particles flocculate. The precipitate was separated by centrifugation and dissolved in [bmim][PF₆] to obtain fluorescent CdTe QDs for studies in ILs.

2.3. Methods for the purification of conventional solvents

Solvents used for the purification and solubility of QDs and ligands were dried following standard procedures available in the literature.⁶

2.3.1. Methanol and ethanol

Initially, Mg turnings (~5 g) and iodine (~0.2 g) were added to the alcohol (80-100 mL) and refluxed for 3-4 h and later distilled under moisture free conditions.

2.3.2. Chloroform

The solvent (~50 mL) was stirred overnight after adding calcium chloride (~5 g) and then distilled under moisture free conditions.

2.3.3. Acetone

The solvent (~50 mL) was first refluxed for 3-4 h with anhydrous phosphorus pentoxide (~3 g) and then distilled under dry conditions.

2.3.4. Water

Milli-Q water used for sample preparation was obtained from Millipore, Synergy Pack.

2.4. Purification of IL

Prior to use, [bmim][PF₆] stored in a desiccator was dried under high vacuum (pressure $10^{-2} - 10^{-3}$ mbar) for ~ 10 h to minimize the water content.

2.5. Sample Preparation

2.5.1. Steady state and time-resolved absorption and emission measurements

For the steady state absorption and steady state and time-resolved emission measurements, the absorbance (1 cm thickness cuvette) of the QDs dissolved in conventional solvents and ILs was maintained around 0.15-0.3 (at the excitation wavelength), to avoid inner filter effect. During these measurements, the cuvette containing the QDs solution was sealed with septum and parafilm. For ultrafast transient absorption measurements, the absorption of the QDs solution was maintained around 0.7-1.0 (at the excitation wavelength).

2.5.2. Transmission electron microscopy (TEM) measurements

The samples were prepared by drop casting the QDs dissolved in conventional solvents and ILs on carbon-coated copper grids followed by evaporation of the solvent under high vacuum.

2.5.3. Inductively coupled plasma-optical emission spectrometer (ICP-OES)

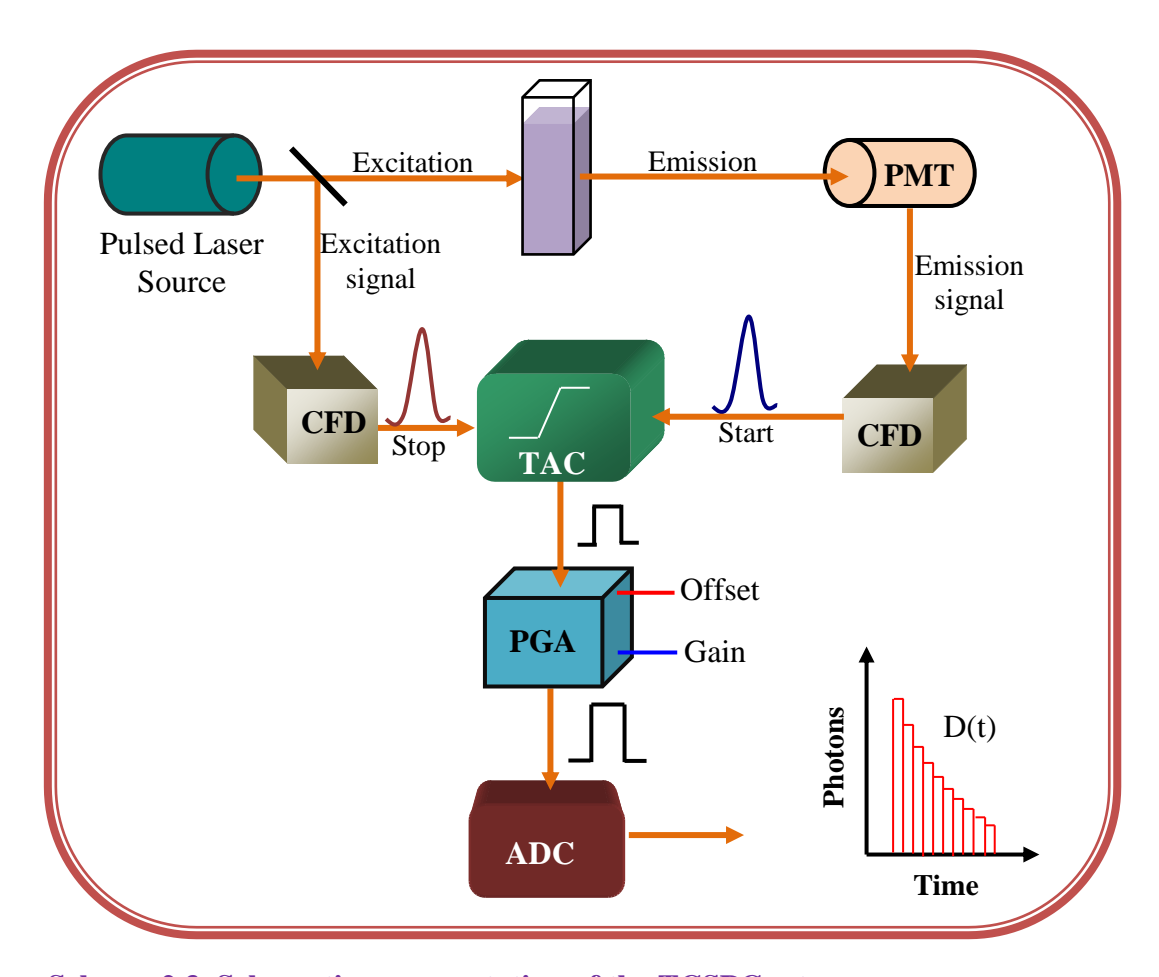
Sample for determination of the compositions of the Cd⁺² and Se⁻² ions of the CdSe QDs by this method was prepared by dissolving the QDs (~ 0.0238 g) in 10 mL of aqua regia (1:3 by volume, HNO₃/HCl).

2.6 Instrumentation and data analysis

The sizes of the QDs were estimated using Tecnai G2 FE1 F12 transmission electron microscope at an accelerating voltage of 200 kV. The compositions of the Cd⁺² and Se⁻² ions of the CdSe QDs were determined using Varian Model Liberty Series inductively coupled plasma-optical emission spectrometer. ¹H and ¹³C NMR spectra for the MBA ligand were recorded using Bruker AVACE 400 MHz NMR spectrometer. Steady state absorption and emission spectra of the samples were recorded using UV-vis spectrophotometer (Cary 100. Varian) spectrofluorimeter (Fluorolog 3, Horiba Jobin Yvon), respectively. The details of other instruments like time-correlated single photon counting fluorimeter and femtosecond pump-probe setup employed in these studies are discussed below.

2.6.1. Time-correlated single photon counting fluorimeter

Time-resolved fluorescence decay profiles were recorded using time-correlated single photon counting (TCSPC) fluorimeter (Horiba Jobin Yvon IBH). The schematic diagram of the experimental setup is shown in Scheme 2.3. A laser source simultaneously excites the sample and sends an excitation signal to the constant fraction discriminator (CFD). The CFD which measures the time corresponding to the photons detected due to the emission of the sample sends a signal to the time-to-amplitude converter (TAC) to start the voltage ramp. The second CFD placed after the laser source receives the reference pulse from the excitation source and sends the pulse to TAC to stop the voltage ramp. The output



Scheme 2.3. Schematic representation of the TCSPC setup.

voltage from the TAC decreases as the arrival times of the emission photons increases. The voltage from TAC is amplified using programmable gain amplifier (PGA) and further converted to a numerical value by analog-to-digital converter (ADC). This numerical value representing the photon detection time is stored as a single event. The above process is repeated several times to construct the histogram of fluorescence intensity over time.

In the present study, Nano LED (439 nm, 1 MHz repetition rate, and 150 ps pulse width) was used as the excitation source and an MCP photomultiplier tube (PMT, Hamamatsu R3809U-50) as the detector. The instrument response function (IRF) containing the pulse shape of the excitation source was recorded by placing a

dilute solution of Ludox (acts as scatter) inside the sample chamber.

2.6.1.1. Data Analysis

The lifetimes of the samples were estimated from the measured emission decay profiles and the instrument response function using a nonlinear least-square iterative fitting procedure (decay analysis software IBH DAS6, Version 2.2). In general, the fluorescence intensity decay of the excited molecules can be expressed as⁷

$$I(t) = I_0 e^{-t/\tau} \tag{2.1}$$

where, I_0 is the intensity at t = 0 and τ represents the lifetime and is given by

 $\tau = 1/(k_r + k_{nr})$ with k_r and k_{nr} as the radiative and non-radiative decay rate constants, respectively and in case of multi-exponential decay, I(t) is expressed as

$$I(t) = \sum_{i=1}^{n} a_i e^{-t/\tau}$$
 (2.2)

where a_i and τ_i represent the amplitude and lifetime of the i^{th} component, respectively.

The measured decay profile containing the actual fluorescence decay and lamp profile is represented as⁸

$$D(t) = \int_{0}^{t} P(t')G(t-t')dt'$$
 (2.3)

where, D(t) is the measured fluorescence intensity at any given time t, P(t') is the IRF and G(t-t') is the actual emission decay function of the sample.

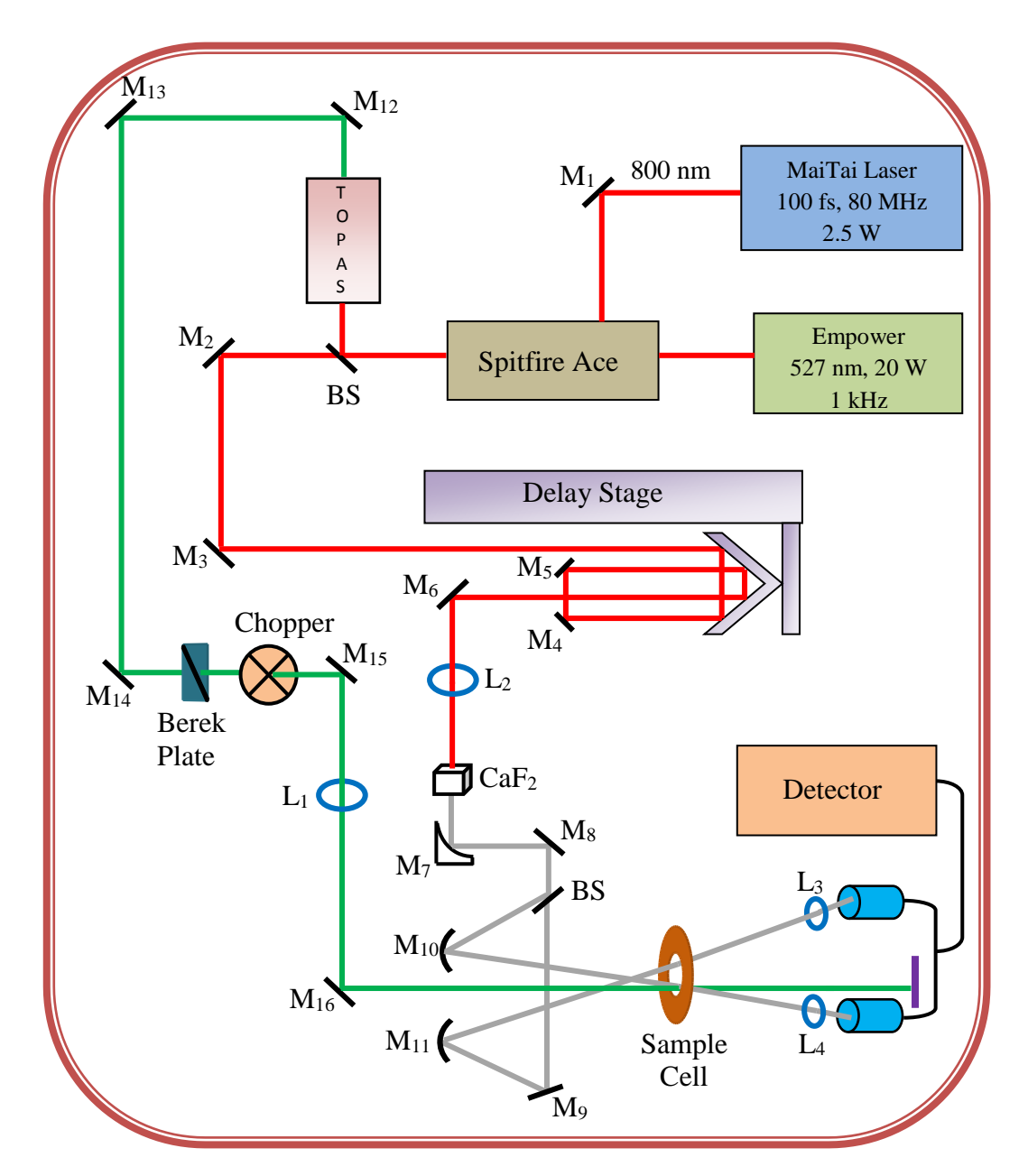
To obtain the actual fluorescence lifetime of the sample, it is essential to deconvolute the IRF from the measured decay profile. The deconvolution of the IRF was done by mixing it with a projected decay to generate a new reconvoluted set. The calculated data was then compared with the measured decay and the difference between the two were added over all the time points to estimate the χ^2 (goodness-of-fit) for the fit. The deconvolution process continued through a series

of iterations till no significant change of χ^2 occurred.

2.6.2 Femtosecond pump-probe setup

The ultrafast transient absorption measurements were performed using a femtosecond time-resolved collinear pump-probe setup (Scheme 2.4). The laser systems (Spectra Physics) of this setup consisted of a mode-locked Ti-sapphire oscillator (seed laser, Mai-Tai), which produced femtosecond pulses (fwhm <100 fs, ~ 2.5 W at 80 MHz) with a wide tunable range of 690-1040 nm. The seed pulse centered around 800 nm was directed to a regenerative amplifier (Spitfire Ace), which was pumped by a frequency-doubled Nd:YLF laser (Empower) at 527 nm. The major output (~75%) from the amplifier (800 nm, <100 fs, 1 kHz, pulse energy ~4.2 mJ) was made to pass through an optical parametric amplifier (TOPAS-Prime) to obtain a wide wavelength tuning range of 290-2600 nm. The output from TOPAS was directed to the transient absorption spectrometer (Excipro, CDP System) and used as the excitation source for the sample. The remaining (25%) portion of the amplifier output was allowed to pass through an optical delay line of 4 ns with a minimum step resolution of 1.5625 fs and then through a rotating CaF₂ crystal to generate a white light continuum (WLC). The white light was split into two parallel beams as probe and reference by using a beam splitter and then projected on to the rotating quartz sample cell. The pump and probe beams were focused on to the sample cell of 1 mm path length by maintaining an angle of less than 5° for better overlap. The transmitted probe and reference beams were directed through an optical fiber to a polychromator and then detected by a pair of photodiode arrays. The difference in optical density of the sample probed by WLC in the presence and absence of excitation pump was analyzed by ExciPro software (CDP Systems). Two-photon absorption (TPA) signal of ethanol was used for the estimation of the time resolution and the 'time zero'. The instrumental resolution after chirp correction was found to be ~ 80 fs. The overall chirp in WLC spectrum was applied to remove the group velocity

dispersion (GVD) effect from the measured data for correct analysis. To improve the signal to



Scheme 2.4. Schematic representation of the femtosecond pump-probe setup (M-mirror, BS-beam splitter and L-Lens)

Materials, Methods...

noise ratio we recorded the spectrum and kinetics with a large number of averaging. To avoid the non-linear interactions between the photo-generated carriers, the transient absorption studies were performed at low pump energy ($< 0.5 \, \mu J$). The average number of electron-hole pairs excited per nanocrystal (N_{e-h}) was calculated to be less than 0.1. The N_{e-h} was estimated using the following relation.^{9,}

$$N_{e-h} = j_p \sigma_a \tag{2.4}$$

where, jp represents the pump fluence (photon per cm²) and σ_a is the nanocrystal absorption cross section (cm²).

2.6.2.1. Data Analysis

The transient absorption spectra were plotted using Origin 8 software. The lifetimes of the species were measured in a similar way as in TCSPC data analysis using nonlinear least-square iterative fitting procedure (IGOR-Pro Software).

2.7. Measurement of emission quantum yield

The fluorescence quantum yields (QY) of the CdTe QDs and CdSe QDs dissolved in aqueous and chloroform medium, respectively, were determined from the QY of the reference compound (rhodamine 6G in ethanol)^{11, 12} using the following equation¹³

$$QY_S = QY_R \left[\frac{I_S \times O.D_R \times n_S^2}{I_R \times O.D_S \times n_R^2} \right]$$
 (2.5)

where, I is the integrated area of the emission spectrum, OD and n represent the optical density at the excitation wavelength and refractive index of the solvent, respectively. The subscript S and R refer to the sample and reference, respectively.

2.8. Determination of the size and concentration of the QDs in solution

The sizes (diameter, D (nm)) of the CdTe and CdSe QDs and their

Chapter 2

concentration were determined using the empirical equations proposed by Peng and co-workers, ¹⁴ given by

$$D_{CdTe} = (9.8127 \text{ X } 10^{-7}) \lambda^3 - (1.7147 \text{ X } 10^{-3}) \lambda^2 + (1.0064) \lambda - (194.84)$$
 (2.6)

$$D_{CdSe} = (1.6122 \text{ X } 10^{-9}) \lambda^4 - (2.6575 \text{ X } 10^{-6}) \lambda^3 + (1.6242 \text{ X } 10^{-3}) \lambda^2 - (0.4277) \lambda + (41.57)$$
(2.7)

where λ is the wavelength at the first exciton absorption peak maximum.

The estimated sizes of the QDs using above equations were well matched with the sizes of the QDs determined from the TEM measurements.^{1, 15} Further, the extinction coefficients (ϵ) of these materials at the first exciton absorption peak maximum were calculated from their sizes using

$$\varepsilon_{\text{CdTe}} = 10043 \text{ (D)}^{2.12}$$
 (2.8)

$$\varepsilon_{\text{CdSe}} = 5857 \text{ (D)}^{2.65}$$
 (2.9)

The concentration of the QDs in the solution was measured from the absorbance using the calculated ϵ values.

2.9. Error Limits

Typical error limits of the experimentally measured values

$$\lambda_{max}$$
 (abs/flu) = ± 2 nm
QY = ± 2 %
 τ (fluorescence) = ± 5 %
QD Size (D/nm) = $\pm 5 - 10$ %

The error limits of the lifetime parameters and their amplitudes obtained from the ultrafast transient absorption measurements are indicated in the following chapters where the experimental results are presented.

Materials, Methods...

References

- 1. Santhosh, K.; Samanta, A., J. Phys. Chem. C 2012 116, 20643.
- 2. Fang, T.; Ma, K.; Ma, L.; Bai, J.; Li, X.; Song, H.; Guo, H., *J. Phys. Chem. C* **2012,** 116, 12346.
- 3. Stevens, M. C.; Tarbell, S. D., J. Org. Chem. 1954, 19, 1996.
- 4. Wuister, S. F.; Swart, I.; Driel, F. V.; Hickey, S. G.; Donega, D. D. M., *Nano. Lett.* **2003**, 3, 503.
- 5. Kloper, V.; Osovsky, R.; Olesiak, J. K.; Sashchiuk, A.; Lifshitz, E., *J. Phys. Chem. C* **2007**, 111, 10336.
- 6. Perrin, D. D.; Armarego, W. L. F.; Perrin, D. R., Purification of Laboratory Chemicals. Pergamon Press: New York. **1980**.
- 7. Lakowicz, J. R., Principles of Fluorescence Spectroscopy, Second ed.; Kluwer Academic/Plenum Publishers. **1999**.
- 8. O'Connor, D. V.; Ware, W. R.; Andre, J. C., J. Phys. Chem. C 1979, 83, 1333.
- 9. Nirmal, M.; Brus, L., Acc. Chem. Res. 1999, 32, 407.
- 10. Murphy, S.; Huang, L., J. Phys.: Condens. Matter 2013, 25, 144203.
- 11. Fischer, M.; Georges, J., Chem. Phys. Lett. 1996, 260, 115.
- 12. Brouwer, M. A., Pure Appl. Chem. **2011**, 83, 2213.
- 13. Austin, E.; M.Gouterman, *Bioonorg. Chem.* **1978,** 9, 281.
- 14. Yu, W. W.; Qu, L.; Guo, W.; Peng, X., Chem. Mater. 2003, 15, 2854.
- 15. Sekhar, M. C.; Samanta, A., J. Phys. Chem. C 2015, 119, 15661.

CdTe Quantum Dots in Ionic Liquid: Stability and Hole Scavenging in the Presence of a Sulfide Salt

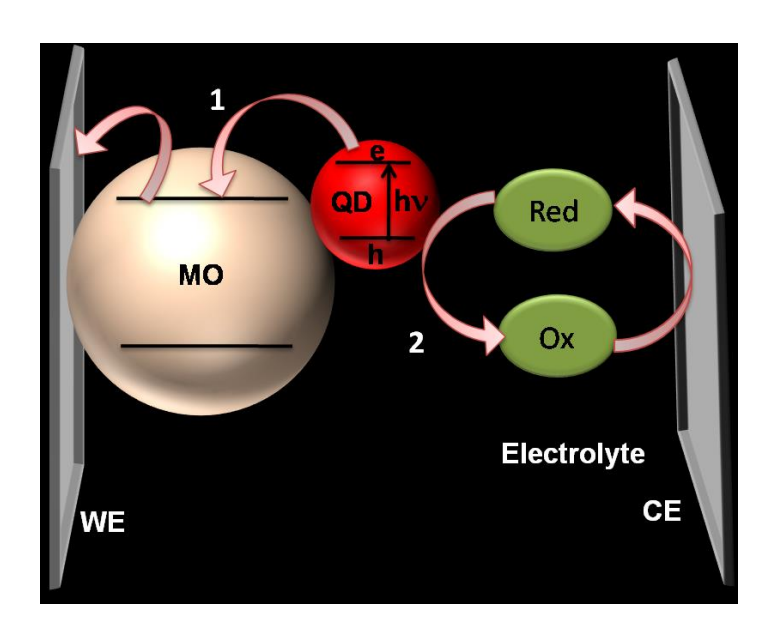
The light harvesting properties of both CdSe and CdTe nanocrystals are ideally suited for their use in quantum dot (QD) sensitized solar cells. However, corrosion of the CdTe QD in an aqueous environment in the presence of sulfide/polysulfide electrolyte renders it unsuitable despite its better electron injection ability (compared to CdSe QD) to a large bandgap semiconductor like TiO₂. In this work, we explore the stability of a CdTe QD, which we have developed exclusively for its liquids, in ionic in 1-butyl-3-methylimidazolium use hexafluorophosphate ionic liquid in the presence of S²⁻ and investigate the hole transfer process from this photo-excited QD to S²⁻. We not only demonstrate that an appropriate capping of the CdTe QD and use of an ionic liquid in place of the aqueous medium enhances the stability of the QD significantly in the presence of S²⁻, but also provide evidence of hole transfer from a photo-excited QD to the sulfide salt using steady state and time-resolved emission and ultrafast transient absorption measurements.

3.1. Introduction

Considerable attention is being paid in recent years to the photovoltaic devices to meet our ever increasing demand of energy using renewable energy sources. Dye-sensitized solar cells (DSSCs) are considered to be the tools for capturing and converting solar energy into electrical energy despite their poor conversion efficiency.² In DSSCs, a dye molecule harvests the solar energy and injects the photo-generated electron to a large band gap semiconductor like TiO₂ or ZnO, which subsequently transfers it to a working electrode.^{2,3} Colloidal quantumconfined semiconductor nanoparticles, commonly termed as quantum dots (QDs), have become promising alternatives to the molecular dyes in solar cells because of their high molar extinction coefficient (10⁴ to 10⁶ M⁻¹ cm⁻¹ at the first exciton transition range), broad absorption, and size-dependent tunability of the bandgap.⁴⁻ ²⁰ Metal chalcogenide based quantum dots, such as CdSe, CdTe, PbS, and PbSe, which have small band gaps, are considered to be ideal sensitizers for harvesting the solar energy in the visible and infrared regions. 12, 21, 22 The energy conversion efficiency of the quantum dot sensitized solar cells (QDSSCs) is mainly governed by the rates of (i) transfer of photo-generated electron to the large band gap semiconductors like TiO₂ or ZnO and its subsequent transfer to the working electrode, and (ii) scavenging of the hole by the redox electrolyte and regeneration of the latter at the counter electrode (Scheme 3.1). Even though the overall power conversion efficiency (reported to be $\sim 6-7\%$)¹³⁻¹⁵ in the QDSSCs is well below that in dye sensitized solar cells (11%),²³ the multiple exciton generation possibility in QDs can boost the energy conversion efficiency of the QDSSCs significantly. 16, 24, 25 As an understanding of the dynamics of electron and hole transfer of the QDs with TiO₂ and a hole scavenger, respectively, is key to improving this efficiency, considerable importance is being given to this aspect in recent years. 17-19 Kamat and coworkers recently found that even though the rate of

CdTe QDs in ionic liquid.....

electron injection to TiO₂ from CdTe QDs is higher by an order of magnitude compared to CdSe QDs,¹⁷ the former is unsuitable in these applications due to its degradation in the presence of very commonly used hole scavenger, sulfide ion, in an aqueous environment.^{17,26}



Scheme 3.1. Functioning of a QDSSC: 1) photo-induced electron injection to a large band gap metal oxide (MO) and its transfer to the working electrode (WE), 2) hole scavenging by the redox electrolyte and its regeneration at the counter electrode (CE).

This drawback of the CdTe QDs can be addressed either by employing a hole scavenger other than S^{2-} (that does not corrode the QDs) or by using a medium in which the hole transfer process is much faster than the corrosion process. Earlier attempts with redox couples such as I_3^{-}/I , ferrocene/ferrocene⁺, $K_4Fe(CN)_6/K_3Fe(CN)_6$ with or without KCN, however, were found to be ineffective, and rapid corrosion of CdTe QDs could not be prevented. ¹⁷ Herein, we explore the alternative strategy of finding a medium that provides enhanced stability to the QDs and at the same time allows hole scavenging by S^{2-} . It is in this

context we evaluate the suitability of an ionic liquid (IL) in place of the aqueous environment.

The ILs, which are salts comprising large ionic constituents having melting point below 100 °C, are often regarded as better alternatives to the conventional solvents for their negligible vapor pressure, high thermal stability, and ability to dissolve large number of inorganic and organic compounds. ²⁷⁻²⁹ High ionic conductivity, wide electrochemical window, and low reactivity have made the ILs popular electrolytes for lithium-ion batteries and fuel cells. ^{30, 31} ILs are also being considered as alternative media in dye/QD sensitized solar cells. ^{20, 32, 33}

$$\begin{array}{c} & & & \\ & &$$

Chart 3.1. Structure of the ligand used in the present study.

As CdSe or CdTe QDs with conventional capping agents are insoluble in ILs, it is necessary to cap these QDs with specific agents for their use in ILs. Recently, we have developed an appropriate ligand (thiol-functionalized imidazolium ionic liquid, MUIM) capped CdTe QD, essentially a QD-IL hybrid (Chart 3.1), which dissolves both in hydrophobic and hydrophilic ILs and provides a greater stability to the QD in ILs.³⁴ In this work, we have employed 1-butyl-3-methylimidazolium

CdTe QDs in ionic liquid.....

hexafluorophosphate, [bmim][PF₆], as the IL (primarily for its excellent optical transmission properties³⁵) to study the stability of this CdTe QD in presence of S^{2-} and hole scavenging of the photo-excited QD by S^{2-} using steady state and time-resolved fluorescence and ultrafast pump-probe measurements.

3.2. Results and Discussion

3.2.1. Steady state and time-resolved experiments

The absorption and emission spectra of the CdTe QD in [bmim][PF₆] are shown in Figure 3.1. The first exciton band absorption maximum of the QD is observed at ~ 510 nm and the emission maximum at ~ 560 nm. The average size of the CdTe QDs estimated from the first exciton band maximum using Peng's

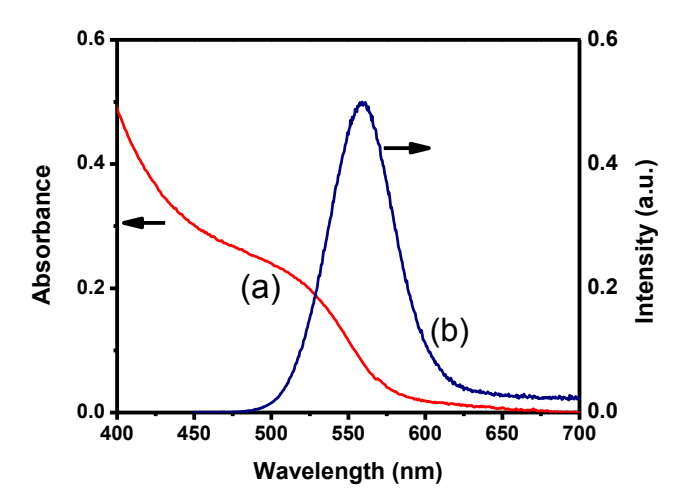


Figure 3.1. Absorption (a) and emission (b) spectra of CdTe QDs in $[bmim][PF_6]$.

equation⁴ is 2.55 nm. Our attempts to determine the size of the QDs by TEM measurements were unsuccessful as clear images could not be obtained due to incomplete removal of the ionic liquid owing to its nonvolatility.

As can be seen from Figure 3.2, addition of Na₂S leads to slight broadening

of the first exciton band of the QD in [bmim][PF₆] perhaps due to the formation of a shell of CdS resulting from the interaction of the sulfide ion with the surface Cd^{+2} .¹⁸ The stability of the QD in [bmim][PF₆] in presence of the sulfide salt is evident from a comparison of the absorption spectra of the QD at different times after addition (shown in Figure 3.2b). Negligible change of the spectrum in presence of S^{2-} even after 72 h indicates no decomposition of the QD in IL. This observation is in stark contrast with the earlier studies of the CdTe QD in aqueous environment in presence of S^{2-} where rapid corrosion was observed.^{17, 26}

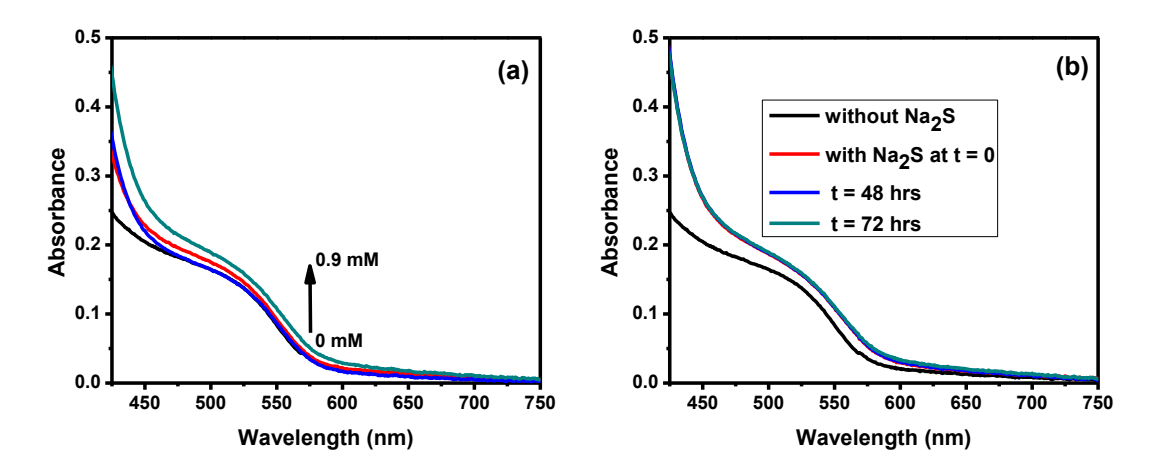


Figure 3.2. (a) Absorption spectra of CdTe QDs in [bmim][PF₆] with increasing concentration of Na₂S (0, 0.3, 0.6 and 0.9 mM). (b) Absorption spectra of the CdTe QDs in [bmim][PF₆] before and after addition of 0.9 mM Na₂S at different times.

The photoluminescence spectra of CdTe QD in [bmim][PF₆] in the presence of various quantity of Na₂S are shown in Figure 3.3. A drastic sulfide salt induced quenching of the emission of CdTe QDs is likely due to the scavenging of the hole of photo-excited CdTe by well-known hole scavenger, sulfide ion^{17, 26} and as can be seen from the energetics of the system (Figure 3.4), the hole transfer process is thermodynamically feasible.

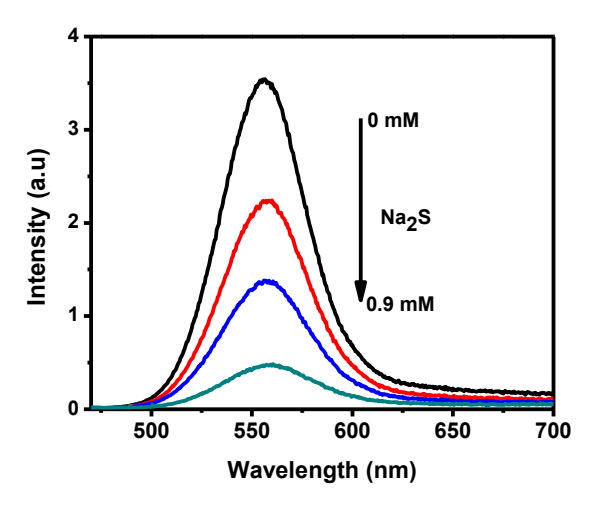


Figure 3.3. Photoluminescence spectra of CdTe QDs in [bmim][PF₆] with increasing concentration of Na₂S (0, 0.3, 0.6 and 0.9 mM). λ_{exc} = 439 nm.

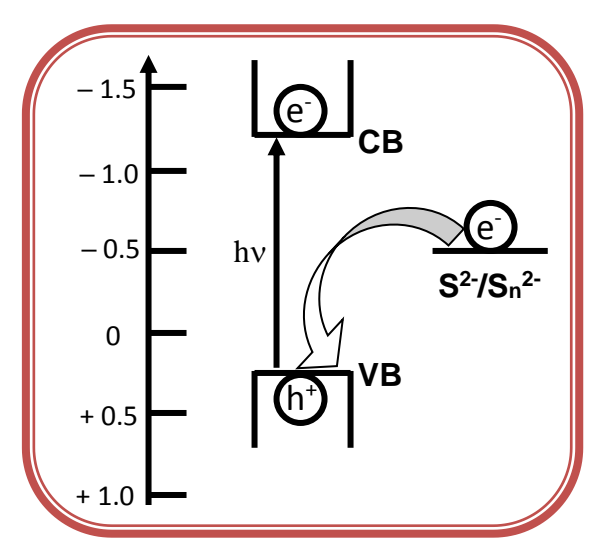


Figure 3.4. Potential Energy diagram of bulk conduction band (CB) and valence band (VB) potentials of CdTe and oxidation potential of S^{2-}/S_n^{2-} (vs NHE). The bulk conduction, valence band potential of CdTe QDs and oxidation potential of sulfide/polysulfide are measured to be at -1.25 V, + 0.25 V and -0.5 V (vs. NHE), respectively^{17, 26} One should note that for highly confined CdTe QDs, the actual separation between the VB and CB levels is much larger than what is shown here.

Chapter 3

The time-resolved fluorescence behavior of the QDs in the absence and in presence of various quantities of Na₂S is studied by monitoring the decay profiles at 560 nm. The emission intensity versus time profiles (Figure 3.5) were fitted to a tri-exponential function of the form, I(t) = $a_1 \exp(-t/\tau_1) + a_2 \exp(-t/\tau_2) + a_3 \exp(-t/\tau_3)$, to obtain the decay parameters, which are presented in Table 3.1, along with the average lifetime $<\tau_a>$, defined by $(a_1\tau_1 + a_2\tau_2 + a_3\tau_3)/(a_1 + a_2 + a_3)$. The measured decay parameters of the QDs in

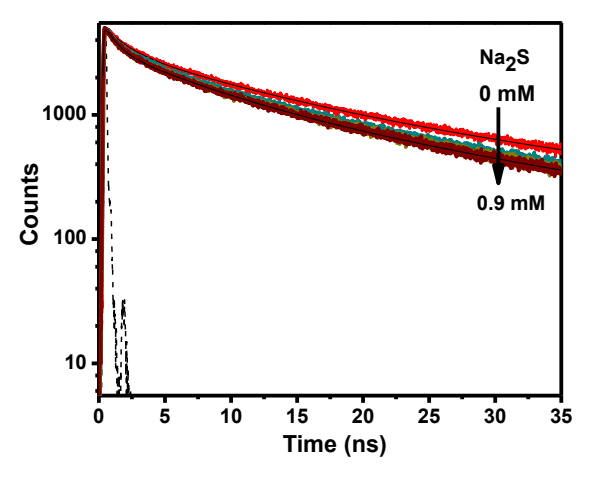


Figure 3.5. Emission decay profiles of CdTe QDs in [bmim][PF₆] in the absence and in presence of different quantities of Na₂S (0.3, 0.6 and 0.9 mM).

Table 3.1. Fluorescence decay parameters \dagger and estimated $<\tau_a>$ of the CdTe QDs in [bmim][PF₆].

Na ₂ S (mM)	τ ₁ (a ₁)	τ ₂ (a ₂)	τ ₃ (a ₃)	$<\tau_{ m a}>$
0	9.10 (0.40)	29.66 (0.27)	1.59 (0.33)	12.17
0.3	7.79 (0.36)	25.63 (0.28)	1.23 (0.36)	10.42
0.6	7.00 (0.44)	24.09 (0.23)	0.99 (0.33)	8.95
0.9	6.92 (0.40)	23.80 (0.20)	0.94 (0.40)	7.91

[†]The lifetime values are expressed in ns

CdTe QDs in ionic liquid.....

the absence of S^{2-} are in good agreement with the literature.³⁶⁻³⁸ Based on literature, the short (1 ns) and the long (~29 ns) lifetime components are believed to be due to the involvement of deep and shallow trap states respectively, in carrier recombination,³⁶ the ~9 ns component to intrinsic recombination of the core states of CdTe ODs.^{39, 40}

The emission quenching of CdTe QDs in [bmim][PF₆], as evident from both steady state and time-resolved studies, is in contrast with the observation made in aqueous environment.¹⁷ Kamat & coworkers observed an increase in the $<\tau_a>$ value of the CdTe QDs on addition of Na₂S in aqueous solution.¹⁷ Interestingly, for CdSe QDs, they observed a decrease of the $<\tau_a>$ value in the presence of Na₂S and attributed it to the hole transfer between photoexcited CdSe QD and sulfide ion.¹⁷ On the basis of the similarity of this finding with ours we attribute the decrease of the $<\tau_a>$ value of CdTe QDs with increasing concentration of sulfide ion in [bmim][PF₆] to the scavenging of the holes of photo-excited CdTe QDs by S²⁻. The fact that, in the presence of 0.9 mM of Na₂S the observed quenching (\sim 85%) of the steady state fluorescence intensity is considerably higher than that evident from the lifetime data implies that a significant contribution of the quenching comes from the static interaction between the quenching partners.

3.2.2 Ultrafast transient absorption measurements

The time-resolved difference absorption spectra of CdTe QDs in [bmim][PF₆] at indicated time delays following 370 nm excitation are shown in Figure 3.6. The spectra are characterized by strong bleach centered at 510 nm and a transient absorption in the 530–580 nm region. The bleach around 500-510 nm, which corresponds to the first exciton absorption band of the system (Figure 3.1), is clearly due to CdTe $\xrightarrow{h\nu}$ CdTe* (e + h) transition. The positive absorption in the 540-580 nm region arises due to the trapped carriers.⁴¹

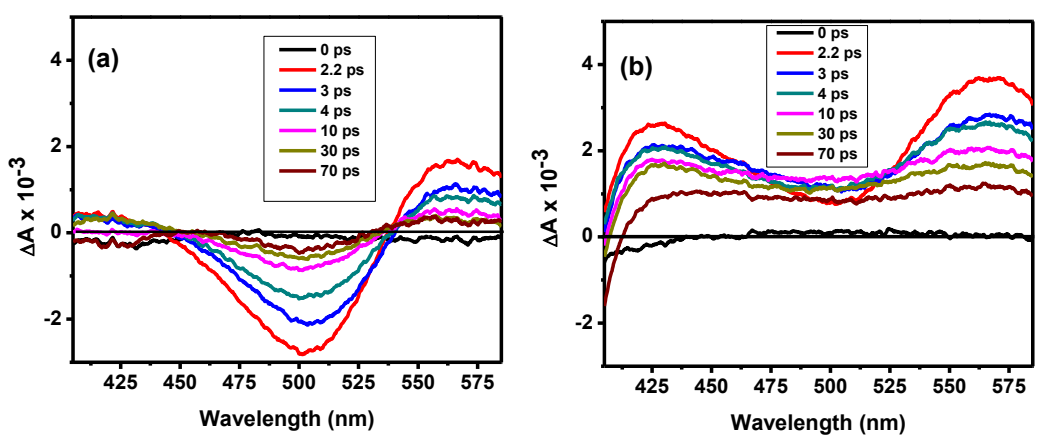


Figure 3.6. Transient absorption spectra of CdTe QDs (4 μ M) in [bmim][PF₆] in the (a) absence and (b) presence of Na₂S (2.7 mM) at different delay times after 370 nm excitation.

In the presence of S^{2-} (Figure 3.6), the bleach portion of the spectrum disappears completely and a strong absorption covering almost the entire region with two well-defined peaks at around 430 and 570 nm and a dip in the 500-510 nm region at the early timescale is observed. The spectra levels off into a broad positive absorption at longer timescales. As the CdTe QD excitonic transition bleach around 500-510 nm is recovered within 70 ps (panel (a) of Figure 3.6), the dip in the positive absorption in presence of S^{2-} at early times is due to both broad positive absorption and the CdTe QD excitonic bleach, where the latter contribution disappears at longer time scales.

In the event of scavenging of the photo-generated hole of CdTe QD by S^{2-} one expects formation of S^{-} and various polysulfide radicals according to the following reaction scheme.

$$CdTe \xrightarrow{h\nu} CdTe^* (e + h)$$
 (3.1)

$$CdTe^* (e + h) + S^{2-} \longrightarrow CdTe (e) + S^{-\bullet}$$
 (3.2)

$$S^{-\bullet} + nS^{2-} \longrightarrow S_{n+1}^{-\bullet}$$
 (3.3)

Considering that the polysulfides absorb in the 400-600 nm region [λ_{max} = 400 nm ($S_2^{-\bullet}$), 580-600 nm ($S_3^{-\bullet}$), and 513 nm ($S_4^{-\bullet}$)] we attribute the absorption around 430 nm to $S_2^{-\bullet}$, 510 nm to $S_4^{-\bullet}$, the one around 570 nm to $S_3^{-\bullet}$.^{18, 42, 43} The bleach due to excitonic transition could not be observed around 510 nm in the presence of $S_4^{-\bullet}$ due to strong absorption of $S_4^{-\bullet}$.

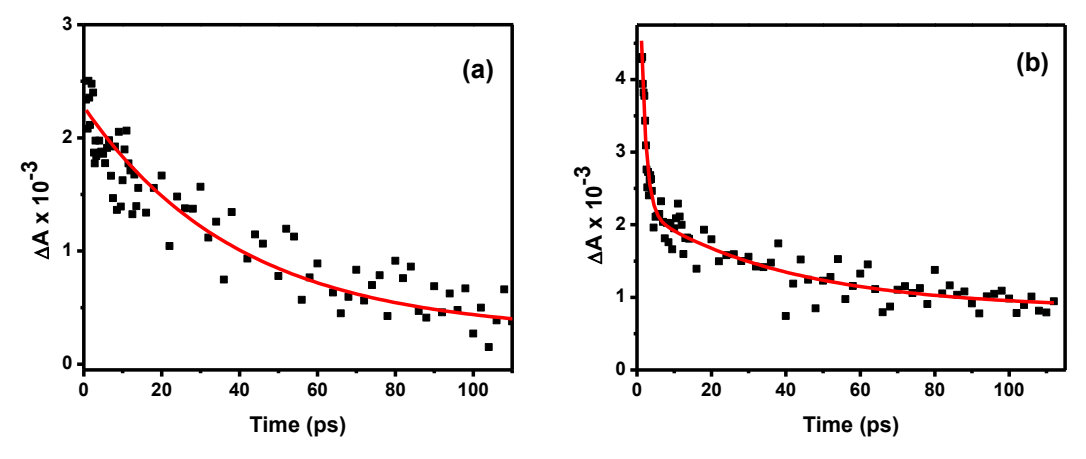


Figure 3.7. Transient absorption decay kinetics of CdTe QDs (4 μ M) in [bmim][PF₆] in the presence of Na₂S (2.7 mM) at 430 nm (a) and 580 nm (b).

The absorption due to $S_2^{-\bullet}$ at 430 nm decays rapidly with a time constant of 35 ± 7 ps in the presence of 2.7 mM S^{2-} primarily due to rapid recombination of $S_2^{-\bullet}$ with CdTe*(e) as illustrated in equation (3.4). We do not consider Chakrapani et. al.'s observation of a much longer lifetime (few microseconds) of $S_2^{-\bullet}$ surprising as their work was carried out also in the presence TiO_2 .¹⁸ The electron CdSe*(e) generated in their case was rapidly injected into TiO_2 and hence, the lifetime of the sulfide radical was determined primarily by the rate of recombination of the electrons in TiO_2 with the $S_{n+1}^{-\bullet}$ (equation 3.5). ¹⁸

$$CdTe^* (e) + S_2^{-\bullet} \longrightarrow CdTe + S_2^{2-}$$
 (3.4)

$$TiO_2(e^-) + S_{n+1}^{-\bullet} \longrightarrow TiO_2 + S_{n+1}^{2-}$$
 (3.5)

The decay kinetics at 580 nm is found to be biexponential with lifetime components of 1.3 ± 0.2 and 36 ± 8 ps indicating the presence of two species. As the 530-580 nm absorption in the absence of sulfide salt due to the trapped carriers⁴¹ has a lifetime of 1.3 ± 0.1 ps (Figure 3.8), the 36 ps component in the presence of S^{2-} can be attributed to S_3^{--} species, which absorbs in this region. The fact that in the presence of S^{2-} no long-lived transient species could be observed implies that the various species generated through reaction (3.1) - (3.5) cannot escape out of the cage of the solvent molecules/ions in viscous IL.

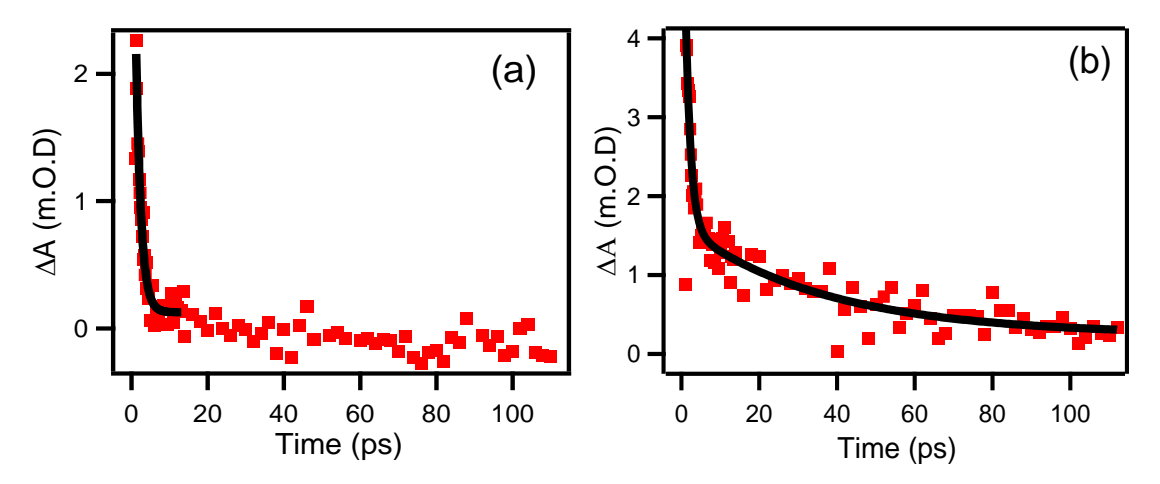


Figure 3.8. Transient absorption decay kinetics of CdTe QDs (4 μ M) monitored at 580 nm in the absence (a) and in presence (b) of 2.7 mM Na₂S in [bmim][PF₆]. The kinetic data were fitted to Δ A (t) = c + a₁ exp (-t/ τ ₁) + a₂ exp (-t/ τ ₂) and the fitting parameters are presented in Table 3.2.

CdTe QDs in ionic liquid.....

Table 3.2. Transient absorption decay parameters of CdTe QDs in [bmim][PF6]

System	$\tau_1 (ps)$	$\mathbf{a_1}$	τ ₂ (ps)	\mathbf{a}_2
CdTe (4 µM)	1.32 ± 0.08	-	-	-
$CdTe + Na_2S (2.7 mM)$	1.32 ± 0.15	0.85 ± 0.09	36.53 ± 8.50	0.15 ± 0.01

3.3. Conclusion

It is shown that a greater stability to the CdTe nanocrystals can be imparted and the photo-generated holes of the CdTe QDs can be scavenged by S²⁻ employing ionic liquid as a medium and by appropriate capping of the QDs. The results reported herein seem to provide a route to overcoming some of the drawbacks of otherwise efficient light harvester and electron injector CdTe nanocrystals that restrict its likely use in quantum dot sensitized solar cells.

Chapter 3

References

- 1. Nayak, P. K.; Garcia-Belmonte, G.; Kahn, A.; Bisquert, J.; Cahen, D., *Energy Environ.* **2012**, 5, 6022.
- 2. Hagfeldt, A.; Boschloo, G.; Sun, L.; Kloo, L.; Pettersson, H., *Chem. Rev.* **2010,** 110, 6595.
- 3. Jensen, R. A.; Ryswyk, H. V.; She, C.; Szarko, J. M.; Chen, L. X.; Hupp, J. T., *Langmuir* **2010**, 26, 1401.
- 4. Yu, W. W.; Qu, L.; Guo, W.; Peng, X., Chem. Mater. 2003, 15, 2854.
- 5. Buhbut, S.; Itzhakov, S.; D.Oron; Zaban, A., J. Phys. Chem. Lett. 2011, 2, 1917.
- 6. Hodes, G., J. Phys. Chem. C 2008, 112, 17778.
- 7. Hod, I.; Gonzalez-Pedro, V.; Tachan, Z.; Fabregat-Santiago, F.; Mora-Sero, I.; Bisquert, J.; Zaban, A., *J. Phys. Chem. Lett.* **2011,** 2, 3032.
- 8. Kamat, P. V., J. Phys. Chem. C 2008, 112, 18737.
- 9. Nozik, A. J., *Physica E* **2002**, 14, 115.
- 10. Kamat, P. V.; Tvrdy, K.; Baker, D. R.; Radich, J. G., Chem. Rev. 2010, 110, 6664.
- 11. Nozik, A. J.; Beard, M. C.; Luther, J. M.; Law, M.; Ellingson, R. J.; Johnson, J. C., *Chem. Rev.* **2010**, 110, 6873.
- 12. Kamat, P. V., J. Phys. Chem. Lett. **2013**, 4, 908.
- 13. Pan, Z. X.; Zhao, K.; Wang, J.; Zhang, H.; Feng, Y. Y.; Zhong, X. H., *ACS Nano* **2013**, 7, 5215.
- 14. Lee, J. W.; Son, D. Y.; Ahn, T. K.; Shin, H. W.; Kim, I. Y.; Hwang, S. J.; Ko, M. J.; Sul, S.; Han, H.; Park, N. G., *Sci. Rep.* **2013**, 3, 1050.
- 15. Wang, J.; Mora-Sero, I.; Pan, Z.; Zhao, K.; Zhang, H.; Feng, Y.; Yang, G.; Zhong, X.; Bisquert, J., *J. Am. Chem. Soc.* **2013**, 135, 15913.
- 16. Semonin, O. E.; Luther, J. M.; Choi, S.; Chen, H. Y.; Gao, J.; Nozik, A. J.; Beard, M. C., *Science* **2011**, 334, 1530.
- 17. Bang, J. H.; Kamat, P. V., ACS Nano 2009, 3, 1467.
- 18. Chakrapani, V.; Baker, D.; Kamat, P. V., J. Am. Chem. Soc. 2011, 133, 9607.
- 19. Robel, I.; Kuno, M.; Kamat, P. V., J. Am. Chem. Soc. 2007, 129, 4136.
- 20. Jovanovski, V.; Gonzalez-Pedro, V.; Gimenez, S.; Azaceta, E.; Cabanero, G.; Grande, H.; Tena-Zaera, R.; Mora-Sero, I.; Bisquert, J., *J. Am. Chem. Soc.* **2011,** 133, 20156.
- 21. Yang, Y.; Rodríguez-Córdoba, W.; Lian, T., J. Am. Chem. Soc. **2011**, 133, 9246.
- 22. Bae, W. K.; Joo, J.; Padilha, L. A.; Won, J.; Lee, D. C.; Lin, Q.; Koh, W.; Luo, H.; Klimov, V. I.; Pietryga, J. M., *J. Am. Chem. Soc.* **2012**, 134, 20160.
- 23. Nazeeruddin, M. K.; Angelis, F. D.; Fantacci, S.; Selloni, A.; Viscardi, G.; Liska, P.; Ito, S.; Takeru, B.; Gratzel, M. G., *J. Am. Chem. Soc.* **2005**, 127, 16835.
- 24. Tisdale, W. A.; Williams, K. J.; Timp, B. A.; Norris, D. J.; Aydil, E. S.; Zhu, X. Y., *Science* **2010**, 328, 1543.
- 25. Schokley, W.; Queisser, H. J., J. Appl. Phys. **1961**, 32, 510.

CdTe QDs in ionic liquid.....

- 26. Ellis, A. B.; Kaiser, S. W.; Bolts, J. M.; Wrighton, M. S., *J. Am. Chem. Soc.* **1977,** 99, 2839.
- 27. Seddon, K. R., *Ionic Liquids, Industrial Applications for Green Chemistry, American Chemical Society, Washington DC* **2002**.
- 28. Dubreuil, J. F.; Bourahla, K.; Rahmouni, M.; Bazureau, J. P.; Hamelin, J., *Catal. Commun.* **2002**, 3, 185.
- 29. Hallett, J. P.; Welton, T., Chem. Rev. 2011, 111, 3508.
- 30. Armand, M.; Endres, F.; MacFarlane, D. R.; Ohno, H.; Scrosati, B., *Nat. Mater.* **2009**, 8, 621.
- 31. Lewandowski, A.; Swiderska-Mocek, A., J. Power Sources 2009, 194, 601.
- 32. Gorlov, M.; Kloo, L., Dalton Trans. 2008, 2655.
- 33. Wang, P.; Klein, C.; Humphry-Baker, R.; Zakeeruddin, S. M.; Grätzel, M., *Appl. Phys. Lett.* **2005**, 86, 123508/1.
- 34. Santhosh, K.; Samanta, A., J. Phys. Chem. C 2012, 116, 20643.
- 35. Santhosh, K.; Banerjee, S.; Rangaraj, N.; Samanta, A., *J. Phys. Chem. B* **2010**, 114, 1967.
- 36. Fitzmorris, B. C.; Cooper, J. K.; Edberg, J.; Gul, S.; Guo, J.; Zhang, J. Z., *J. Phys. Chem. C* **2012**, 116, 25065.
- 37. Santhosh, K.; Patra, S.; Soumya, S.; Khara, D. C.; Samanta, A., *ChemPhysChem* **2011,** 12, 2735.
- 38. Boulesbaa, A.; Huang, Z.; Wu, D.; Lian, T., J. Phys. Chem. C 2010, 114, 962.
- 39. Klimov, V. I.; McBranch, D. W.; Leatherdale, C. A.; Bawendi, M. G., *Phys. Rev. B: Condes. Matter Mater. Phys* **1999**, 60, 13740.
- 40. Wang, X.; Qu, L.; Zhang, J.; Peng, X.; Xiao, M., *Nano Lett.* **2003,** 3, 1103.
- 41. Rawalekar, S.; Kaniyankandy, S.; Verma, S.; Ghosh, H. N., *J. Phys. Chem. C* **2010**, 114, 1460.
- 42. Chivers, T.; Drummond, I., *Inorg. Chem.* **1972**, 11, 2525.
- 43. Clark, R. J. H.; Cobbold, D.G., *Inorg. Chem.* **1978**, 17, 3169.

Chapter 3

Nature of Interaction between Oppositely Charged Photo-excited CdTe Quantum Dots and Cresyl Violet

Understanding the dynamics of exciton quenching of the quantum dots (QDs) is of great importance considering the fact that the applications of these substances are based mainly on luminescence. In this work, we have studied exciton quenching of the CdTe QDs by cresyl violet (CV) employing steady state and time-resolved absorption and emission techniques. Efficient luminescence quenching of these QDs is observed in the presence of CV. Interestingly, despite an excellent overlap of the absorption and emission spectra of CV and QD, respectively, the emission quenching of the QD is not accompanied by an increase in the steady state fluorescence intensity of CV or a rise in its fluorescence time profile that can be considered as evidence for the Förster resonance energy transfer process. The time-resolved fluorescence measurements suggest that the quenching is partially due to static interaction of the two species. The transient absorption studies in the 0 -100 ps time scale show that recovery of the 1S exciton bleach of the QDs is much faster in the presence of CV when compared with that in its absence, indicating that ultrafast photoinduced electron transfer from the conduction band of the QDs to CV is responsible for the emission quenching of the former. The recombination of the charge-separated species is found to occur in ~ 2 ps.

4.1 Introduction

Three-dimensionally confined semiconductor nanoparticles, which are commonly termed as Quantum Dots (QDs), are considered as promising alternatives to the molecular dyes in several applications such as in solar cells, biological imaging and light emitting diodes because of their superior photostability, broad absorption with high molar extinction coefficient, and size-dependent tunability of their band gap. 1-14 Because of the spatial confinement, photo-excitation of the QDs leads to the formation of bound electron-hole pairs (excitons), whose recombination gives rise to the emission of the QDs. Any process that contributes to dissociation of the exciton prior to electron-hole recombination of the QDs gives rise to quenching of its emission. Because the dynamics of exciton dissociation plays a crucial role in determining the utility of the QDs in a wide variety of applications ranging from lasing and photovoltaics to biological imaging, it is absolutely essential to have a clear understanding of the exciton quenching dynamics. 5-14

The exciton quenching of the QDs is mainly governed by charge- (electron or hole) transfer and energy-transfer processes. The dissociation of exciton by photo-induced charge transfer between the QDs and metal oxides, ^{15, 16} molecular acceptors ^{17, 18} or polymers ^{19, 20} has been studied extensively while exploring possible applications of the QDs in solar cell. The low energy conversion efficiency (~6-7 %)²¹⁻²⁴ in the quantum dot sensitized solar cells (QDSSCs) compared to other (dye or silicon based) solar cell devices ²⁴⁻²⁶ makes the QDSSCs not attractive for real-world applications; however, multiple exciton generation, which is an important characteristic of the QDs, where a photon of higher energy (ħω≥ 2Eg, Eg is the bandgap of the QD) generates two or more excitons, is a new approach to enhancing the conversion efficiency of QDSSCs and is being seriously explored by many researchers. ²⁷⁻³⁰ Klimov and coworkers reported photon-to-

Nature of interaction...

exciton conversion efficiency of 700 % for PbS and PbSe QDs by generating seven excitons from a photon with an energy of 7.8 Eg.²⁸ Hence, optimization of multiple exciton generation and subsequent dissociation of the exciton by ultrafast charge transfer to acceptors prior to exciton-exciton annihilation has become an active area of research in the context of improving the solar energy conversion efficiency of the QDSSCs.

Dissociation of the QD excitons by molecular system or metal nanoparticles via Förster resonance energy transfer (FRET) is extensively studied. 31-35 Kamat and coworkers recently developed a QD-dye dual sensitized solar cell, where they have succeeded in enhancing the energy conversion efficiency by coupling the energy transfer between the QD and dye with the charge transfer between dye and TiO₂.³⁶ It is important to note in this context that the mechanism of emission quenching of the QDs by molecular systems in a large majority of cases is established as FRET merely on the basis of spectral overlap criterion between the QD emission and quencher absorption and a decrease in the average emission lifetime of the QD in the presence of the quencher. 37-39 Not many instances could be observed where kinetic evidence of the FRET process is provided through the time profile of the acceptor emission. In one of our earlier works, while we highlighted this important point using one specific example, we could not provide evidence of the alternate mechanism due to lack of ultrafast pump-probe facility at that time.40 In this work, we study the interaction between water soluble mercaptopropanoic acid-capped photo-excited CdTe QDs and CV, a pair is chosen for having an excellent overlap of the emission spectrum of the former with the absorption spectrum of the latter. We show that despite fulfilling the overlap criteria the emission quenching of the QDs is not governed by FRET interaction of the two species, and employing femtosecond time-resolved transient absorption measurements, we demonstrate that ultrafast photo-induced electron transfer from the conduction band of the QDs to CV is the primary response for the exciton quenching process.

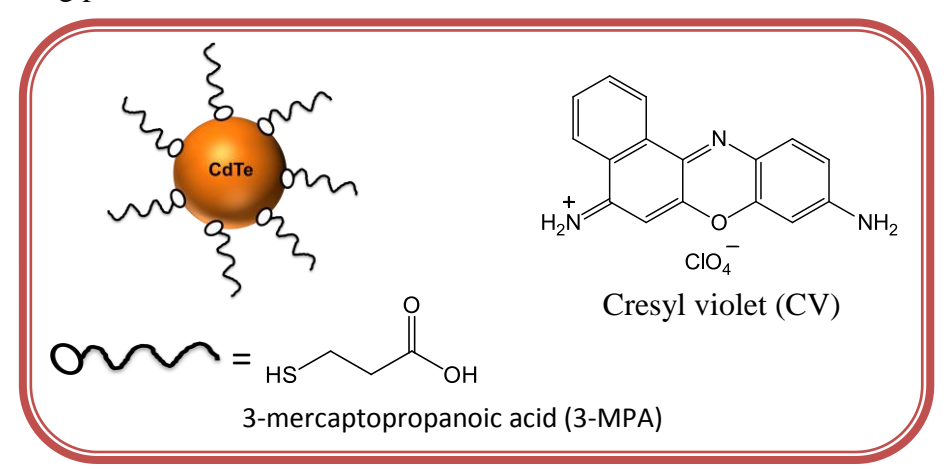


Chart 4.1. CdTe QDs and chemical formula of CV and 3-MPA

4.2. Results

4.2.1. Steady state measurements

Figure 4.1a depicts the absorption and emission spectra of CdTe QDs in aqueous medium. The broad absorption spectrum is characterized by the exciton

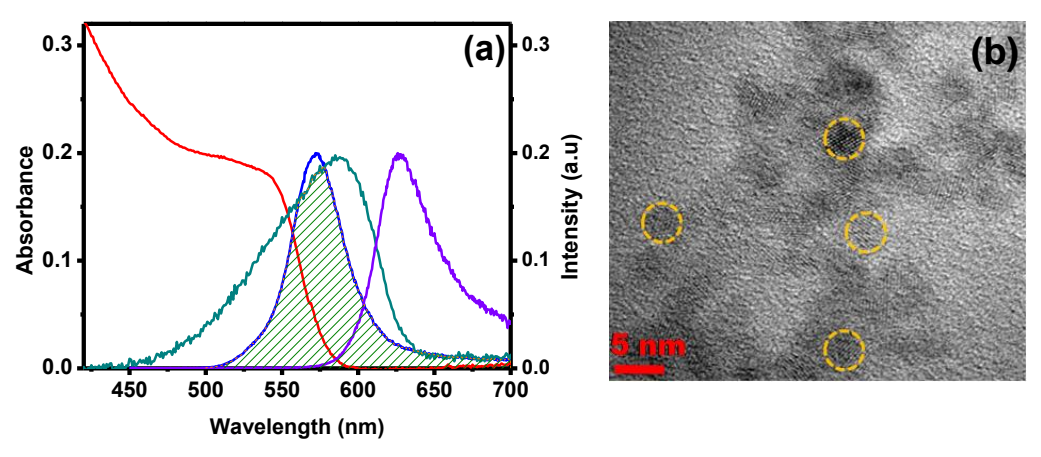


Figure 4.1. a) Absorption spectra of CdTe QDs (red) and CV (cyan) and emission spectra of CdTe QDs (blue) and CV (violet) in aqueous medium. The overlapped region of the QD emission and CV absorption is shown as shaded area. The spectra are normalized to the peak heights. b) TEM image of CdTe QDs

band maximum at ~ 530 nm and the narrow emission spectrum shows peak at ~570 nm. The average size of these QDs, estimated from the first exciton band maximum using the empirical relation suggested by Peng and coworkers, is found to be 3.0 ± 0.2 nm. This value matches reasonably well with the size $(3.3 \pm 0.2 \text{ nm})$ determined from the TEM image (Figure 4.1b). Figure 4.1a also shows the absorption ($\lambda_{max} = 585 \text{ nm}$) and emission ($\lambda_{max} = 630 \text{ nm}$) spectra of CV in aqueous solution. A good overlap between the emission spectrum of the QDs and the absorption spectrum of CV is also clearly evident from Figure 4.1a.

Figure 4.2 shows the changes in the emission spectrum of the QDs with increasing concentrations of CV. These measurements (and the times resolved ones presented in the next section) were carried out by exciting the solution at 439 nm, at which, as can be seen from Figure 4.1, the absorption due to CV is negligible. A drastic quenching of the CdTe QDs emission is observed with minor contribution from the CV emission (vide Discussion section).

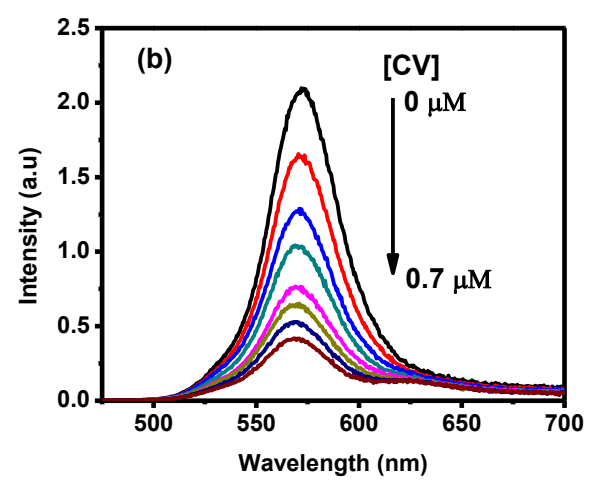


Figure 4.2. Photoluminescence spectra (λ_{exc} = 439 nm) of the QDs (1 μ M) with increasing concentration of CV (0, 0.1, 0.2, 0.3, 0.4, 0.5, 0.6, and 0.7 μ M).

4.2.2 Time-resolved measurements

The emission decay profiles of the QDs monitored at 570 nm in the absence and presence of CV are shown in Figure 4.3. The decay curves are found to be

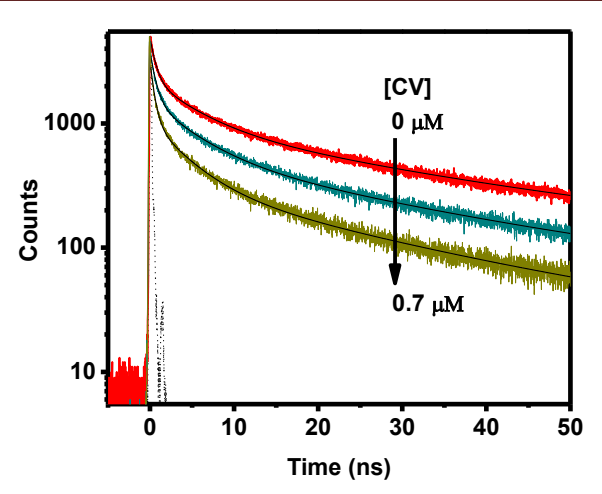


Figure 4.3. Fluorescence decay profiles of CdTe QDs as a function of the concentrations (0, 0.4, 0.7 μ M) of CV. (The decay profiles for intermediate concentrations of CV are not shown for clarity). The exciting lamp profile is also shown as dotted line. The excitation and monitoring wavelengths were 439 and 570 nm, respectively.

Table 4.1. Emission decay parameters (τ values are expressed in nanoseconds) and estimated average lifetime of the QDs for different concentrations of CV.

CV (µM)	τ ₁ (a ₁)	$ au_2\left(\mathbf{a}_2 ight)$	τ ₃ (a ₃)	<τ _a >
0	5.24 (0.19)	30.30 (0.76)	0.66 (0.05)	24.06
0.1	5.20 (0.23)	28.69 (0.71)	0.68 (0.06)	21.61
0.2	5.18 (0.22)	28.43 (0.72)	0.70 (0.06)	21.65
0.3	5.13 (0.23)	28.17 (0.70)	0.68 (0.06)	20.94
0.4	4.86 (0.24)	27.13 (0.69)	0.62 (0.07)	19.93
0.5	4.36 (0.25)	25.22 (0.68)	0.56 (0.07)	18.28
0.6	4.41 (0.25)	25.48 (0.68)	0.55 (0.07)	18.47
0.7	4.25 (0.26)	24.67 (0.65)	0.53 (0.05)	17.18

Nature of interaction...

best represented by a triexponential function of the form $I(t) = a_1 \exp(-t/\tau_1) + a_2 \exp(-t/\tau_2) + a_3 \exp(-t/\tau_3)$. The lifetime values of the components, associated amplitudes and the average lifetime $<\tau_a>$ of the QDs, defined as $<\tau_a> = (a_1\,\tau_1^2 + a_2\,\tau_2^2 + a_3\,\tau_3^2)$ / $(a_1\tau_1 + a_2\tau_2 + a_3\tau_3)$, in the absence and presence of CV are presented in Table 4.1. The triexponential nature of the emission time profile and measured decay parameters of the QDs in the absence of CV are in agreement with literature. According to the literature, the \sim 5 ns component arises from core-state recombination 42, 43 whereas the short (\sim 0.6 ns) and long (\sim 30 ns) components are due to carrier recombination of the deep and shallow trap states, respectively. In the presence of CV, a decrease in the average lifetime of the CdTe QDs is observed.

It is to be noted that while the steady state fluorescence intensity of the QDs decreases by 80%, the average lifetime decreases only by 30% for the same amount of CV, thus indicating that static interaction between the two species significantly contributes to the quenching of emission of the QDs.

4.2.3. Ultrafast transient absorption measurements

To understand the nature of the quenching interaction between the QDs and CV, we have carried out the time-resolved ultrafast transient absorption studies. The transient absorption spectra of CdTe QDs recorded at the indicated delay times after 350 nm excitation in both the absence and presence of CV are shown in Figure 4.4. The spectra are characterized by bleach around 530 nm, which corresponds to the first exciton absorption band maximum of QDs (Figure 4.1) and hence can be attributed to the state-filling of the 1S exciton (equation 4.1). In the presence of CV, a similar spectral feature is observed but with ~ 50 % reduction in the amplitude of the 1S exciton bleach at the early time (vides the two panels of Figure 4.4).

$$CdTe \xrightarrow{h\nu} CdTe^* (1S_h \rightarrow 1S_e)$$
 (1)

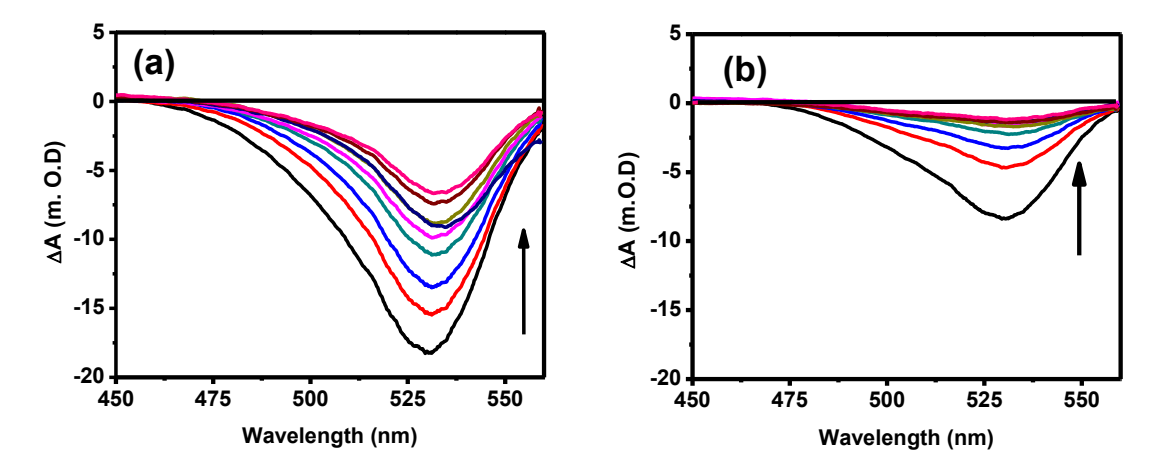


Figure 4.4. Difference absorption spectra of the QDs (7 μ M) in aqueous medium in the absence (a) and presence (b) of CV (7 μ M) at different delay times (2, 5, 10, 20, 30, 40, 60, 70, 100 ps) after 350 nm excitation.

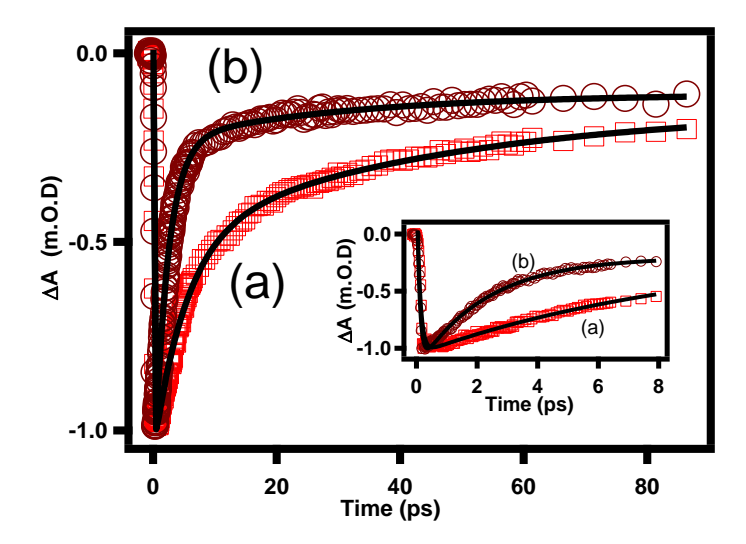


Figure 4.5. Normalized bleach recovery kinetics monitored at 535 nm of the QDs alone (a) and CdTe in the presence of CV (b). Inset: The inset shows the kinetics decay traces at shorter time scales in the early time regime.

Figure 4.5 compares the bleach recovery kinetics of the QDs in the absence and presence of CV at 535 nm. The kinetics are best represented by a biexponential function of the form, ΔA (t) = c + a_1 exp (-t/ τ_1) + a_2 exp (-t/ τ_2), where τ_1 and τ_2

Nature of interaction...

represent the lifetimes and a_1 and a_2 are the amplitudes at t=0. The recovery parameters of QDs in the absence and presence of CV are shown in Table 2. As can be seen from Figure 4.5 and data presented in Table 2, the bleach recovery kinetics becomes much faster in the presence of CV. While in the case of CdTe QDs alone, the two time components of the kinetics are 6.2 ± 0.2 and 51 ± 5 ps, respectively, in the presence of CV, these values are 2.4 ± 0.3 and 39 ± 5 , respectively.

Table 4.2. 1S bleach recovery parameters of CdTe QDs in H₂O.

System	Lifetime Parameters			
	τ1, ps	\mathbf{a}_1	$ au_2, \mathbf{ps}$	\mathbf{a}_2
CdTe (7 μM)	6.2 ± 0.2	0.64 ± 0.03	51 ± 5	0.36 ± 0.01
$CdTe + CV (7 \mu M)$	2.4 ± 0.3	0.88 ± 0.02	39 ± 5	0.12 ± 0.01

4.3. Discussion

Because CV is fluorescent, in the event of energy transfer between photo-excited QD and CV (irrespective of the non-radiative or radiative nature of the process), emission quenching of the former should have been accompanied by a buildup of the emission intensity of CV; however, Figure 4.2 shows that this is not the case. One may argue that small intensity in the 600-650 nm region that is better seen for higher concentrations of the quencher, is the outcome of this energy-transfer process; however, the results of the control experiments, which are presented in Figure 4.6, clearly rule out this possibility. Specifically, a comparison of the spectra of the QDs containing 0.7 μ M of CV (highest concentration used in emission quenching experiments) with another solution containing the same amount of CV but no QDs under identical experimental conditions shows that the hump at ~ 625 nm is not due to energy transfer from the QDs but due to direct excitation of CV.

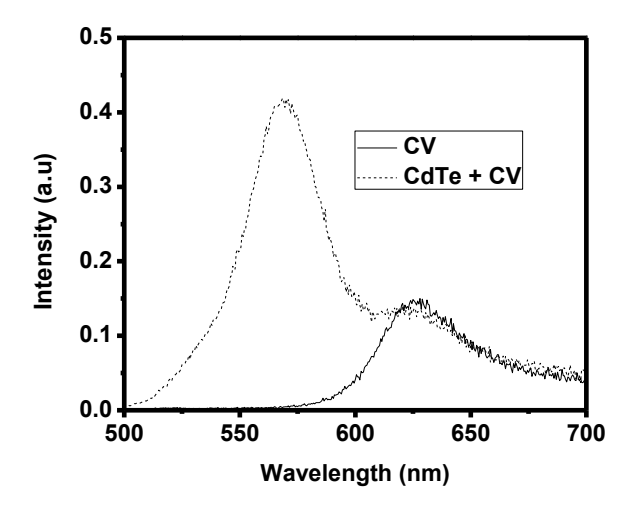


Figure 4.6. Comparison of the emission spectrum of an aqueous solution of a mixture of CdTe QDs (1 μ M) and CV (0.7 μ M) with the one containing same concentration of CV alone. These spectra were recorded under identical experimental conditions. $\lambda_{exc} = 439$ nm.

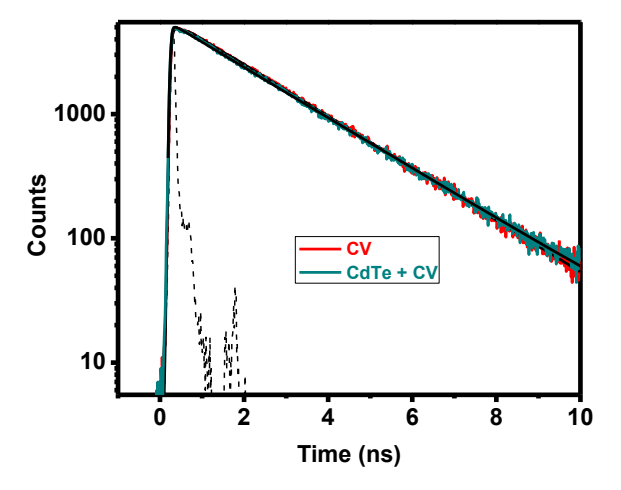


Figure 4.7. A comparison of the emission decay profiles of an aqueous solution of (i) CdTe QD (1 μ M) + CV (1 μ M) with that containing same concentration of CV alone. These spectra were recorded under identical experimental condition. The exciting lamp profile is also shown as dotted line. The excitation and monitoring wavelengths were 439 and 630 nm, respectively.

Nature of interaction...

The time-resolved measurements also confirm the absence of any energy-transfer process. In the case of energy transfer from QDs to CV, one should observe a time-dependent rise of the acceptor (CV) emission intensity; however, no rise component (characterized by a negative pre-exponential factor) could be observed while monitoring the fluorescence time profile of CV of a solution containing a mixture of the two (Figure 4.7).

The excellent overlap of the absorption spectrum of CV and emission spectrum of the QDs suggests that the QDs and CV form an ideal FRET pair. According to Förster theory,^{44, 45} the rate of energy transfer from a donor to an acceptor is given by

$$k_T(r) = \frac{1}{\tau_D} \left[\frac{R_0}{r} \right]^6 \tag{4.2}$$

where τ_D is the emission lifetime of the donor in the absence of acceptor, r is the distance between the donor and acceptor, R_o is the Förster distance (in angstroms), which is defined as the distance between the donor and acceptor at which the energy transfer efficiency is 50 % and is given by

$$R_0 = 0.211 \left[\kappa^2 n^{-4} Q_D J(\lambda) \right]^{\frac{1}{6}}$$
 (4.3)

where κ^2 is the relative orientation of the transition dipoles of donor and acceptor in space, Q_D is the emission quantum yield of the donor, n is the refractive index of the medium and J (λ) is the overlap integral representing the spectral overlap between the donor emission and acceptor absorption and given by

$$J(\lambda) = \int_{0}^{\infty} F_{D}(\lambda) \varepsilon_{A}(\lambda) \lambda^{4} d\lambda \tag{4.4}$$

where $F_D(\lambda)$ is the corrected fluorescence intensity of the donor normalized to unity and $\varepsilon_A(\lambda)$ is the extinction coefficient of the acceptor at λ . By using the

equations 4.3 and 4.4, the spectral overlap and employing a κ^2 value of 2/3, a refractive index of 1.33, and a Q_D value of 0.03 for the CdTe QDs, the spectral overlap and Förster distance are calculated to be 6.7 X 10^{15} M⁻¹cm⁻¹nm⁴ and 36.8 Å, respectively. Because the QDs and CV are oppositely charged, they are expected to held together tightly, and their actual distance is expected to be much shorter than the estimated Förster distance. It is therefore surprising that despite such a favorable condition, the energy transfer process does not occur.

Because the emission quenching is not due to energy transfer between photo-excited QDs and CV, charge (electron or hole) transfer between the two species, which is mainly governed by their redox potentials, could be an alternative mechanism of quenching. An examination of the potentials of the valence band (VB) and conduction band (CB) of CdTe QDs and the reduction and oxidation potentials of CV (Figure 4.8) reveals that charge transfer can indeed be the possible pathway for emission quenching of QDs by CV.

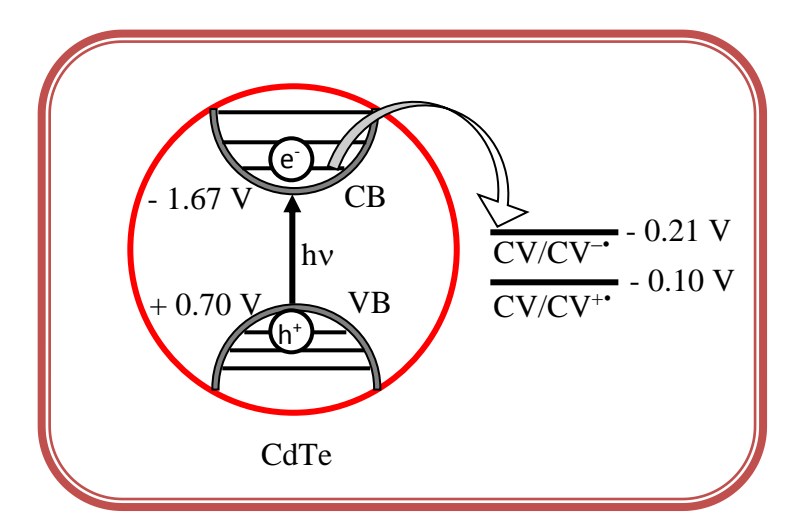


Figure 4.8. Conduction band (CB) and valence band (VB) potentials of CdTe QDs and reduction and oxidation potentials of CV (vs NHE).

The band gap of the semiconductors nanocrystals is high compared to their bulk counterparts due to the quantum size confinement. 46-48 The extent of the shift

Nature of interaction...

in the potentials of the VB and CB of the semiconductor nanocrystals from their bulk band potentials varies with the size of the QDs. $^{47,\ 48}$ The bulk VB and CB potentials of the CdTe QDs are +0.54 V and -1.0 V (vs NHE) respectively. 49 The size dependent shift of the bandgap of QDs with respect to bulk bandgap is given by $^{48,\ 50,\ 51}$

$$E_{CdTe^*}(1S_e,1S_h) = E_{bulk} + \frac{\hbar^2 \pi^2}{2R^2 m_e^*} + \frac{\hbar^2 \pi^2}{2R^2 m_h^*} - \frac{1.786e^2}{\varepsilon R} - 0.248 E_{Ry}^* \quad (4.5)$$

where, E_{bulk} is the bulk bandgap (for CdTe, $E_{\text{bulk}} = 1.54 \text{ eV}$) and R is the radius of the QD (1.5 nm). The second and third terms in equation 4.5 are the confinement energies of the electron and hole with effective masses $m_e^* = 0.096m_0$ and $m_h^* = 0.4m_0$ respectively, for CdTe QDs where m_0 is the rest mass of an electron. The fourth term represents the Coulomb attraction between the electron and hole with ε as the dielectric constant ($\varepsilon = 7.1$ for CdTe QDs). The last term is due to the spatial correlation between electron and hole, where E_{Ry}^* is the exciton Rydberg energy. The potentials of the VB and CB of the QDs used in this study are estimated to be +0.70 V and -1.67 V, respectively. The reduction and oxidation potentials of CV are -0.21 V and -0.10 V, respectively. Depiction of these potentials (Figure 4.8) shows that both electron and hole transfer are possible from the QDs to CV; however, the estimated free-energy values suggest that electron transfer ($\Delta G = -140.86 \text{ kJ/mol}$) process is thermodynamically more feasible compared to hole transfer ($\Delta G = -77.18 \text{ kJ/mol}$) process.

The electron transfer from photo-excited QDs to CV should lead to the formation of CV radical anion, which may be possible to detect by transient absorption measurements; however, the CV⁻⁺ molecule, which absorbs at ~390 nm⁵⁴ could not be observed (Figure 4.9) presumably due to very strong absorption of QDs in this wavelength region.

$$CdTe^*(e^- + h^+) + CV \longrightarrow CdTe(h^+) + CV^{-\bullet}$$
 (4.6)

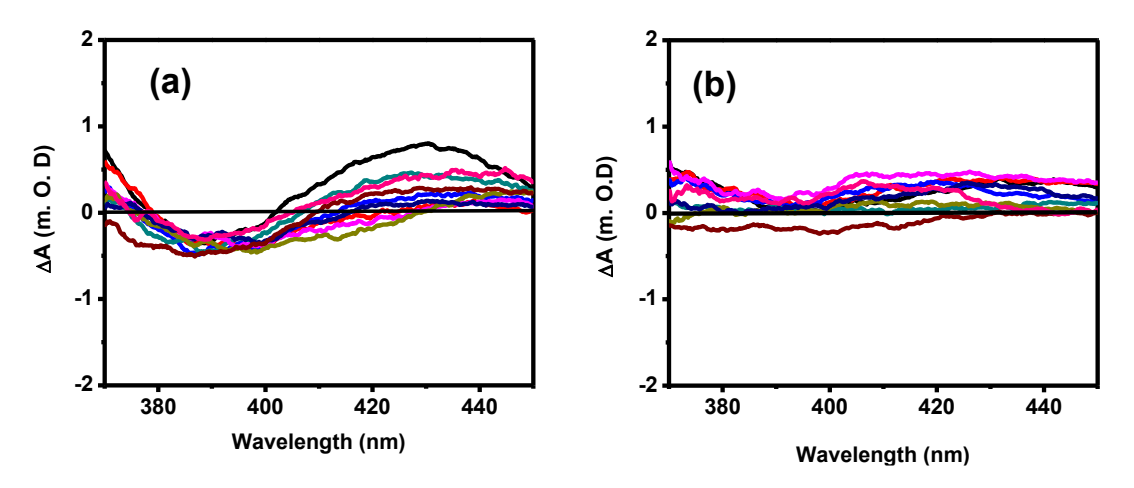


Figure 4.9. Transient absorption spectra of CdTe QDs (7 μ M) in aqueous medium in the absence (a) and presence of CV (7 μ M) (b) at different delay times (2, 5, 10, 20, 30, 40, 60, 70, 100 ps) after 350 nm excitation.

It is known that the amplitude of the state-filling induced bleach of the interband optical transitions is proportional to the sum of the occupation numbers of the electron and hole states involved in these transitions. Because of the degeneracy of the valence band and a high effective mass of the hole compared to the electron (for CdTe, $m_h^*/m_e^* = 4$), the room-temperature occupation probabilities of the lowest electron state are greater than the coupled hole states. Consequently, the state-filling induced bleach signal is highly dominated by the electron populations.

Because the 1S exciton bleach is sensitive to electrons, the evidence for the electron transfer between QDs and molecular systems can be obtained by monitoring the bleach recovery dynamics in the absence and presence of acceptor. ^{15,56-58} Because the 1S exciton bleach recovery dynamics of the QDs in the presence of electron acceptor is faster compared to free QDs due to additional decay route for the removal of 1S electron by electron transfer, ⁵⁶⁻⁵⁸ we have investigated the bleach recovery dynamics of the CdTe QDs in the absence and

presence of CV very carefully.

As already stated, the 1S exciton bleach of the CdTe QDs recovers with short and long lifetime components of ~ 6 ps and ~ 50 ps, respectively in the absence of CV. A similar two component bleach recovery dynamics of CdSe QDs with lifetimes of ~ 5 ps and ~ 70 ps was reported by Burda et. al., and the short and long lifetime components were attributed to electron trapping by the shallow and deep trap states, respectively.⁵⁹ On the basis of this literature, we attributed the short lifetime component (~ 6 ps) to the electron trapping by the shallow trap states and the long lifetime component (~ 50 ps) to the electron trapping by the deep trap states.

Our observation of a much faster bleach recovery of the QDs (88 % of bleach is recovered in about 2 ps) in the presence of CV, is similar to that observe by El-Sayed and coworkers, who reported that the bleach recovery dynamics of CdSe QDs is accelerated upon addition of benzoquinone (BQ, an electron acceptor) due to rapid transfer of the electron of the photoexcited QDs to the adsorbed BQ molecule.⁵⁷ They observed formation of a short-lived charge transfer complex between CdSe and BQ which decayed with a lifetime of ~ 2 ps.⁵⁷ Ghosh and coworkers also observed 50 % bleach recovery of CdTe QDs by the addition of BQ with a time constant of ~ 1 ps and attributed it to the fast decay of the charge-transfer complex between CdTe and BQ.⁵⁸ Considering the above literature, the majority of the bleach recovery of the CdTe QDs in the presence of CV in ~ 2 ps in our study, suggests the formation of charge transfer complex between photoexcited CdTe and CV (Reaction 4.7), and the time constant of ~ 2 ps in the bleach recovery dynamics of the QDs is attributed to the recombination time of the electron in CV⁻⁺ with the hole of the CdTe QD (reaction 4.8).

$$CdTe (e^{-} + h^{+}) + CV \longrightarrow (CdTe (h^{+}) - CV^{-\bullet})$$
 (4.7)

$$(CdTe (h^{+}) - CV^{-\bullet}) \longrightarrow CdTe + CV$$
 (4.8)

Chapter 4

It is thus evident that photo-induced electron transfer process and static interaction contribute to the emission quenching of the QDs by CV. No evidence of FRET between photo-excited QDs and CV could be found despite the interacting species fulfilling the required criteria strictly. This implies that quenching due to the other two interactions is too rapid for the FRET process to compete with them.

4.4. Conclusion

Quenching of the CdTe QDs exciton by fluorescent molecule, CV, is studied using steady state and time-resolved absorption and emission techniques. We conclusively establish that emission quenching is not due to energy transfer between photo-excited QDs and CV even though the pair meets the spectral overlap criteria of the FRET mechanism. Using ultrafast transient absorption measurements, we show that ultrafast PET interaction is largely responsible for the quenching process, and the time constant for the back electron transfer process is found to be ~ 2 ps. The study also highlights once again the importance of a careful analysis of the fluorescence quenching data to avoid erroneous conclusion.

Nature of interaction...

References

- 1. Yu, W. W.; Qu, L.; Guo, W.; Peng, X., Chem. Mater. 2003, 15, 2854.
- 2. Hodes, G., J. Phys. Chem. C 2008, 112, 17778.
- 3. Hod, I.; Gonzalez-Pedro, V.; Tachan, Z.; Fabregat-Santiago, F.; Mora-Sero, I.; Bisquert, J.; Zaban, A., *J. Phys. Chem. Lett.* **2011**, 2, 3032.
- 4. Resch-Geneger, U.; Grabolle, M.; Cavaliere-Jaricot, S.; Nitschke, R.; Nann, T., *Nature Methods* **2008**, 5, 763.
- 5. Kamat, P. V.; Trvdy, K.; Baker, D. R.; Radich, J. G., Chem. Rev. **2010**, 110, 6664.
- 6. Nozik, A. J.; Beard, M. C.; Luther, J. M.; Law, M.; Ellingsono, R. J.; Jhonson, J. C., *Chem. Rev.* **2010,** 110, 6873.
- 7. Nozik, A. J., *Physica E* **2002**, 14, 115.
- 8. Kamat, P. V., J. Phys. Chem. C 2008, 112, 18737.
- 9. Achermann, M.; Petruska, M. A.; Koleske, D. D.; Crawford, M. H.; Klimov, V. I., *Nano. Lett.* **2006**, 6, 1396.
- 10. Steckel, J. S.; Snee, P.; Coe-Sullivan, S.; Zimmer, J. P.; Anikeeva, P.; Kim, L. A.; Bulovic, V.; Bawendi, M. G., *Angew. Chem. Int. Ed.* **2006**, 45, 5796.
- 11. Colvin, V. L.; Schlamp, M. C.; Alivisatos, A. P., *Nature* **1994,** 370, 354.
- 12. Bruchez, M.; Moronne, M.; Gin, P.; Weiss, S.; Alivisatos, A. P., *Science* **1998**, 281, 2013.
- 13. Chan, W. C. W.; Nie, S., Science **1998**, 281, 2016.
- 14. Medintz, I. L.; Clapp, A. R.; Brunel, F. M.; Tiefenbrunn, T.; Uydea, H. T.; Chang, E. L.; Deschamps, J. R.; Dawson, P. E.; Mattoussi, H., *Nat. Mater.* **2006**, 5, 581.
- 15. Trvdy, K.; Frantsuzov, A. P.; Kamat, P. V., PNAS **2011**, 108, 29.
- 16. Zidek, K.; Abdellah, M.; Zheng, K.; Pullerits, T., Sci. Rep. 2014, 4, 7244.
- 17. Huang, J.; Huang, Z.; Jin, S.; Lian, T., J. Phys. Chem. C 2008, 112, 19734.
- 18. Cui, S. C.; Tachikawa, T.; Fujitsuka, M.; Majima, T., *J. Phys. Chem. C* **2008,** 112, 19625.
- 19. Xu, Z.; Hine, C. R.; Maye, M. M.; Meng, Q.; Cotlet, M., ACS Nano **2012**, 6, 4984.
- 20. Couderc, E.; Greaney, J. M.; Brutchey, L. R.; Bradforth, E. S., *J. Am. Chem. Soc.* **2013,** 135, 18418.
- 21. Pan, Z. X.; Zhao, K.; Wang, J.; Zhang, H.; Feng, Y. Y.; Zhong, X. H., *ACS Nano* **2013**, 7, 5215.
- 22. Lee, J. W.; Son, D. Y.; Ahn, T. K.; Shin, H. W.; Kim, I. Y.; Hwang, S. J.; Ko, M. J.; Sul, S.; Han, H.; Park, N. G., *Sci. Rep.* **2013**, *3*, 1050.
- 23. Wang, J.; Mora-Sero, I.; Pan, Z.; Zhao, K.; Zhang, H.; Feng, Y.; Yang, G.; Zhong, X.; Bisquert, J., *J. Am. Chem. Soc.* **2013**, 135, 15913.
- 24. Kim, R. M.; Ma, D., J. Phys. Chem. Lett. **2014**, 6, 85.
- Yella, A.; Lee, H. W.; Tsao, H. N.; Yi, C.; Chandiran, A. K.; Nazeeruddin, M. K.; Diau, E. W.; Yeh, C. Y.; Zakeeruddin, S. M.; Gratzel, M., *Science* **2011**, 334, 629.
- 26. Green, M. A.; Emery, K.; Hishikawa, Y.; Warta, W.; Dunlop, E. D., *Prog. Photovoltaics* **2012**, 20, 12.
- 27. Semonin, O. E.; Luther, J. M.; Choi, S.; Chen, H. Y.; Gao, J.; Nozik, A. J.; Beard, M. C., *Science* **2011**, 334, 1530.
- 28. Schaller, R. D.; Sykora, M.; Pietryga, J. M.; Klimov, V. I., *Nano. Lett.* **2006,** 6, 424.

Chapter 4

- 29. Schokley, W.; Queisser, H. J., J. Appl. Phys. J. Appl. Phys. 1961, 32, 510.
- 30. Nozik, A. J., Chem. Phys. Lett. 2008, 457, 3.
- 31. Funston, A. M.; Jasieniak, J. J.; Mulvaney, P., Adv. Mater. 2008, 20, 4274.
- 32. Medintz, I. L.; Mattoussi, H., Phys. Chem. Chem. Phys. 2009, 11, 17.
- 33. Curutchet, C.; Franceschetti, A.; Zunger, A.; Scholes, G. D., *J. Phys. Chem. C* **2008**, 112, 13336.
- 34. Wang, X.; Guo, X., Analyst **2009**, 134, 1348.
- 35. Li, M.; Cushing, S. K.; Wang, Q.; Shi, X.; Hornak, A. L.; Hong, Z.; Wu, N., *J. Phys. Chem. Lett.* **2011,** 2, 2125.
- 36. Choi, H.; Santra, P. K.; Kamat, P. V., ACS Nano **2012**, 6, 5718.
- 37. Zhou, D.; Piper, J. D.; Abell, C.; Klenerman, D.; Kang, D. J.; Ying, L., *Chem. Comm.* **2005**, 4807.
- 38. Goldman, E. R.; Medintz, I. L.; Whitley, J. L.; Hayhurst, A.; Clapp, A. R.; Uyeda, J. R.; Deschamps, J. R.; Lassman, M. E.; Mattoussi, H., *J. Am. Chem. Soc.* **2005**, 127, 6744.
- 39. Sadhu, S.; Tachiya, M.; Patra, A., J. Phys. Chem. C **2009**, 113, 19488.
- 40. Santhosh, K.; Patra, S.; Soumya, S.; Khara, D. C.; Samanta, A., *ChemPhysChem* **2011,** 12, 2735.
- 41. Fitzmorris, B. C.; Cooper, J. K.; Edberg, J.; Gul, S.; Guo, J.; Zhang, J. Z., *J. Phys. Chem. C* **2012**, 116, 25065.
- 42. Klimov, V. I.; McBranch, D. W.; Leatherdale, C. A.; Bawendi, M. G., *Phys. Rev. B: Condes. Matter Mater. Phys* **1999**, 60, 13740.
- 43. Wang, X.; QU, L.; Zhang, J.; Peng, X.; Xiao, M., Nano. Lett. **2003**, 3, 1103-1106.
- 44. Forster, T., *Discuss. Faraday Soc.* **1959,** 27, 7.
- 45. Lakowicz, J. R., Principles of Fluorescence Spectroscopy, 2nd ed., Kluwer/Plenum, New York. **1999**.
- 46. Smith, A. M.; Nie, S., Acc. Chem. Res. **2010**, 43, 190.
- 47. Brus, L. E., *J. Chem. Phys.* **1983**, 79, 5566.
- 48. Brus, L. E., J. Chem. Phys. **1984**, 80, 4403.
- 49. Bang, J. H.; Kamat, P. V., ACS Nano **2009**, 3, 1467.
- 50. Wang, Y.; Herron, N., J. Phys. Chem. **1991,** 95, 525.
- 51. Kayanuma, Y., Phys. Rev. B 1988, 38, 9797-.
- 52. Masumaoto, Y.; Sonobe, K., *Phys. Rev. B* **1997**, 56, 9734.
- 53. Lei, C.; Hu, D.; Ackerman, E. J., *Chem. Comm.* **2008**, 5490.
- 54. Liu, D.; Kamat, P. V., Langmuir **1996**, 12, 2190.
- 55. Klimov, V. I., J. Phys. Chem. B **2000**, 104, 6112.
- 56. Song, N.; Zhu, H.; Jin, S.; Zhan, W.; Lian, T., ACS Nano **2011,** 5, 613.
- 57. Burda, C.; Link, S.; Mohamed, M.; El-Sayed, M., *J. Phys. Chem. B* **2001**, 105, 12286.
- 58. Rawalekar, S.; Kaniyankandy, S.; Verma, S.; Ghosh, H. N., *J. Phys. Chem. C* **2010**, 114, 1460.
- 59. Burda, C.; Link, S.; Green, T. C.; El-Sayed, M. A., *J. Phys. Chem. B* **1999,** 103, 10775.

Influence of Capping Agents on the Carrier Trapping Dynamics of Photo-excited CdTe Quantum Dots

As applications of the quantum dots (QDs) are based mainly on their luminescence, synthesis of QDs with appropriate ligands that results in highly fluorescent QDs is essential. A recent study of the effect of a series of mercapto acids on CdTe QDs synthesized in aqueous medium shows much higher emission quantum yield (QY) for the 3-mercaptobutyric acid (MBA)capped QDs compared to the 3-mercaptopropanoic acid (3-MPA) capped system. However, the emission QY of the QDs obtained by this route with capping agents, 2-mercaptoethanoic acid and 2-mercaptopropanoic acid are found to be low. In this work, we have synthesized these water soluble CdTe QDs using a different synthetic route, ligand-replacement method, and found that while MBA-capped CdTe QDs exhibit fluorescence QY similar to those obtained by direct aqueous synthesis, the other mercapto acid-capped QDs are much more fluorescent. Interestingly, maximum QY is observed for 3-MPAcapped CdTe QDs, not for MBA capped system. The evidence for efficient passivation of surface defect states of CdTe QDs by 3-MPA is further provided using time-resolved emission and ultrafast transient absorption studies.

5.1. Introduction

The semiconductor materials of size similar or smaller than their bulk exciton Bohr radius experience quantum confinement effect due to restricted spatial motion of electrons and holes.²⁻⁶ The spatial confinement of these charge carriers induces discrete electronic energy levels in the conduction and valence bands of nanomaterials (commonly termed as quantum dots (QDs)) and favors radiative recombination of photo-generated carriers.²⁻⁵ The optical properties of these few nanometer size QDs are majorly governed by the surface atoms because of high surface area to volume ratio.⁵ The incomplete bonding of these surface atoms leads to energy states, which act as carrier traps, and if these levels lie in between the semiconductor band gap, they often enhance the probability of non-radiative transitions.⁵ Efficient passivation of these surface trap states is required for the potential use of the QDs in wide variety of applications.⁷⁻¹⁵ This passivation is commonly achieved by coating these nanocrystals with organic ligands (such as trioctylphospine oxide or hexadecylamine) or forming an inorganic shell (such as ZnS, CdS) around the nanocrystals. ^{16,17}

There are two commonly used procedures for preparation of QDs for their use in aqueous environment; (i) direct synthesis of QDs in aqueous medium and (ii) synthesis of QDs in high boiling non-aqueous solvents followed by replacement of the ligand with a water soluble ligand (ligand-replacement method). The synthesis of QDs by former method leads to nanocrystals with poor surface quality and wide size distribution, whereas in the case of latter the emission is sometimes quenched (in case of CdSe QDs)²¹ and the stability after ligand replacement is reduced. ^{22, 23}

The effect of different mercapto acids on the photoluminescence of QDs has been studied by various groups. ¹⁸⁻²⁵ 2-mercaptoethanoic acid (MEA) and 3-mercaptopropionoic acid (3-MPA) are the most commonly used capping agents for CdTe QDs. ¹⁸⁻²⁴ 6-mercaptohexanoic acid and 11-mercaptoundecanoic acid have

Influence of capping agent...

also been used, but such capped QDs show significantly low QY compared to 3-MPA.²⁵ Recently, Guo and co-workers have studied the effect of a series of mercapto acids (3-MPA, MBA, 2-MPA, MEA, Chart 6.1) on the luminescence behavior of CdTe QDs synthesized in aqueous environment by the direct method. They found the MBA-capped QDs to be most fluorescent (70 %).¹ The huge enhancement in the quantum yield (QY) of MBA-capped CdTe QDs compared to 3-MPA-capped ones (31 %) was attributed to better passivation of the surface trap states of QDs by the carbonyl oxygen of the carboxyl group of MBA.¹

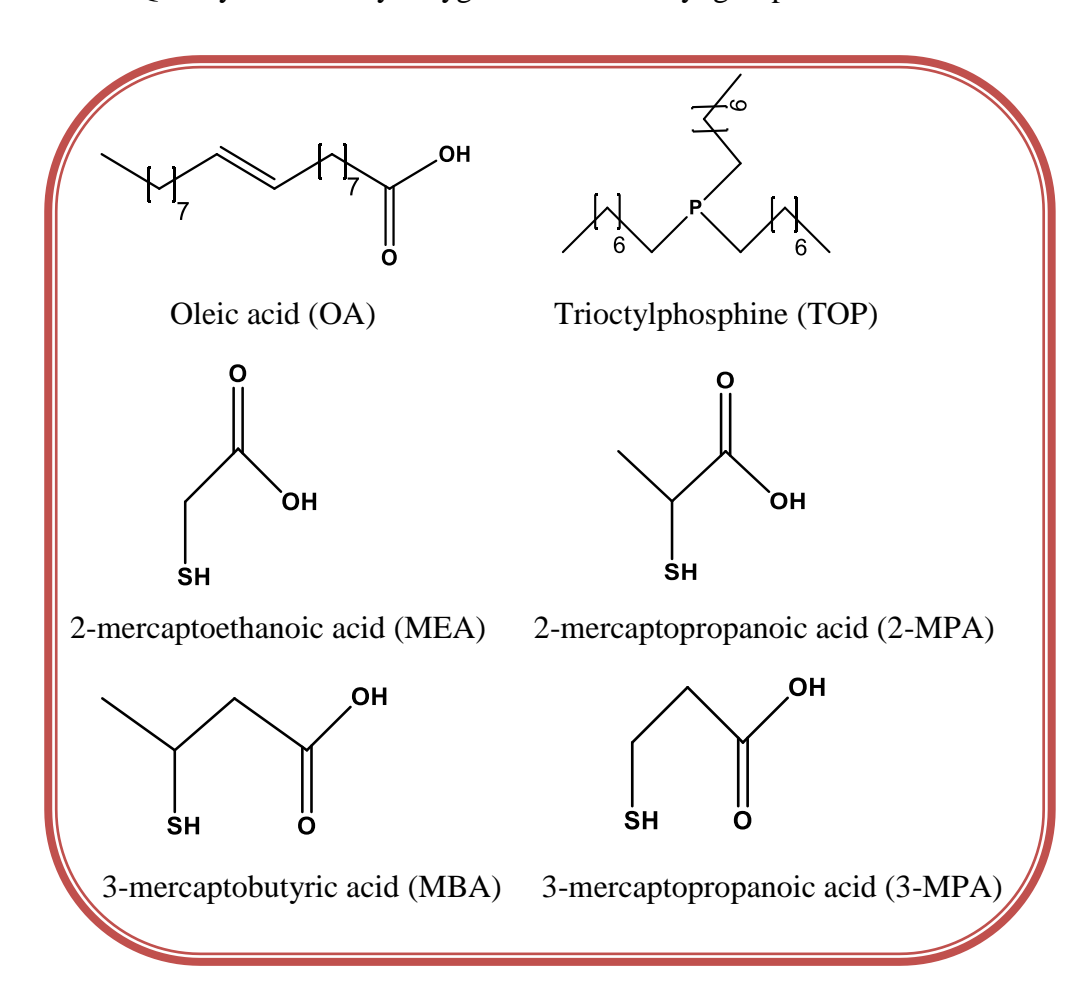


Chart 5.1. Structures of the capping agents used in this study

As the ligand replacement method generally produces QDs with high QY, ²⁰ we thought it might be possible to obtain even higher luminescent CdTe QDs by first synthesizing them with organic ligand capping²⁶ and later replacing the organic ligands by mercapto acids (Chart 1).²⁰ Herein, we demonstrate that this is indeed the case. What we find really very interesting is that 3-MPA-capped CdTe QDs show higher QY than the MBA-capped QDs indicating a better passivation of the QDs surfaces by the latter.

5.2. Results

5.2.1. Steady state measurements

Figure 5.1a shows the broad absorption and narrow emission spectra of the TOP/OA-capped CdTe QDs synthesized in chloroform. This broad absorption, which shows the first exciton peak maximum at \sim 622 nm, indicates an average size of 3.8 \pm 0.3 nm of the QDs according to the empirical equation of Peng.²⁷ This size matches reasonably well with the size (4.2 \pm 0.2 nm) obtained from the TEM image (Figure 5.1b).

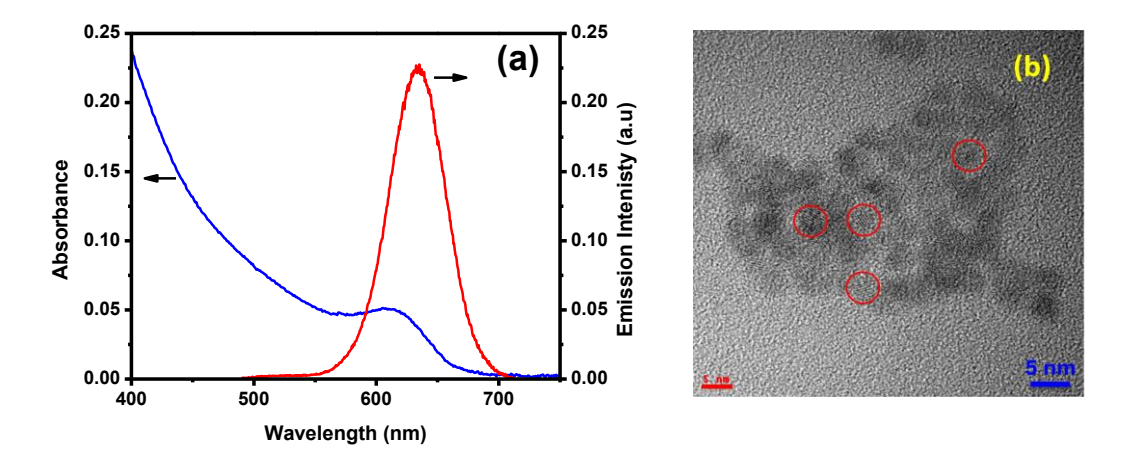


Figure 5.1. a) Absorption (blue) and emission (red) spectra (λ_{exc} = 439 nm) of CdTe QDs (0.3 μ M) in chloroform. b) TEM image of the TOP/OA-capped CdTe QDs.

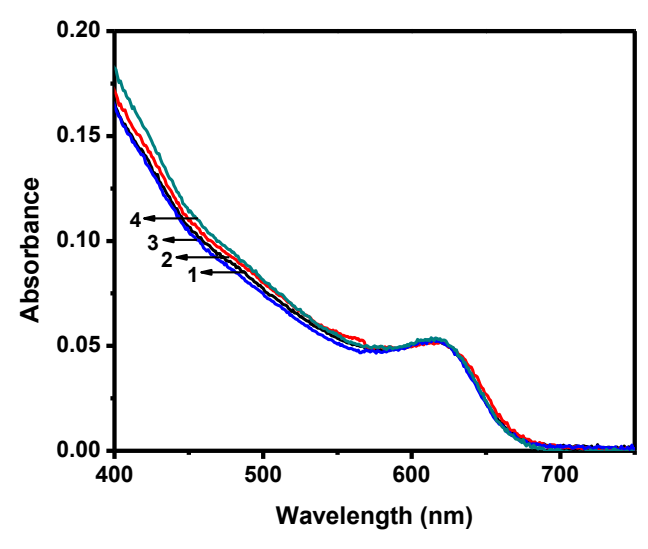


Figure 5.2. Absorption spectra of water soluble CdTe QDs (0.3 μ M) capped with (1) 2-MPA, (2) MEA, (3) MBA and (4) 3-MPA.

The water soluble CdTe QDs were obtained from the TOP/OA-capped QDs by replacement of the capping agents with different mercapto acids (Chart 5.1) via ligand-replacement method. The absorption spectra of water soluble CdTe QDs with various capping agents, shown in Figure 5.2, show very similar features with the first exciton peak maximum at ~624 nm, indicating negligible change in the size of the QDs, which is substantiated by the TEM images of the particles (Figure 5.3).

Figure 5.4 depicts the emission spectra of the water soluble CdTe QDs capped with different ligands. The enhancement of the photoluminescence of CdTe QDs is clearly observed in the aqueous medium compared to chloroform. Further, among the different mercapto acids, 3-MPA capped CdTe QDs exhibits the highest photoluminescence. The photoluminescence quantum yield (QY) of CdTe QDs with various capping agents is presented in Table 5.1.

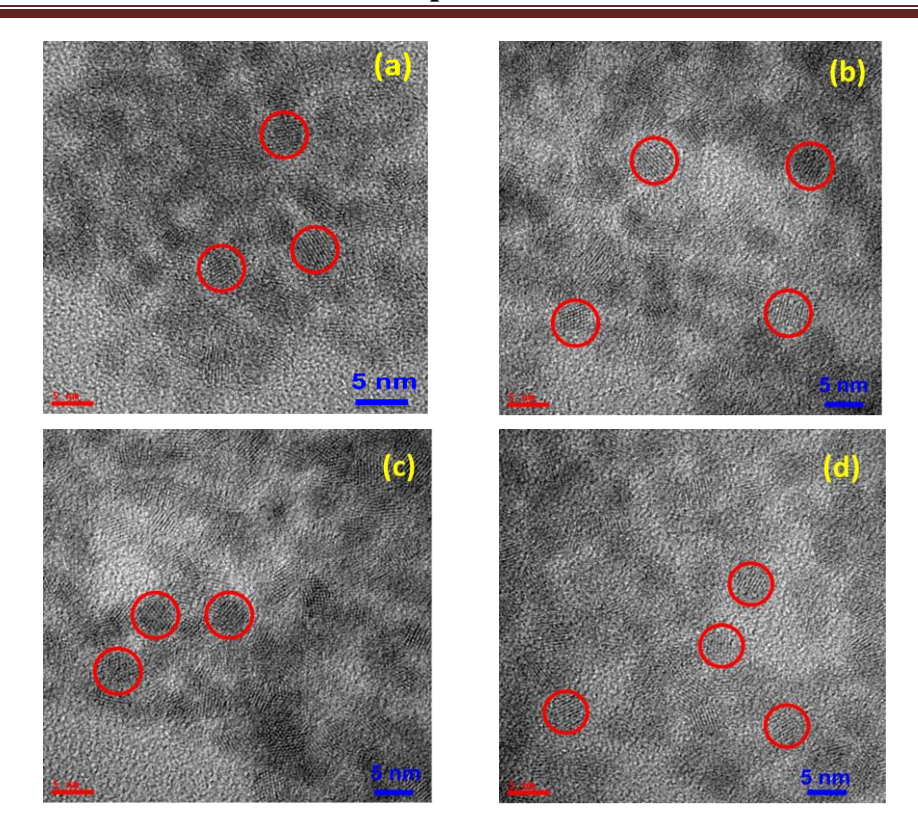


Figure 5.3.TEM images of CdTe QDs capped with (a) 2-MPA, (b) MEA, (c) MBA and (d) 3-MPA

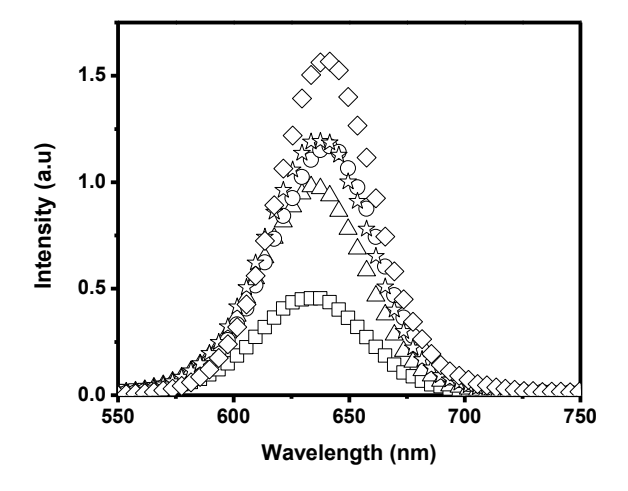


Figure 5.4. Emission spectra of CdTe QDs (0.3 μ M) with different capping agents TOP/OA (\square) dissolved in chloroform, 2-MPA (Δ), MEA (o), MBA (*) and 3-MPA (\Diamond) dissolved in aqueous medium. ($\lambda_{exc} = 439 \text{ nm}$)

Table 5.1. Quantum yield of the CdTe QDs with various capping agents and comparison with earlier literature.¹

System	Quantum Yield		
	Obtained	Reported	
CdTe @ TOP/OA	35		
CdTe @ 2-MPA	59	45	
CdTe @ MEA	63	19	
CdTe @ MBA	70	70	
CdTe @ 3-MPA	75	31	

5.2.2. Time-resolved photoluminescence measurements

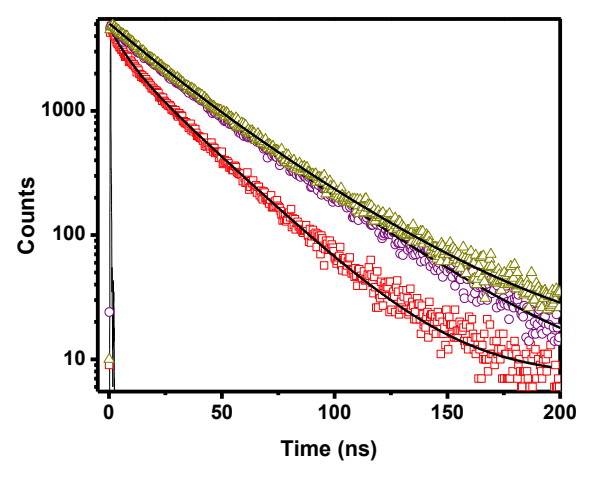


Figure 5.5. Emission decay profiles of the CdTe QDs (0.3 μ M) capped with TOP/OA (\Box), 2-MPA (o) and 3-MPA (Δ), decay profiles of the QDs capped with other agents are omitted for clarity. The excitation and monitoring wavelengths are 439 and 635 nm, respectively.

The emission decay profiles of QDs monitored at 635 nm are shown in Figure 5.5. The decay profiles are best represented by a biexponential function of the form $I(t) = a_1 \exp(-t/\tau_1) + a_2 \exp(-t/\tau_2)$, where τ_1 and τ_2 represent the lifetimes

and a_1 and a_2 are the amplitudes. The average lifetime $\langle \tau_a \rangle$, defined by $\langle \tau_a \rangle = (a_1\tau_1 + a_2\tau_2)$ / $(a_1 + a_2)$, along with the lifetime components and associated amplitudes are presented in Table 5.2. The measured decay parameters of CdTe QDs match reasonably well with the literature.^{28, 29} The short lived emission component can be attributed to the core state recombination and the long lived component to the carrier recombination involving the surface states. ^{28, 29} The replacement of TOP/OA with mercapto acids leads to ~ 1.5 -fold enhancement of the average lifetime of the QDs.

Table 5.2. Emission decay parameters and average lifetime (in ns) of CdTe QDs with various capping agents.

	τ ₁ (a ₁)	τ ₂ (a ₂)	<τ _a >
CdTe @ TOP/OA	7.93 (0.39)	26.60 (0.61)	19.36
CdTe @ 2-MPA	20.39 (0.41)	36.97 (0.59)	30.17
CdTe @ MEA	19.67 (0.40)	37.83 (0.60)	30.57
CdTe @ MBA	23.02 (0.44)	39.56 (0.56)	32.28
CdTe @ 3-MPA	22.96 (0.56)	40.98 (0.44)	30.89

5.2.3. Ultrafast transient absorption measurement

The ultrafast transient absorption studies are carried out to understand the effect of capping agent on the trapping dynamics of CdTe QDs. Figure 5.6 shows that the transient absorption spectra of QDs with various capping agents (pumped with 480 nm laser pulse) are very similar. These are characterized by a strong bleach in the region 550 - 750 nm centered at ~ 622 nm, which corresponds to the first exciton peak maximum of CdTe QDs (Figure 5.1) due to $1S(e)-1S_{3/2}(h)$ transition.^{28, 30}

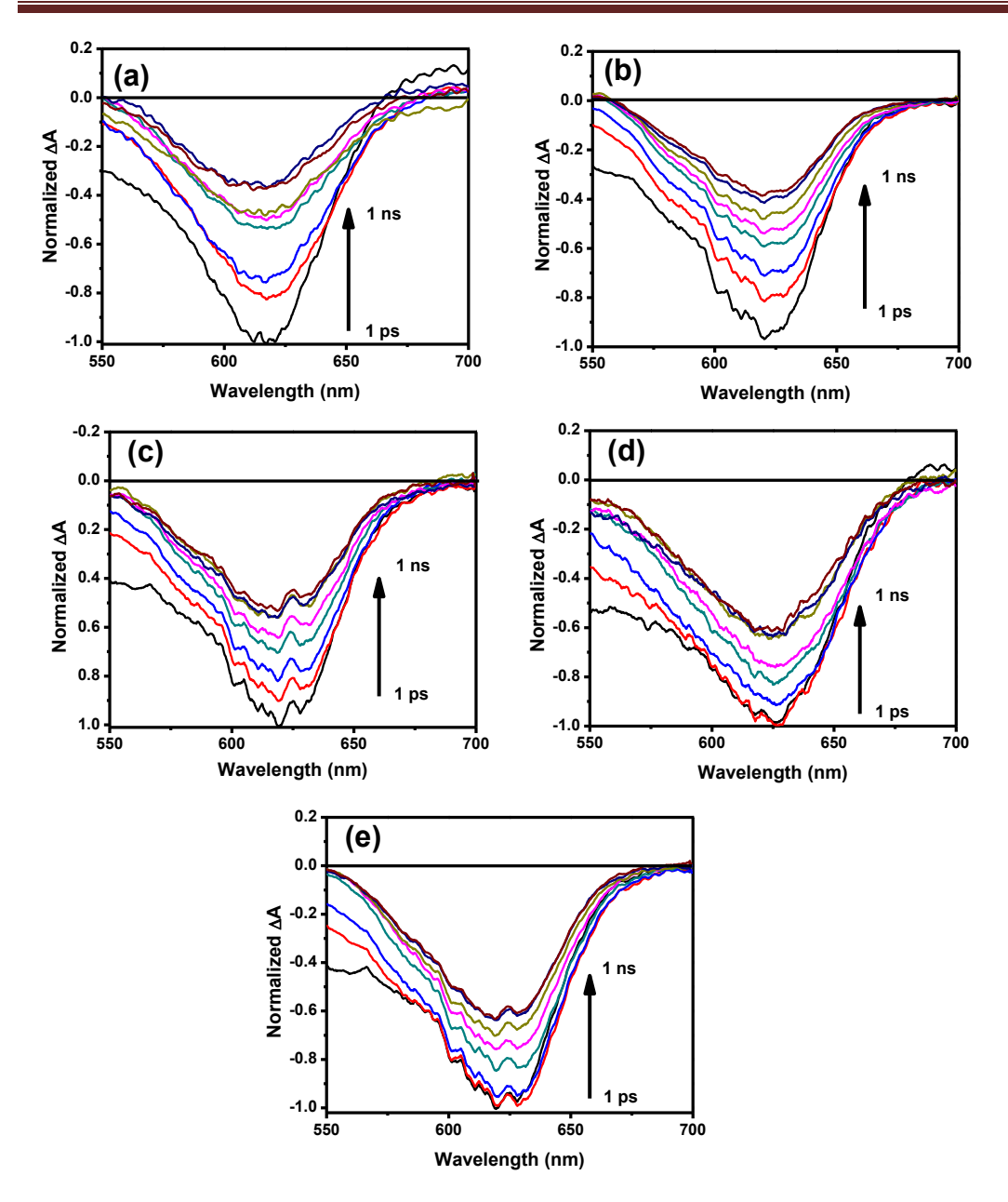


Figure 5.6. Normalized transient absorption spectra of CdTe QDs (3 μ M) capped with TOP/OA (a), 2-MPA (b), MEA (c), MBA (d) and 3-MPA (e).

The bleach recovery kinetics of the QDs (monitored at 620 nm) in the 0-250 ps time domain are shown in Figure 5.7. These time-profiles are represented by a bi-exponential function of the form ΔA (t) = c + a₁ exp (-t/ τ_1) + a₂ exp (-t/ τ_2),

where τ_1 and τ_2 are the lifetimes and a_1 and a_2 are the amplitudes at t=0. The 1S bleach recovery parameters of the QDs obtained from the fits are collected in Table 5.3. The data shows that, in the 0-250 ps time domain, for TOP/OA capped CdTe

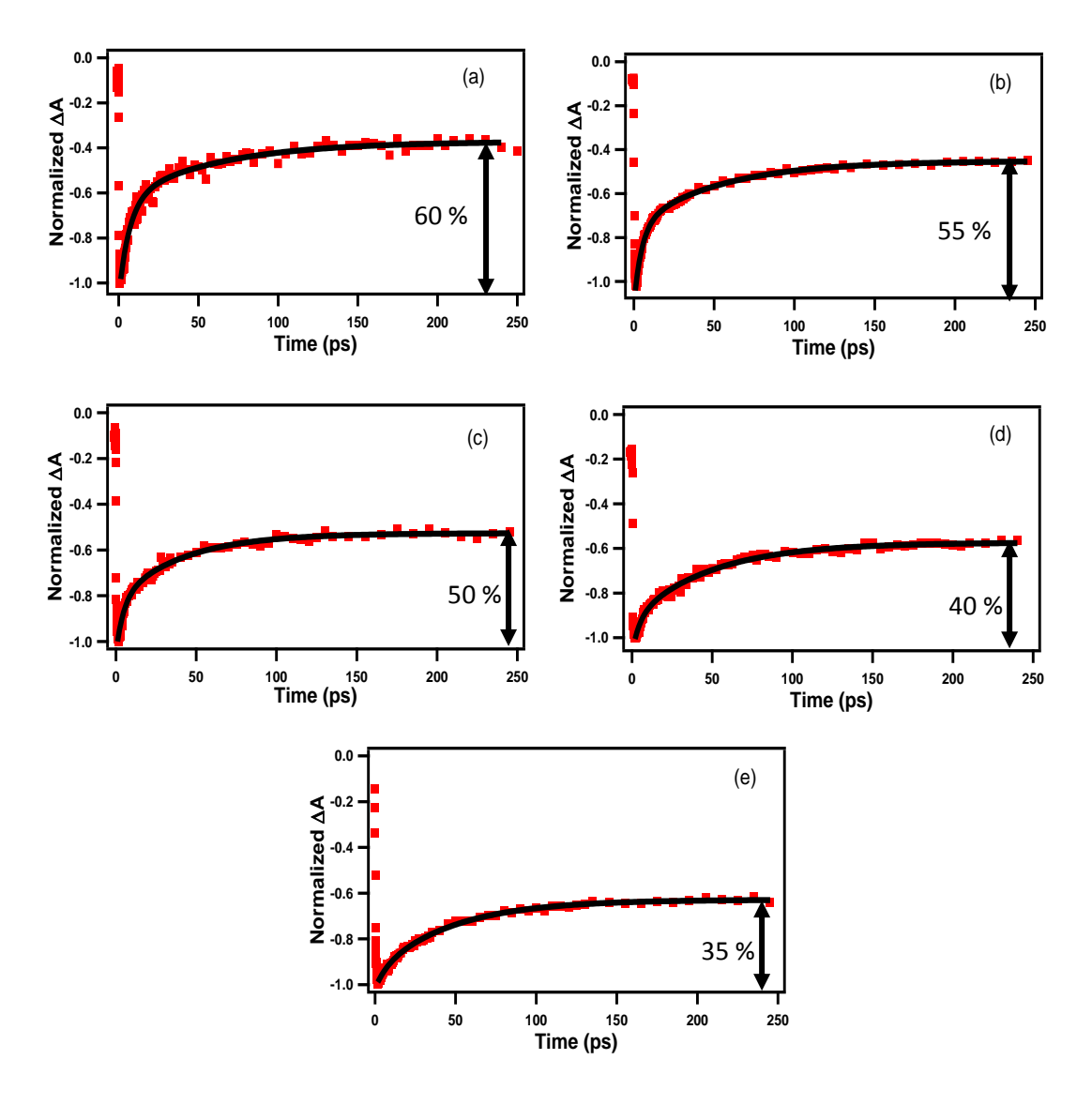


Figure 5.7. 1S transient absorption bleach recovery kinetics (monitored at 620 nm) of CdTe QDs capped with TOP/OA (a), 2-MPA (b), MEA (c), MBA (d), and 3-MPA (d) in the 0-250 ps time domain.

Influence of capping agent...

QDs, 61 % of the bleach is recovered with 7 ps time constant and the remaining by 60 ps. In case of mercapto acid-capped QDs, though these time constants (5-6 and 40-53 ps) remained similar, a decrease in the amplitude (54 to 17 %) of the short time constant is observed. Further, it is obvious from Figure 5.7 that the bleach is not completely recovered within the 0-250 ps time domain. For TOP/OA-capped QDs, 60 % of the bleach is recovered within the 250 ps time window, whereas, for mercapto acid-capped QDs, the amplitude (55 to 35 %) of this bleach recovery is decreased. Further, among the various mercapto acid-capped QDs, the amplitude (35 %) of this bleach recovery is lowest in case of 3-MPA-capped QDs.

Table 5.3. 1S bleach recovery parameters of CdTe QDs with various capping agents.

	a 1	τ ₁ (ps)	\mathbf{a}_2	τ ₂ (ps)
CdTe @ TOP/OA	0.61 ± 0.04	6.89 ± 0.74	0.39 ± 0.03	60.26 ± 12
CdTe @ 2-MPA	0.54 ± 0.01	4.94 ± 0.27	0.46 ± 0.01	52.51 ± 4.05
CdTe @ MEA	0.44 ± 0.04	4.68 ± 0.55	0.56 ± 0.04	41.08 ± 3.98
CdTe @ MBA	0.31 ± 0.02	4.74 ± 0.79	0.69 ± 0.02	48.70 ± 2.75
CdTe @ 3-MPA	0.17 ± 0.02	6.50 ± 1.59	0.83 ± 0.03	46.28 ± 2.42

The bleach recovery kinetics of CdTe QDs with various capping agents on a larger time scale of 0-2 ns is compared in Figure 5.8. It is evident from the figure, there occurs hardly any recovery between 250 ps and 2 ns.

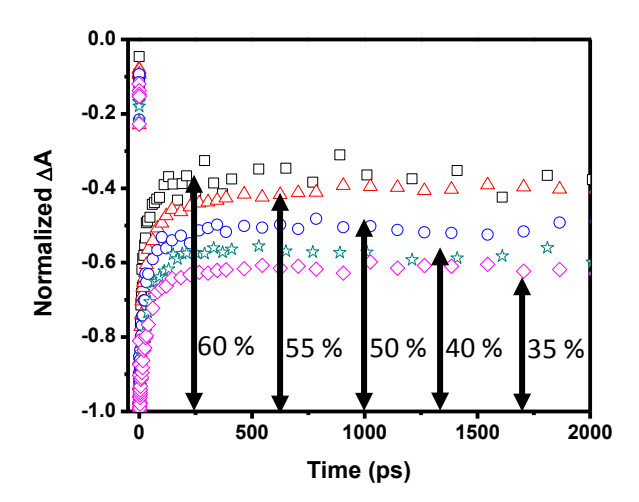


Figure 5.8. Normalized bleach recovery kinetics (monitored at 622 nm) of CdTe QDs (3 μ M) with TOP/OA (\square), 2-MPA (Δ), MEA (o), MBA (*) and 3-MPA (\Diamond) as capping agents.

5.3. Discussion

The enhancement of QY of CdTe QDs on replacement of the capping agents TOP/OA with mercapto acids indicates passivation of the surface trap states arising from the unsaturated or dangling bonds, which provide a pathway for non-radiative carrier recombination resulting in the quenching of QDs photoluminescence.^{5, 6} Effective passivation of the surface trap states by mercapto acids is due to strong binding interaction between the –SH group (a soft base) of the capping agent and the Cd⁺² ions (soft acid) of the QDs when compared with that between the –COOH group (hard base) and Cd⁺² ions. In addition to the strong interaction between the – SH group and Cd sites, the carbonyl oxygen of mercapto acids also coordinates to the Cd sites of QDs thus further contributing to passivation of the unsaturated bonds on the surface atoms.^{18, 31}

Efficient passivation of the surface trap states of QDs by mercapto acids is also evident from the time-resolved emission and absorption studies. An enhancement of the short lifetime component from 8 to 23 ns and long lifetime

Influence of capping agent...

component from 27 to 41 ns and a decrease in the amplitude of the long lifetime component from 61 % to 44 % (Table 5.2) of mercatpo acid-capped CdTe QDs compared to the TOP/OA-capped ones.^{28, 29} Further, the fact that among different mercapto acid-capped QDs, the luminescence contribution due to the core-state recombination is the largest for the 3-MPA-capped QDs (Table 5.2), suggests that a higher degree of surface passivation can be achieved using 3-MPA as a capping agent.

In the transient absorption studies, as mentioned earlier, we observed a 2component recovery (5-7 and 40-60 ps) of the 1S bleach within 250 ps time window beyond which negligible recovery was observed up to 2 ns. These two fast components can be due to the relaxation of the photo-excited carriers of QDs by many particle interactions or by trapping at their surface trap states.²⁸ In order to avoid the influence of many particle interactions on the carrier relaxation dynamics of the QDs, these studies were carried out at low pump energies (where the average number of electron-hole pairs generated per nanocrystal is < 0.1). Hence, as the 1S bleach is dominated by electrons, we attribute the observed bleach recovery to the trapping of photo-excited electrons by various trap states of QDs.²⁸ The long component (> 2 ns) of the recovery (the time constant of which is not measured here) is attributed to the radiative recombination of the photo-generated carriers.²⁸ A larger recovery (60 %) of the 1S bleach in the case of TOP/OA capped-QDs compared to all mercapto acid-capped QDs (55 to 35 %) is a reflection of the efficient trapping of photo-excited carriers. The fact that the recovery is the smallest in the case of 3-MPA-capped QDs indicates the most efficient passivation by 3-MPA.

As 3-MPA differs from MEA and MBA by methylene and methyl group, respectively (Chart 5.1), we first discuss the effect of the methylene unit and then the methyl group on surface passivation of the QDs.

- i) Effect of methylene group: A higher fluorescence QY of the 3-MPA-capped CdTe QDs compared to MEA was attributed to better surface passivation by the former due to the secondary coordination between the carbonyl oxygen of the carboxyl group of mercapto acid and Cd site of the CdTe QDs in addition to the strong –SH- Cd⁺² interaction.¹⁸ Möhwald and co-workers, who observed a higher stability of colloidal 3-MPA capped CdTe QDs compared to the MEA capped ones, explained their observation considering coordination of the -SH and carbonyl oxygen to the same Cd site by the former, whereas, in case of MEA (one methylene unit shorter than 3-MPA), the two moieties coordinate to two adjacent sites.³¹ Hence, the enhancement in the photoluminescence of 3-MPA capped QDs observed in our study, can be assigned to the better surface passivation due to the binding of SH and carbonyl group of 3-MPA to the same Cd site.
- ii) Effect of methyl group: The observation of an enhancement in fluorescence of CdTe QDs in the presence of polyacrylic acid (PAA) at low pH, ¹⁸ but no enhancement in the presence of polymethylacrylic acid (PMAA) by Gao and coworkers was attributed to the spatial hindering effect of the methyl group preventing the secondary coordination of the carbonyl oxygen from binding the Cd sites on the nanoparticle surface. Breus and coworkers also observed the effect of spatial hindrance by the methyl groups present on the β-carbon atom of D-penicillamine that reduces interactions between the carbonyl oxygen and the Cd sites, when they capped CdSe/ZnS QDs with cysteine and D-penicillamine. ³² Based on above literature, we can speculate that the presence of methyl group on the β-carbon atom of the MBA hinders the secondary coordination between the carbonyl oxygen and the Cd sites of CdTe QDs thus explaining poor performance in surface passivation.

Influence of capping agent...

5.4. Conclusion

It is shown that highly luminescent water soluble mercapto acid-CdTe QDs developed through ligand-replacement method instead of their direct aqueous growth. With the help of steady state and time-resolved absorption and emission studies it is shown that efficient passivation of the surface trap states of CdTe QDs can be achieved using 3-MPA as a capping agent.

Chapter 5

References

- 1. Fang, T.; Ma, K.; Ma, L.; Bai, J.; Li, X.; Song, H.; Guo, H., *J. Phys. Chem. C* **2012,** 116, 12346.
- 2. Alivisatos, A. P., J. Phys. Chem. **1996**, 100, 13226.
- 3. Nirmal, M.; Brus, L., Acc. Chem. Res. **1999**, 32, 407.
- 4. Murray, C. B.; Norris, D. J.; Bawendi, M. G., J. Am. Chem. Soc. **1993**, 115, 8706.
- 5. Smith, A. M.; Nie, S., Acc. Chem. Res. **2010**, 43, 190.
- 6. Chen, X.; Lou, Y.; Samia, A. C.; Burda, C., Nano Lett. **2003**, 3, 799.
- 7. Kamat, P. V.; Trvdy, K.; Baker, D. R.; Radich, J. G., *Chem. Rev.* **2010,** 110, 6664.
- 8. Nozik, A. J.; Beard, M. C.; Luther, J. M.; Law, M.; Ellingsono, R. J.; Jhonson, J. C., *Chem. Rev.* **2010**, 110, 6873.
- 9. Kamat, P. V., J. Phys. Chem. C 2008, 112, 18737.
- 10. Achermann, M.; Petruska, M. A.; Koleske, D. D.; Crawford, M. H.; Klimov, V. I., *Nano. Lett.* **2006**, *6*, 1396.
- 11. Steckel, J. S.; Snee, P.; Coe-Sullivan, S.; Zimmer, J. P.; Anikeeva, P.; Kim, L. A.; Bulovic, V.; Bawendi, M. G., **2006**, 45, 5796.
- 12. Colvin, V. L.; Schlamp, M. C.; Alivisatos, A. P., *Nature* **1994**, 370, 354.
- 13. Bruchez, M.; Moronne, M.; Gin, P.; Weiss, S.; Alivisatos, A. P., *Science* **1998,** 281, 2013.
- 14. Chan, W. C. W.; Nie, S., Science 1998, 281, 2016.
- 15. Medintz, I. L.; Clapp, A. R.; Brunel, F. M.; Tiefenbrunn, T.; Uydea, H. T.; Chang, E. L.; Deschamps, J. R.; Dawson, P. E.; Mattoussi, H., *Nat. Mater.* **2006**, 5, 581.
- 16. Pokrant, S.; Whaley, K. B., Eur. Phys. J. D. **1999**, 6, 255.
- 17. Chaudhuri, R. G.; Paria, S., Chem. Rev. 2012, 112, 2373.
- 18. Zhang, H.; Zhou, Z.; B, Y.; Gao, M., J. Phys. Chem. B 2003, 107, 8.
- 19. Green, M.; Harwood, H.; Barrowman, C.; Rahman, P.; Eggeman, A.; Festry, F.; Dobson, P.; Ng, T., *J. Mater. Chem.* **2007,** 17, 1989.
- 20. Wuister, S. F.; Swart, I.; Driel, F. V.; Hickey, S. G.; Donega, D. D., *Nano. Lett.* **2003**, 3, 503.
- 21. Wuister, S. F.; Donega, C. M.; Meijerink, A., J. Phys. Chem. B 2004, 108, 17393.
- 22. Gaponik, N.; Talapin, D. V.; Rogach, A. L.; Hoppe, K.; Shevchenko, V. E.; Kornowski, A.; Eychmüller, A.; Weller, H., *J. Phys. Chem. B* **2002**, 106, 7177.
- 23. Lim, S. J.; Chon, B.; Joo, T.; Shin, S. K., *J. Phys. Chem. C* **2008**, 112, 1744.
- 24. Gaponik, N.; Rogach, L. A., Phys. Chem. Chem. Phys. **2010**, 12, 8685.
- 25. Aldeek, F.; Balan, L.; Lambert, J.; Schneider, R., *Nanotechnology* **2008**, 19, 475401.
- 26. Kloper, V.; Osovsky, R.; Olesiak, J. K.; Sashchiuk, A.; Lifshitz, E., *J. Phys. Chem. C* **2007**, 111, 10336.
- 27. Yu, W. W.; Qu, L.; Guo, W.; Peng, X., Chem. Mater. 2003, 15, 2854.
- 28. Klimov, V. I.; McBranch, D. W.; Leatherdale, C. A.; Bawendi, M. G., *Phys. Rev. B: Condes. Matter Mater. Phys* **1999**, 60, 13740.
- 29. Wang, X.; QU, L.; Zhang, J.; Peng, X.; Xiao, M., *Nano. Lett.* **2003,** 3, 1103.

Influence of capping agent...

- 30. Burda, C.; Link, S.; Green, T. C.; El-Sayed, M. A., *J. Phys. Chem. B* **1999**, 103, 10775.
- 31. Zhang, H.; Wang, D.; Möhwald, H., Angew. Chem. Int. Ed. 2006, 45, 748.
- 32. Breus, V. V.; Heyes, D. C.; Tron, K.; Nienhaus, G. U., ACS Nano 2009, 3, 25730.

Charge Separation and Recombination Dynamics between CdSe QDs and Methyl Viologen: Dependence on the Stoichiometry of the Nanocrystals

The interaction between photo-excited CdSe QDs of various surface stoichiometry and methyl viologen (MV⁺²) is studied using steady state and time-resolved absorption and emission techniques. The ultrafast transient absorption measurements provide convincing evidence of the transfer of electron between CdSe QDs and MV⁺² and show that the rate of forward and back electron transfer process is independent of the QDs stoichiometry. Interestingly, however, the electron transfer efficiency is found dependent on the QDs stoichiometry with maximum efficiency observed in the case of Cd-rich QDs. The low electron transfer efficiency in Se-rich QDs is attributed to efficient hole trapping at the selenium sites, which enhances the non-radiative carrier recombination.

6.1. Introduction

Quantum dots (QDs), the three dimensionally confined semiconductor nanocrystals, which exhibit size-dependent optical and electronic properties ¹⁻⁴ are considered as ideal sensitizers for harvesting the solar energy. ⁵⁻⁹ They also have the ability to generate multiple (two or more) excitons by absorbing photon of higher energy ($hv \ge 2Eg$, Eg is the band gap of the QD), which increases the energy-to-current conversion efficiency of the Quantum Dot Sensitized Solar Cells (QDSSCs) beyond Schokley and Queisser limit. ¹⁰⁻¹⁴ However, the energy conversion efficiency exhibited by these QDSSCs ($\sim 8-9$ %)^{8, 9} is low compared to the other (dye and silicon based) solar cells. ¹⁵⁻¹⁷ Trapping of the photo-generated charge carriers by the states that arise due to incomplete bonding of the surface atoms present on the QDs is regarded as one of the factors in limiting the energy conversion efficiency in QDSSCs. ^{9, 18}

The passivation of the unsaturated dangling orbitals on the surface atoms of the QDs can be accomplished by growing inorganic shell of larger band gap around the core. Though the photoluminescence of the QDs is enhanced by this process, the rate of the electron (hole) transfer between the photo-excited QDs and the electron (hole) acceptors is decreased. On the other hand, these unsaturated dangling orbitals are also passivated with organic ligands. The organic ligands such as alkylamine, alkylphosphine oxides and alkylphosphonic acids are shown to bind to the cationic sites of the QDs strongly, whereas the anionic sites are majorly passivated by the alkylphosphine. Hence, the ability to passivate the trap states of the QDs with these organic ligands depends on the surface stoichiometry of the QDs.

Mulvaney and co-workers modified the surface stoichiometry of the CdSe QDs from Cd-rich to Se-rich and observed significantly higher photoluminescence

Charge Separation and recombination...

quantum yield (QY) for the Cd-rich QDs.²⁶ They also observed a dramatic increase in the QY of the Se-rich QDs after treating with trioctylphosphine indicating different surface stoichiometry of the QDs requires different ligand passivation. Further, Heyes and co-workers synthesized CdTe QDs by varying their stoichiometry and studied the effect of the interaction between the surface atoms and ligands on the radiative and non-radiative relaxation rates of the CdTe QDs.²⁸ Though the effect of surface stoichiometry of the QDs on their photoluminescence properties is well-studied, its influence on the charge separation and recombination dynamics between the QDs and acceptors is largely unexplored.

In this work, we have investigated the effect of QDs stoichiometry on the charge separation and recombination dynamics between the photo-excited CdSe QDs and MV^{+2} (Chart 6.1). Using femtosecond transient absorption measurements, we show that the rate of both forward and back electron transfer between CdSe QDs and MV^{+2} is independent of the QDs stoichiometry, but not the efficiency of the electron transfer process from CdSe QDs to MV^{+2} .

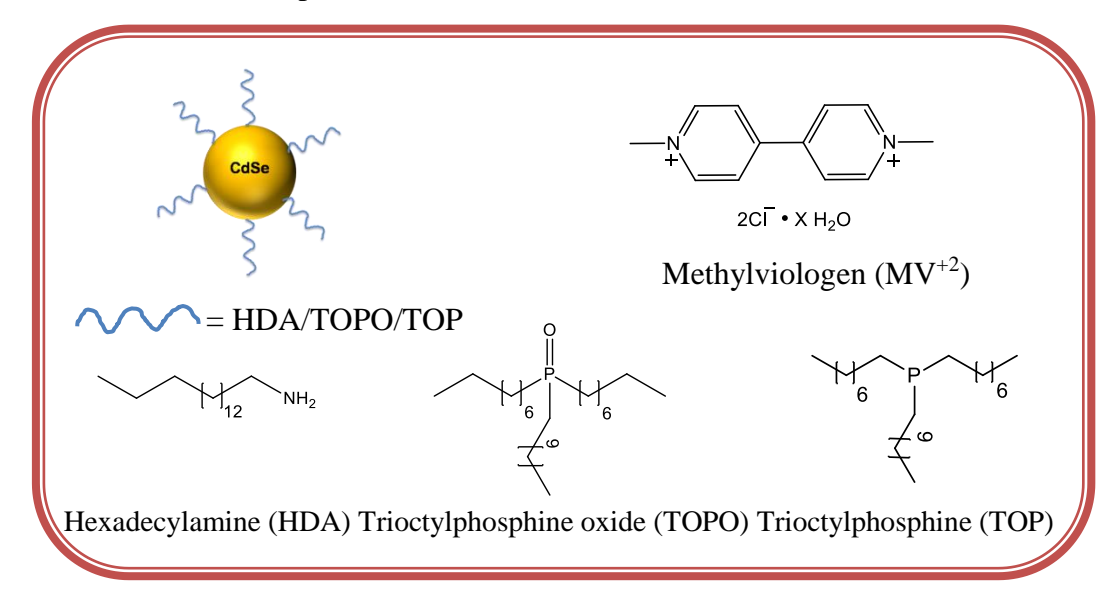


Chart 6.1. CdSe QDs and chemical formula of MV⁺² and capping agents.

6.2. Results

6.2.1. Steady state and time-resolved measurements

Figure 6.1a depicts the absorption spectra of CdSe QDs of different stoichiometry in chloroform. These spectra are featured with three well-resolved bands with maxima around ~ 560 , ~ 525 and ~ 475 nm corresponding to the interband transitions $1S_{e}-1S_{3/2(h)}$, $1S_{e}-2S_{3/2(h)}$, and $1P_{e}-1P_{3/2(h)}$, respectively.^{29, 30} A very similar first exciton peak maximum for the QDs with different stoichiometry indicates similar sizes (3.2 \pm 0.1 nm, calculated from the first exciton peak maximum)³¹ which is confirmed by the TEM micrographs (Figure 6.2). The emission spectra of the CdSe QDs with different stoichiometry are shown in Figure 6.1b and the quantum yields (QY) are given in Table 6.1. Compared to the CdSe (1:1) QDs, small enhancement of the QY values in the case of CdSe (2.5:1) and a decrease in the case of CdSe (1:1.5) is observed.

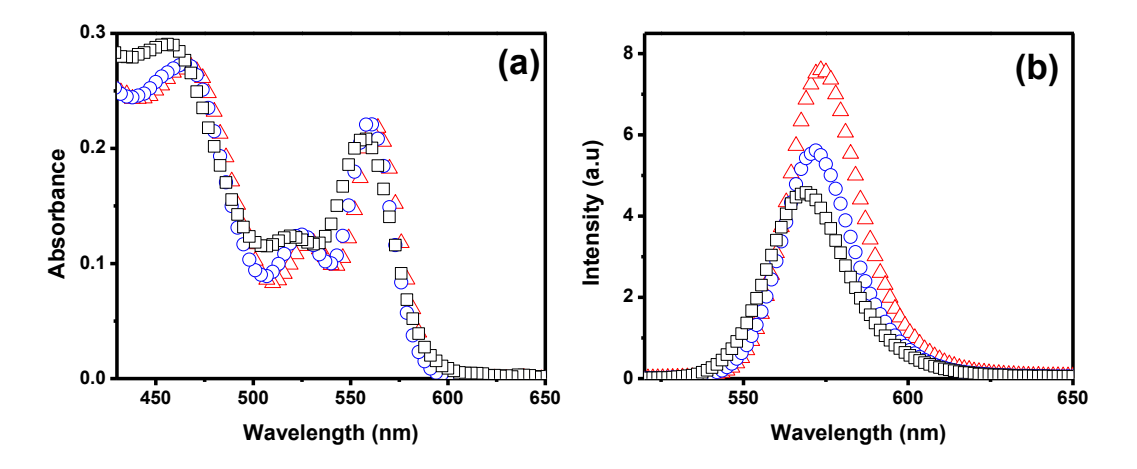


Figure 6.1. (a) Absorption and (b) emission spectra of 1.5 μ M solution (CHCl₃) of CdSe QDs with different stoichiometry; (2.5:1, Δ), (1:1, 0) and (1:1.5, \Box).

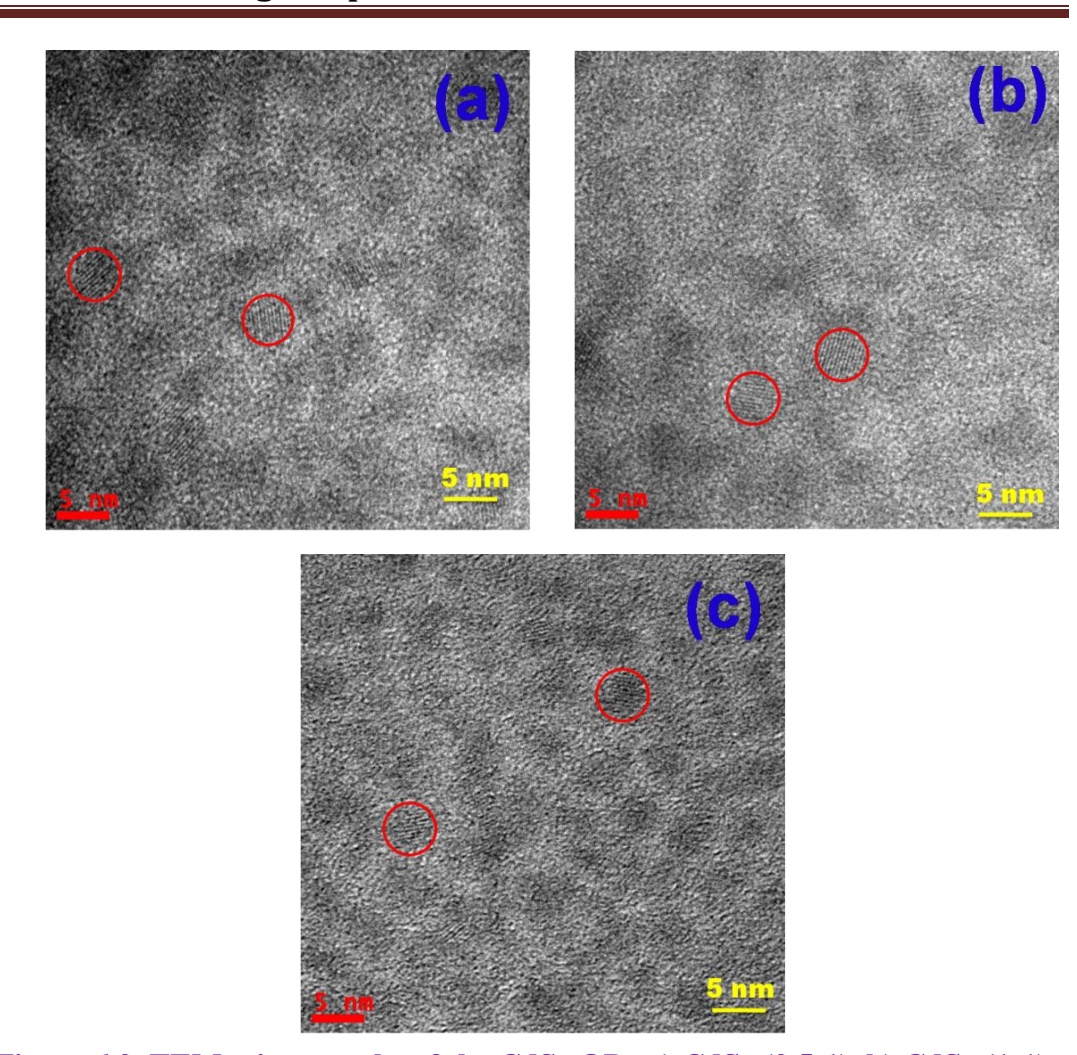


Figure 6.2. TEM micrographs of the CdSe QDs a) CdSe (2.5:1), b) CdSe (1:1) and c) CdSe (1:1.5).

Table 6.1. Quantum yield of CdSe QDs with different stoichiometry.

System	Quantum yield (%)
CdSe (2.5:1)	24
CdSe (1:1)	21
CdSe (1:1.5)	18

On addition of MV^{+2} , a huge quenching of emission is observed in all cases (Figure 6.3) though the absorption spectra of the CdSe QDs remained similar (Figure 6.4).

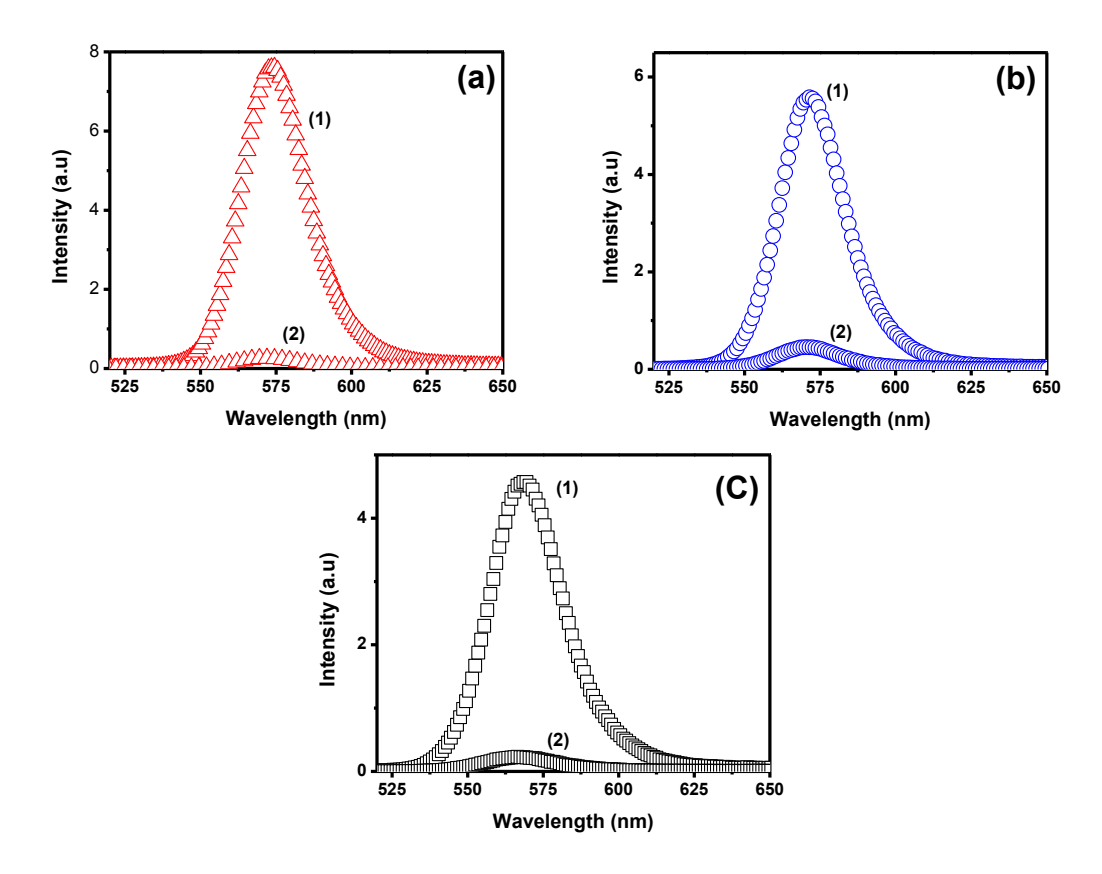


Figure 6.3. Emission spectra of the a) CdSe (2.5:1), b) CdSe (1:1) and c) CdSe (1:1.5) QDs (1.5 μ M) in the (1) absence and (2) presence of MV⁺² (3 μ M).

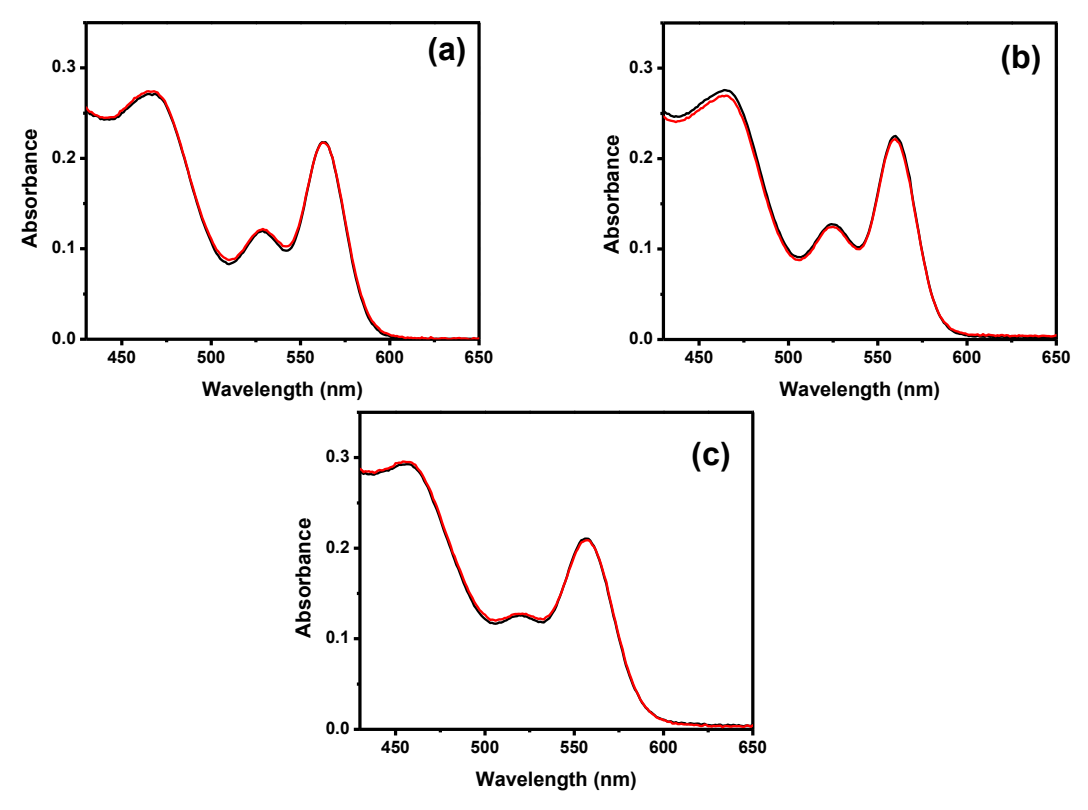


Figure 6.4. Absorption spectra of the a) CdSe (2.5:1), b) CdSe (1:1) and c) CdSe (1:1.5) QDs (1.5 μ M) in the absence (black) and presence (red) of MV⁺²(3 μ M).

The fluorescence decay profiles of the CdSe QDs of different stoichiometry in the absence and presence of MV^{+2} , monitored at their emission maxima, are shown in Figure 6.4. These decay profiles are best represented by a triexponential function of the form $I(t) = a_1 \exp(-t/\tau_1) + a_2 \exp(-t/\tau_2) + a_3 \exp(-t/\tau_3)$. The lifetime components and associated amplitudes of the QDs including their average lifetime $<\tau_a>$, given by $<\tau_a> = (a_1\tau_1 + a_2\tau_2 + a_3\tau_3)/(a_1+a_2+a_3)$, are presented in Table 6.2. The triexponential nature of the decay and the measured decay parameters are in agreement with literature.³² We attribute the \sim 18 ns component to recombination of

the core-state electrons and holes, whereas the shortest (\sim 2 ns) and the longest (\sim 52 ns) components to the electron-hole recombination involving the deep and shallow trap states, respectively. ³²⁻³⁴ In the presence of MV⁺², a small decrease (30 %) in the average lifetimes of the QDs is observed. The huge decrease observed in the steady state fluorescence intensities of the QDs compared to their average lifetimes on addition of MV⁺² implies that the quenching of the QDs emission occurs mainly by the static interaction between the donor and acceptor.

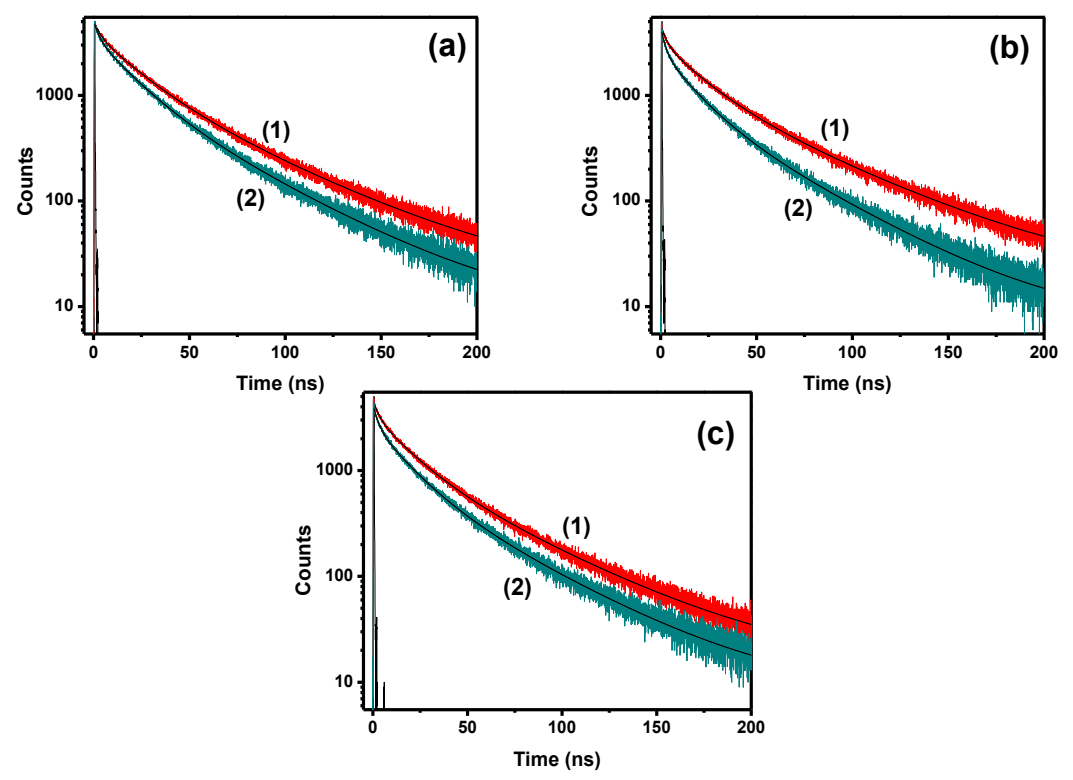


Figure 6.4. Emission decay profiles of the a) CdSe (2.5:1), b) CdSe (1:1) and c) CdSe (1:1.5) QDs (1.5 μ M) in the (1) absence and (2) presence of MV⁺² (3 μ M).

Charge Separation and recombination...

Table 6.2. Fluorescence decay parameters and average lifetime ($\langle \tau_a \rangle$, ns) of the QDs of different stoichiometry in the absence and presence of MV⁺².

System	τ ₁ (a ₁)	τ ₂ (a ₂)	τ ₃ (a ₃)	<τ _a >
CdSe (2.5:1)	18.15 (0.47)	52.84 (0.32)	2.05 (0.21)	25.87
$CdSe + MV^{+2}$	16.16 (0.49)	45.50 (0.22)	2.45 (0.29)	19.10
CdSe (1:1)	18.21 (0.44)	52.89 (0.29)	2.71 (0.27)	24.08
$CdSe + MV^{+2}$	14.67 (0.43)	42.53 (0.22)	2.24 (0.35)	16.45
CdSe (1:1.5)	17.33 (0.47)	49.25 (0.27)	2.79 (0.26)	22.18
$CdSe + MV^{+2}$	15.97 (0.46)	44.89 (0.23)	2.69 (0.31)	18.06

6.2.2. Ultrafast transient absorption measurements

The ultrafast transient absorption measurements enable us to determine the mechanism of quenching of the QDs emission on addition of MV^{+2} and also to find out the effect of QDs stoichiometry on the nature of interaction between the quenching partners. Figure 6.5 shows the transient absorption spectra of the various CdSe QDs recorded at indicated delay times in the absence and presence of MV^{+2} after 480 nm excitation. These spectra show two well resolved bleach features centered at ~530 nm and ~ 562 nm, which can be assigned to the $1S_{e^{-1}} S_{3/2(h)}$ and $1S_{e^{-2}} S_{3/2(h)}$ inter-band optical transitions, respectively, considering the absorption spectra of the sample (Figure 6.1).^{29, 30} In the presence of MV^{+2} , a faster recovery of the QDs bleach is observed along with a new broad positive absorption band in the 580-650 nm range.

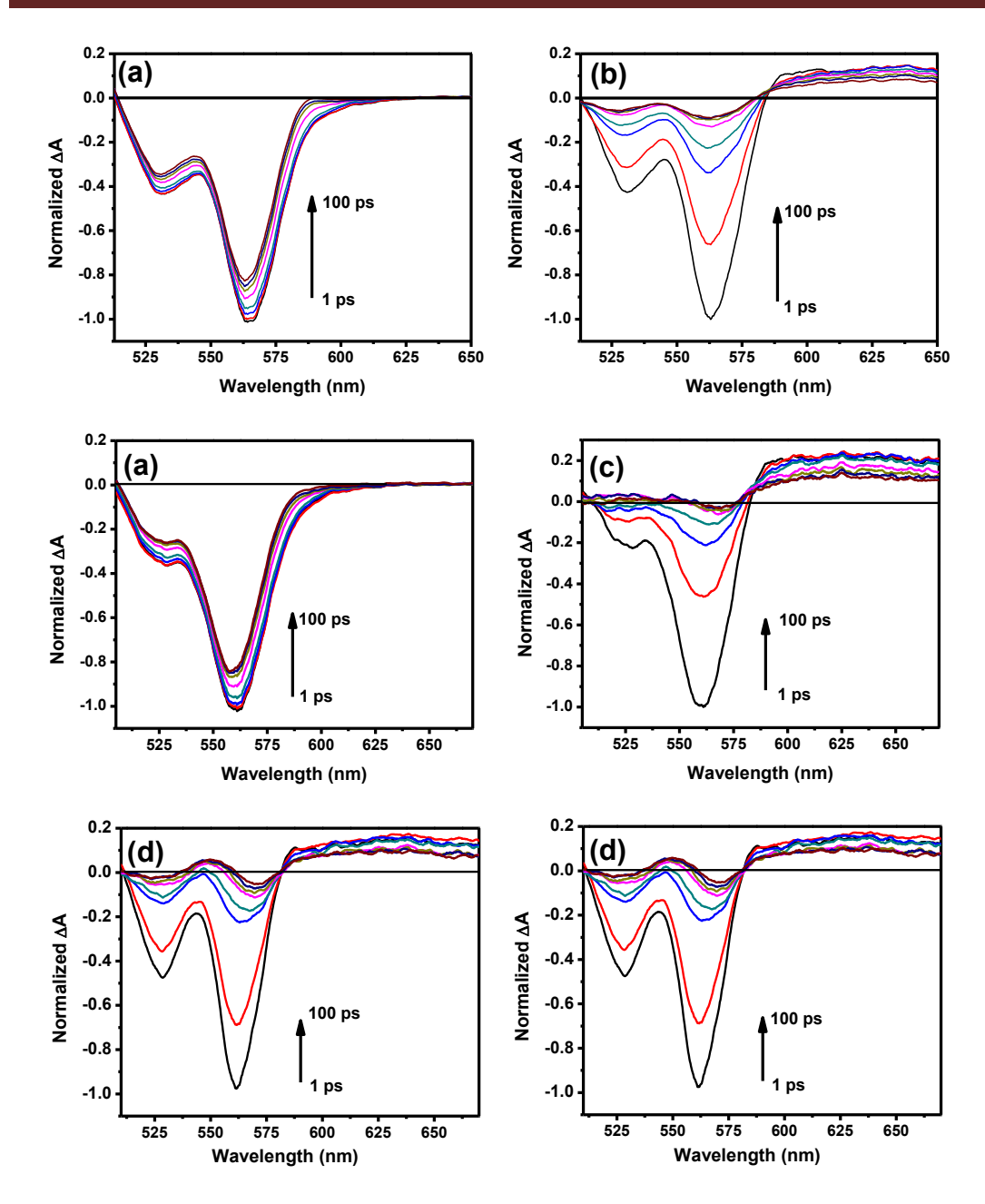


Figure 6.5. Normalized difference absorption spectra of the a) CdSe (2.5:1) and b) CdSe (1:1) and c) CdSe (1:1.5) QDs (10 μ M) in the (a,b,c) absence and (d,e,f) presence of MV⁺² (50 μ M) at various delay time (1, 2, 5, 10, 30, 50, 70, 100 ps) after 480 nm excitation.

The decay kinetics of the new transient absorption band observed in presence of MV⁺² monitored at 640 nm are compared in Figure 6.6 for the different CdSe QDs. The overlap of the decay profile indicates very similar growth and decay kinetics for the three different QDs.

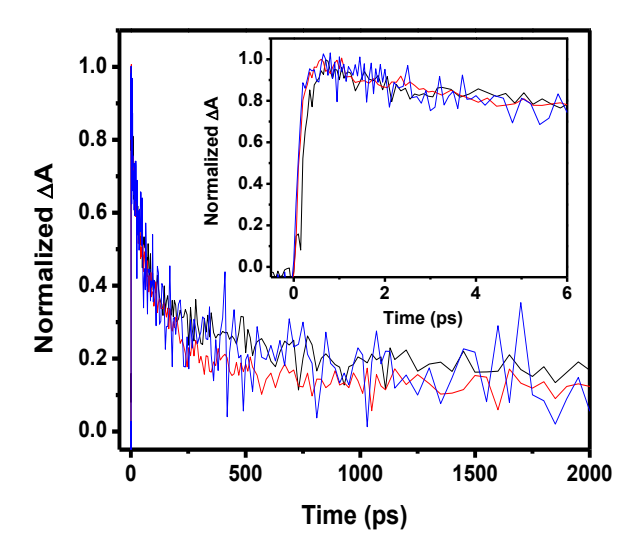


Figure 6.6. Normalized transient absorption decay kinetics of the CdSe (2.5:1, black), CdSe (1:1, red) and CdSe (1:1.5, blue) QDs (10 μ M) in the presence of MV⁺²(50 μ M) monitored at 640 nm. The Inset shows the decay kinetics at early time scale.

The transient absorption decay profiles of the QDs (Figure 6.7) can be fitted to a biexponential function of the form ΔA (t) = c + $a_1 exp$ (-t/ τ_1) + $a_2 exp$ (-t/ τ_2), where τ_1 and τ_2 represent the lifetimes and a_1 and a_2 are the corresponding amplitudes at t = 0. The measured decay parameters of the QDs in the presence of MV^{+2} along with the rise time (τ_{rise}) and average lifetime $<\tau_a>$, given by $<\tau_a>$ = $(a_1\tau_1 + a_2\tau_2)/(a_1+a_2)$ are presented in Table 6.3.

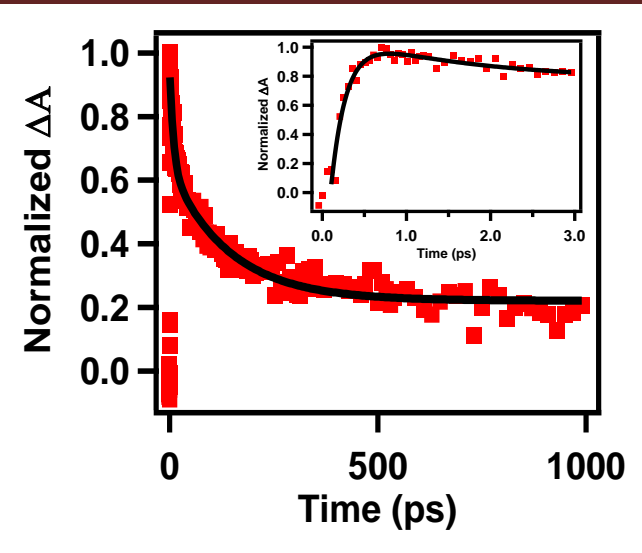


Figure 6.7. Representative decay kinetics monitored at 640 nm for CdSe (2.5:1) QDs (10 μ M) in the presence of MV⁺² (50 μ M). Inset show the kinetics at shorter time scale.

Table 6.3. The measured rise and decay parameters of the kinetics monitored at 640 nm for different QDs stoichiometry.

System	τ_{rise}, fs	τ ₁ , ps	a 1	$ au_2, \mathbf{ps}$	a 2	$ au_{avg}, ps$
CdSe (2.5:1)	105 ± 8	9 ± 1	0.42 ± 0.02	141 ± 11	0.58 ± 0.01	85.53
CdSe (1:1)	136 ± 6	8 ± 1	0.39 ± 0.01	136 ± 6	0.61 ± 0.01	86.11
CdSe (1:1.5)	114 ± 3	8 ± 3	0.31 ± 0.04	107 ± 15	0.69 ± 0.04	76.21

Though the transient absorption decay kinetics for different CdSe QDs-MV⁺² systems show very little dependence on the QDs stoichiometry, an interesting difference in the amplitude of the transient absorption signal is observed on varying the stoichiometry of the QDs, which is evident from Figure 6.8 showing a much stronger signal for CdSe (2.5:1) QDs compared to the CdSe (1:1.5) QDs.

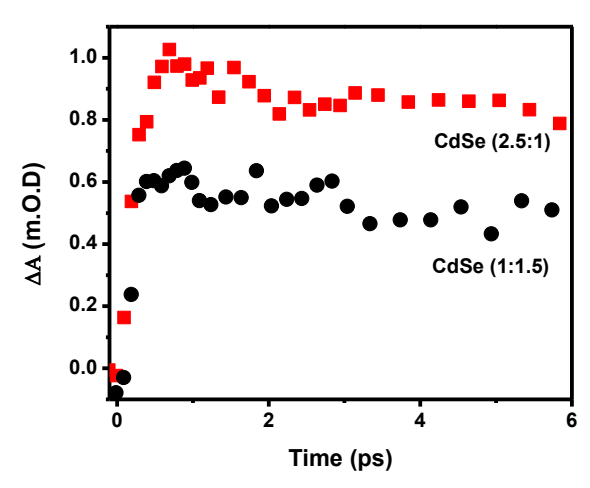


Figure 6.8. Transient absorption decay kinetics of the CdSe (2.5:1, \blacksquare) and CdSe (1:1.5, \bullet) QDs (10 μ M) in the presence of MV⁺² (50 μ M) monitored at 640 nm. These decay kinetics are recorded under same experimental conditions.

6.3. Discussion

As there is no change in the absorption spectra of the CdSe QDs on addition of MV^{+2} (Figure 6.2), the quenching of the QDs emission by of MV^{+2} is due to an

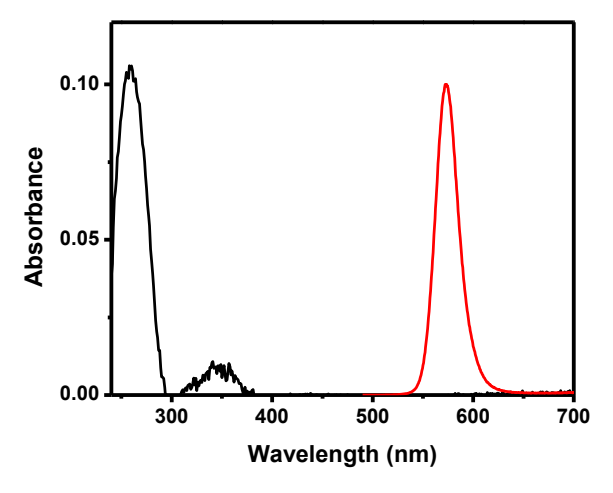


Figure 6.9. Absorption (black) and emission (red) spectra of MV^{+2} and CdSe QDs, respectively.

additional non-radiative relaxation pathway. The lack of spectral overlap of the donor (QD) emission and acceptor absorption (MV^{+2}) spectra (Figure 6.9) eliminates the possibility of energy transfer between the two. On examining the potentials of the valence band (VB) and conduction band (CB) of the CdSe QDs and the reduction potential of the MV^{+2} (Figure 6.10), it is evident that photo-induced electron transfer between QDs and MV^{+2} is a thermodynamically feasible route for quenching of the QDs emission by MV^{+2} . The potentials of the VB and CB of the CdSe QDs are estimated to be + 0.6 V and -1.57 V, respectively.^{35, 36} and the reduction potential of MV^{+2} is - 0.5V.³⁷

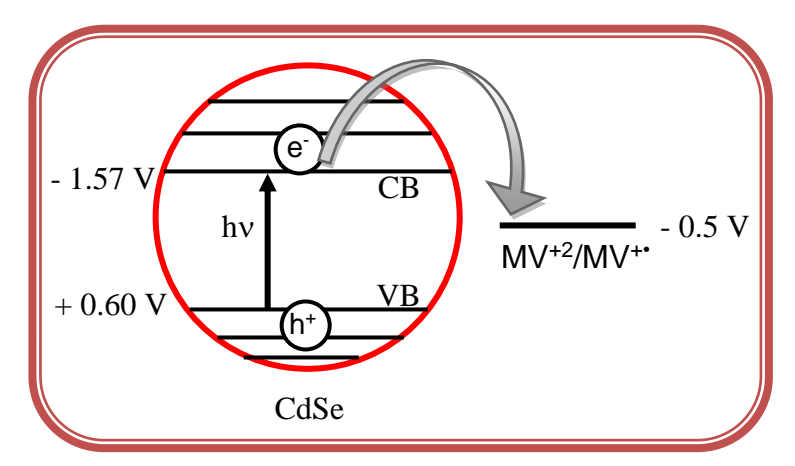


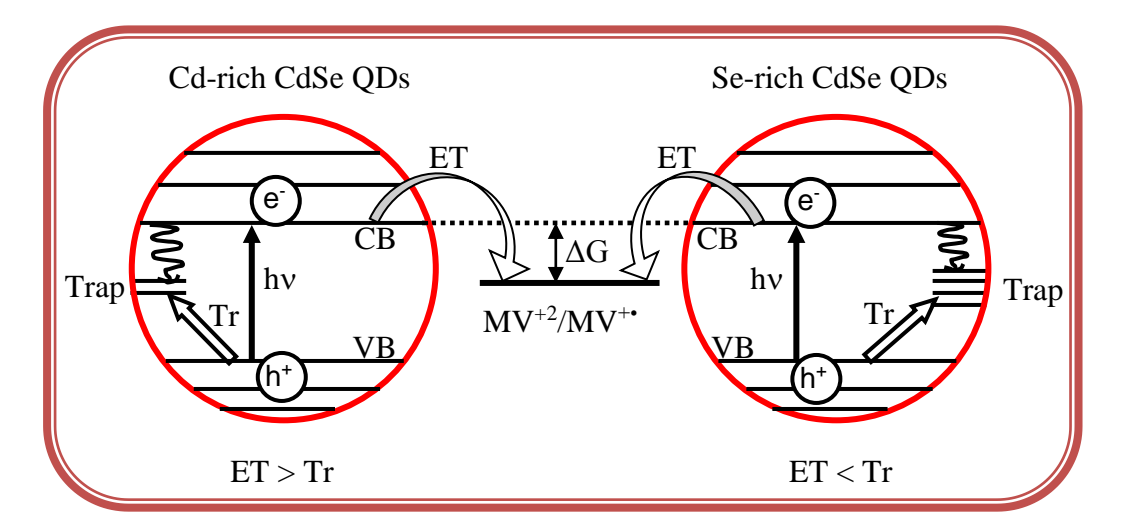
Figure 6.10. Valence band (VB) and conduction band (CB) potentials of the CdSe QDs and reduction potential of MV^{+2} (vs NHE).

Matylitsky and coworkers studied photo-induced electron transfer between CdSe QDs and MV⁺² using ultrafast transient absorption spectroscopy and observed the formation of monocationic radical species of MV⁺² (MV^{+*}),³⁸ which exhibits a broad absorption in the regions 300–400 nm and 470-750 nm.³⁹ As, the broad positive absorption (580-650 nm) observed in our case on addition of MV⁺² (Figure 6.5) is very similar to the well-known absorption band of the MV^{+*} radical species, we can conclude photo-induced electron transfer between the CdSe QDs

Charge Separation and recombination...

and MV⁺². Wachtveitl and co-workers found that the photo-induced electron transfer rate constant between CdSe QDs and MV+2 varies with the size of the QD,⁴⁰ which they attributed to the change in the QDs energy levels.⁴⁰ Markus et. al., studied electron transfer between the CdSe QDs and TiO2 by varying the sizes of the CdSe QDs and observed that efficient electronic coupling between CdSe QDs and TiO₂ modifies the energetics of the CdSe-TiO₂ system.⁴¹ Further, Canovas and coworkers synthesized the PbS QDs on the oxide matrix (SnO₂) through successive ionic layer adsorption and reaction (SILAR) method and investigated the effect of QDs stoichiometry and their size on the photo-induced electron transfer between PbS QDs and SnO2. 42 They observed that the rate of photo-induced electron transfer between the PbS QDs and SnO₂ is independent of the QDs stoichiometry and their size, and concluded that the energy difference (ΔG) between the CB of the PbS QDs and the CB of the SnO₂ which influence the transfer of electron is not affected by the QDs stoichiometry and their size. Based on the above literature, the invariance in the rate of forward ($k_{ET} = 1/\tau_{rise} = -8 \text{ x}$ $10^{12}~s^{\text{--}1})$ and back (k_BET = $1/\tau_{avg}$ = $\sim\!1~x~10^{10}~s^{\text{--}1})$ electron transfer between the CdSe QDs of different QDs stoichiometry and MV⁺² (Figure 6.6), suggests that the QD-MV⁺² energetics and their coupling strength are independent of the QDs stoichiometry (Scheme 6.1).

Though the formation and decay kinetics of the MV⁺⁺ radical species is independent of the QDs stoichiometry, the larger ΔA value for CdSe (2.5:1) in Figure 6.8 shows that electron transfer is more efficient in the case of CdSe (2.5:1) QDs. It is known that trapping of photo-generated carriers by the surface trap states competes with the electron transfer process between the QDs and acceptors and can influence their efficiency.⁴² To find out whether the stoichiometry of the QDs affects this trapping process, we compared the 1S bleach recovery kinetics of the various QDs (Figure 6.11), considering that the bleach signal mostly represents the



Scheme 6.1. Schematic representation of the CdSe-MV⁺² system energetics as a function of the stoichiometry of the CdSe QDs. CdSe (2.5:1) QDs are populated with less number of trap states and hence increases the probability of electron transfer to the MV^{+2} . CdSe (1:1.5) QDs are populated with more number of trap states that enhances the probability of carrier trapping (Tr).

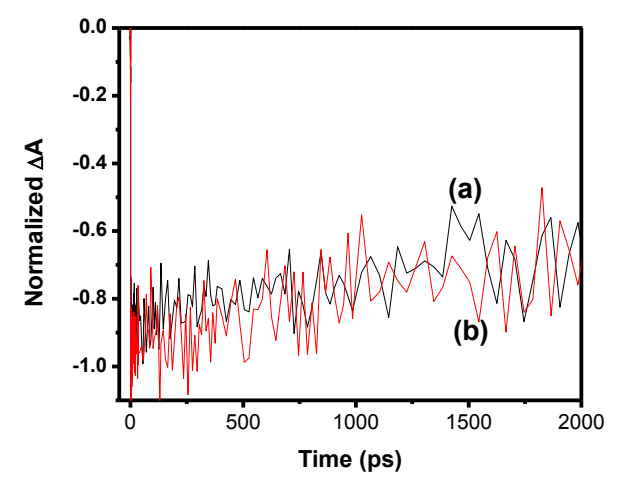


Figure 6.11. 1S bleach recovery kinetics of a) CdSe (2.5:1) and b) CdSe (1:1) QDs (10 μ M). To avoid many particle interactions on the carrier relaxation dynamics, these bleach recovery kinetics are measured at low pump energies such that the number of excitons generated per nanocrystal is less than 0.05.

Charge Separation and recombination...

dynamics of electrons in the conduction band.^{29, 33} A similar bleach recovery kinetics observed for different stoichiometric QDs suggest that the trapping of the photo-excited electrons is independent of QDs stoichiometry. In view of this and recognizing a more efficient hole trapping in case of Se-rich QDs,^{26, 43} the decrease in electron transfer efficiency and a low emission QY for CdSe (1:1.5) QDs is attributed to more efficient hole trapping process at the surface selenium sites, which enhances the non-radiative carrier recombination (Scheme 6.1).

6.4. Conclusion

Quenching of the emission of QDs with different surface stoichiometry is studied using steady state and time-resolved absorption and emission techniques. We found that the rate of forward and back electron transfer process between the QD and MV⁺² is independent of QDs stoichiometry. Interestingly, we observed higher electron transfer efficiency from QDs to MV⁺² in the case of cationic-rich QDs.

Chapter 6

References

- 1. Alivisatos, A. P., *Science* **1996**, 271, 933.
- 2. Norris, D. J.; Efros, A. L.; Rosen, M.; Bawendi, M. G., *Phys. Rev. B* **1996**, 53, 16347.
- 3. Talapin, D. V.; Lee, J. S.; Kovalenko, M. V.; Shevchenko, E. V., *Chem. Rev.* **2009**, 110, 389.
- 4. Norris, D. J.; Bawendi, M. G., *Phys. Rev. B* **1996**, 53, 16347.
- 5. Kamat, P. V.; Trvdy, K.; Baker, D. R.; Radich, J. G., Chem. Rev. 2010, 110, 6664.
- 6. Nozik, A. J., *Physica E* **2002**, 14, 115.
- 7. Kamat, P. V., J. Phys. Chem. C 2008, 112, 18737.
- 8. Chuang, C. H. M.; Brown, P. R.; Bulovic, V.; Bawendi, M. G., *Nat. Mater.* **2014,** 13, 796.
- 9. Yang, J.; Wang, J.; Zhao, K.; Izuishi, T.; Li, Y.; Shen, Q.; Zhong, X., *J. Phys. Chem. C* **2015,** 119, 28800.
- 10. Nozik, A. J.; Beard, M. C.; Luther, J. M.; Law, M.; Ellingsono, R. J.; Jhonson, J. C., *Chem. Rev.* **2010**, 110, 6873.
- 11. Semonin, O. E.; Luther, J. M.; Choi, S.; Chen, H. Y.; Gao, J.; Nozik, A. J.; Beard, M. C., *Science* **2011**, 334, 1530.
- 12. Schaller, R. D.; Sykora, M.; Pietryga, J. M.; Klimov, V. I., *Nano. Lett.* **2006,** 6, 424.
- 13. Nozik, A. J., Chem. Phys. Lett. 2008, 457, 3.
- 14. Schokley, W.; Queisser, H. J., J. Appl. Phys. **1961,** 32, 510.
- 15. Kim, R. M.; Ma, D., J. Phys. Chem. Lett. **2014,** 6, 85.
- 16. Yella, A.; Lee, H. W.; Tsao, H. N.; Yi, C.; Chandiran, A. K.; Nazeeruddin, M. K.; Diau, E. W.; Yeh, C. Y.; Zakeeruddin, S. M.; Gratzel, M., *Science* **2011**, 334, 629.
- 17. Green, M. A.; Emery, K.; Hishikawa, Y.; Warta, W.; Dunlop, E. D., Solar Cell Efficiency Tables (Version 39). *Prog. Photovoltaics* **2012**, 20, 12-20.
- 18. Abdellah, M.; Marschan, R.; Zidek, K.; Messing, E. M.; Abdelwahab, A.; Chabera, P.; Zheng, K.; Pullerits, T., *J. Phys. Chem. C* **2014**, 118, 25802.
- 19. Chaudhuri, R. G.; Paria, S., Chem. Rev. 2012, 112, 2373.
- 20. Zhu, H.; Song, N.; Lian, T., J. Am. Chem. Soc. 2010, 112, 15038.
- 21. Xu, Z.; Hine, R. C.; Maye, M. M.; Meng, Q.; Cotlet, M., ACS Nano **2012**, 6, 4984.
- 22. Pokrant, S.; Whaley, K. B., Eur. Phys. J. D. 1999, 6, 255.
- 23. Kalyuzhny, G.; Murray, R. W., J. Phys. Chem. B **2005**, 109, 7012.
- 24. Bullen, C.; Mulvaney, P., Langmuir 2006, 22, 3007.
- 25. Woo, Y. J.; Lee, S.; Lee, S.; Kim, D. W.; Lee, K.; Kim, K.; An, J. H.; Lee, C. D.; Jeong, S., J. Am. Chem. Soc. **2016**, 138, 876.
- 26. Jasieniak, J.; Mulvaney, P., J. Am. Chem. Soc. **2007**, 138, 876.
- 27. Gao, Y.; Peng, X., J. Am. Chem. Soc. **2015**, 137, 4230.
- 28. Omogo, B.; Aldana, F. J.; Heyes, D. C., *J. Phys. Chem. C* **2013**, 117, 2317.
- 29. Klimov, V. I., J. Phys. Chem. B **2000**, 104, 6112.
- 30. Liu, C.; J, P. J.; Krauss, T. D., J. Phys. Chem. Lett. **2014,** 5, 3032.
- 31. Yu, W. W.; Qu, L.; Guo, W.; Peng, X., Chem. Mater. 2003, 15, 2854.

Charge Separation and recombination...

- 32. Fitzmorris, B. C.; Cooper, J. K.; Edberg, J.; Gul, S.; Guo, J.; Zhang, J. Z., *J. Phys. Chem. C* **2012**, 116, 25065.
- 33. Klimov, V. I.; McBranch, D. W.; Leatherdale, C. A.; Bawendi, M. G., *Phys. Rev. B: Condes. Matter Mater. Phys* **1999**, 60, 13740.
- 34. Wang, X.; QU, L.; Zhang, J.; Peng, X.; Xiao, M., *Nano. Lett.* **2003,** 3, 1103.
- 35. Brus, L. E., J. Chem. Phys. **1983**, 79, 5566.
- 36. Brus, L. E., J. Chem. Phys. 1984, 80, 4403.
- 37. Aulenta, F.; Catervi, A.; Majone, M.; Panero, S.; Reale, P.; Rosetti, S., *Environ. Sci. Technol.* **2007**, 41, 2554-2559.
- 38. Matylitsky, V. V.; Dworak, L.; Breus, V. V.; Basche, T.; Wachtveitl, J., Ultrafast *J. Am. Chem. Soc.* **2009**, 131, 2424.
- 39. Watanabe, T.; Honda, K., J. Phys. Chem. **1982**, 86, 2617.
- 40. Scholz, F.; Dworak, L.; Matylitsky, V. V.; Wachtveitl, J., *ChemPhysChem* **2011,** 12, 2255.
- 41. Markus, T. Z.; Itzhakov, S.; Alkotzer, Y. I.; Cahen, D.; Hodes, G.; Oron, D.; Naaman, R., *J. Phys. Chem. C* **2011**, 115, 13236.
- 42. Wang, H.; Barcelo, I.; Villarreal, L. T.; Gomez, R.; Bonn, M.; Canovas, E., *Nano. Lett.* **2014**, 14, 5780.
- 43. Busby, E.; Anderson, C. N.; Owen, S. J.; Sfeir, Y. M., *J. Phys. Chem. C* **2015,** 119, 27797.

Concluding remarks

This chapter summarizes the results of present work outlined in this thesis. Based on the present findings, the scope of future studies is highlighted.

7.1. Overview

The work presented in this thesis discusses the exciton quenching dynamics of three-dimensionally confined semiconductor nanoparticles (quantum dots, QDs) in the presence of molecular systems in ionic liquid, aqueous and organic media. The stability of CdTe QDs in presence of sulfide ion and transfer of photogenerated holes of former to S2- is studied in ionic liquid to overcome the limitations of these QDs in quantum dot sensitized solar cells (QDSSCs) due to their degradation in presence of sulfide/polysulfide electrolyte in aqueous medium. Very often the emission quenching of QDs in presence of molecular systems is attributed to Förster resonance energy transfer (FRET) merely on the basis of spectral overlap criterion between emission of the former and absorption of latter and a decrease of emission lifetime of QDs in the presence of the quencher. Our study of fluorescence quenching of CdTe QDs by cresyl violet show that the emission quenching is not due to energy transfer between photo-excited QDs and CV, but due to charge transfer, even though the pair meets the spectral overlap criteria of the FRET mechanism. Further, the influence of capping agents on the luminescence properties of QDs and the effect of stoichiometry of QDs on their charge separation and recombination dynamics is also studied.

Various techniques, which include Transmission Electron Microscopy (TEM) for determining the morphology and size of the QDs, Nuclear Magnetic Resonance (NMR) Spectroscopy for the characterization of molecular systems, steady state and time-resolved absorption and emission for spectral and kinetic measurements have been employed to execute the work presented in this thesis. The results of the present work are summarized below.

The stability of CdTe QDs in presence of sulfide ion and the hole transfer between the photo-excited CdTe QDs and S²⁻ are investigated in ionic liquid instead of aqueous medium. In ionic liquids, we not only found an enhancement in the stability of the appropriate ligand (thiol-functionalized imidazolium ionic

Concluding remarks

liquid, MUIM) capped CdTe QDs in presence of sulfide ion, but also observed hole transfer between photo-excited CdTe QDs and S²⁻, through our steady state and time-resolved emission and ultrafast transient absorption measurements.

The exciton quenching dynamics of the CdTe QDs in presence of fluorescent molecule, cresyl violet (CV), is studied by employing steady state and time-resolved absorption and emission techniques. Surprisingly, though the criterion of spectral overlap between the QDs emission and CV absorption required for FRET is satisfied, the emission quenching of the QD is not accompanied by enhancement in the steady state emission of the CV and also no rise in its time-resolved emission profile (evidence for energy transfer process) is observed. The transient absorption studies (0-100 ps time window), which reveals a faster recovery of the CdTe QDs 1S exciton bleach in the presence of CV as compared in its absence, indicates that electron transfer between the photo-excited CdTe QDs and CV is responsible for the quenching of the QDs emission.

We have synthesized water soluble mercapto acid-capped CdTe QDs through a two-step ligand replacement method and observed that even though MBA-capped CdTe QDs exhibits QY similar to that reported for the QDs obtained through direct aqueous synthesis, a huge enhancement in the QY is achieved for other mercapto acid-capped CdTe QDs. Moreover, the highest QY is obtained for 3-MPA-capped QDs, not for MBA-capped QDs, indicating efficient passivation of the unsaturated or dangling bonds of the CdTe QDs by MPA and consequent enhancement of their radiative carrier recombination. The evidence for efficient passivation of the surface atoms in case of MPA-capped CdTe QDs is further provided using time—resolved emission and ultrafast transient absorption measurements.

The charge separation and recombination dynamics between photoexcited CdSe QDs of varying stoichiometry and methyl viologen (MV⁺²) is investigated employing steady state and time-resolved emission and absorption techniques. The

ultrafast transient absorption studies show that the rate constant of forward and back electron transfer process between CdSe QDs and MV⁺² is independent of the QDs stoichiometry. Interestingly, the electron transfer efficiency is found to be dependent on the QDs stoichiometry. The maximum efficiency of the electron transfer process is observed in Cd-rich QDs. The low electron transfer efficiency observed in case of Se-rich QDs is attributed to the unpassivated selenium sites (compared to Cd-rich QDs), which enhances the hole trapping resulting in non-radiative carrier recombination.

7.2. Future scope

Use of conventional solvents in liquid-junction solar cells is limited due to the evaporation of these solvents which deteriorates the energy conversion efficiency of the cell. Ionic liquids (ILs) are considered as alternatives to conventional solvents due to their non-volatility, high thermal stability and wide electrochemical window. When ILs are used instead of aqueous medium, we not only observe a higher stability of CdTe QDs in the presence of sulfide ion, but also observe hole transfer between CdTe QDs and sulfide ion. However, the high viscosity of ILs compared to conventional solvents limits the charge separation process between the QDs and electron/hole acceptors. This is a serious problem for the development of solar cells using these promising materials. We consider design and development of new ILs with low viscosities and study of the charge separation dynamics between the QDs and molecular systems are key to expand the scope of their utility in real world applications.

As discussed earlier, majority of QDs applications ranging from photovoltaics to light-emitting diodes are related to their luminescence. However, synthesis of these materials with high emission quantum yields is still a challenge. The trapping of photo-generated carriers by surface trap states of the QDs is one factor which leads to their non-radiative recombination. Passivation of this surface

Concluding remarks

trap states by capping the QDs with ligands is one of the possible routes by which the non-radiative recombination of the photo-generated carriers can be reduced. Though we are successful in enhancing the emission quantum yields of the CdTe QDs by using appropriate capping agents employing a different synthetic approach, complete passivation of these QDs surface states is not achieved. Therefore, further studies on exploration of novel synthetic routes and appropriate capping agents, which completely passivate the trap states of the QDs and increase their radiative recombination, are necessary.

Chapter 7

ULTRA FAST TRANSIENT ABSORPTION AND FLUORESCENCE STUDIES

ORIGINALITY REPORT

SIMILARITY INDEX

2%

INTERNET SOURCES **PUBLICATIONS**

7%

2%

STUDENT PAPERS

PRIMARY SOURCES

Sekhar, M. Chandra, Kotni Santhosh, Jaini Praveen Kumar, Navendu Mondal, S. Soumya, and Anunay Samanta. "CdTe Quantum Dots in Ionic Liquid: Stability and Hole Scavenging in the Presence of a Sulfide Salt", The Journal of Physical Chemistry C, 2014.

Publication

Sekhar, M Chandra, and Anunay Samanta. "An Ultrafast Transient Absorption Study of the Nature of Interaction Between Oppositely Charged Photo-excited CdTe Quantum Dots and Cresyl Violet", The Journal of Physical Chemistry C, 2015.

1%

Publication

Santhosh, Kotni, and Anunay Samanta. "Exploring the CdTe Quantum Dots in Ionic Liquids by Employing a Luminescent Hybrid of the Two", The Journal of Physical Chemistry C, 2012.

Publication

<1%

4	properties and organic reactivity", Journal of Physical Organic Chemistry, 04/2005 Publication	<1%
5	Regulacio, Michelle D., and Ming-Yong Han. "Composition-Tunable Alloyed Semiconductor Nanocrystals", Accounts of Chemical Research, 2010. Publication	<1%
6	Biofuels and Biorefineries, 2014. Publication	<1%
7	Da Lei. "Recent progress in the fields of tuning the band gap of quantum dots", Science China Technological Sciences, 02/22/2012 Publication	<1%
8	Xie, Renguo. "Synthesis and surface modification of semiconductor nanocrystals", 09: Chemie, Pharmazie und Geowissenschaft. 09: Chemie, Pharmazie und Geowissenschaft, 2007. Publication	<1%
9	Sadeghi, R "Effect of alkyl chain length and temperature on the thermodynamic properties of ionic liquids 1-alkyl-3-methylimidazolium	<1%

bromide in aqueous and non-aqueous

solutions at different temperatures", The

Journal of Chemical Thermodynamics, 200902